Nonlocal Quantum Transport through the Edge State in Two-Dimensional Electron Systems

by

Kenichi Oto

Dissertation in Physics

Department of Physics
Faculty of Science
Osaka University
1993

Contents

Abstract

The quantum transport of two-dimensional electron systems (2DES) in GaAs/AlGaAs heterostructures and Si-MOS FETs is investigated at high magnetic fields and low temperatures. The mesoscopic size ($\approx\mu$m) and macroscopic size ($\approx$mm) multi-terminal wires are fabricated from GaAs/AlGaAs heterostructure wafers. The magnetoresistance shows nonlocal features, such as a geometry dependent resistivity, an influence of the contact probe and a current dependent resistivity, which can not be explained only by considering local conductivity tensor. The nonlocal features in 2DES are understood by considering both edge and bulk state as current carrying channels. A nonlocal resistance, where the voltage probes are well separated from the nominal current path, is observed in 2DES samples; not only in the high mobility GaAs/AlGaAs heterostructures, but also in the Si-MOS FETs. The observed nonlocal resistance is explained quantitatively by the Landauer-Büttiker formula. A negative four-terminal resistance is observed when a probe is not ideal. The anomalous transmission probability to the edge and bulk channels at the probe causes an anomalous population of electrons in the channels when the probe is used as a current source. By using the probe as a voltage probe, selective detection of the channels is made. The negative resistance is understood by considering the property of the non-ideal probe and non-equilibrium conduction in the edge state. In order to investigate the influence of the properties of the probe on the measured resistivity, the transmission probability of the channels is artificially controlled by a gate near the probe. Since the chemical potential equilibration among channels occurs in the probe, it affects the electronic transport, whether it is in use or not. The nonlocal features of the electronic

transport in 2DES are also changed by variable confinement potential of 2DES at the sample edge which is controlled by surrounding Schottky gate. The magnetocapacitance between a metal gate on the sample and 2DES in GaAs/AlGaAs heterostructure shows minima at the quantum Hall plateau regime. The capacitance minima are governed by the area of the current carrying edge state, and is not reflected by the density of states at Fermi level. The width of the edge state is estimated.

1 Introduction

The electronic transport property of the two-dimensional electron system (2DES) has attracted both theoretical and experimental interest as the quantum effects[1]. Owing to the technical development of the semiconductor crystal growth and fabrication process in recent years, the high quality 2DES in the heterostructures and metal-oxide-semiconductor (MOS) structures can be made. When the magnetic fields applied normal to the 2DES, the energy band of the electrons split into the Landau levels. At low temperatures, the magnetoresistance shows Shubnikov-de Haas (SdH) oscillations, and the peak value of longitudinal conductivity σ_{xx} at a $n-th$ Landau level shows a good agreement with the theoretical value $2e^2(n+1/2)/\pi h$, calculated on a self-consistent Born approximation[2]. The Hall resistance shows quantized plateaus h/ie^2 (i=1,2,$\cdots$), which is well known as the quantum Hall effect[3] (QHE). The QHE has been understood as follows. The Landau levels are broaden by the scatterers, and only states near the center of Landau level acts as an extended state (bulk state), and rest states are localized as shown in Fig. 1. When the Fermi level exists in the localized state between $i-th$ and $(i+1)-th$ extended states, the conductivity shows $\sigma_{xx}=0$ and $\sigma_{xy}=i\,e^2/h$. The QHE has been applied to the international resistance standard, because the quantum Hall (QH) plateau resistance ($=h/ie^2$) is not influenced by the sample geometry and quality. The accuracy of measured QH plateau resistance is 10^{-7}, and the fine structure constant $\alpha = e^2/\hbar c$ can be measured precisely.

The electronic quantum transport in 2DES shows novel properties such as size dependent resistivity[4,5], and a nonlocal resistance, which can not be understood only by considering the local conductivity σ_{xx} and σ_{xy}[8,9]. The nonlocal resistance is defined as a four terminal resistance where the nominal current path and voltage

probes are separated well, as shown in Fig. 2. The nonlocal resistance is hardly observed, in a classical view. Especially in the high quality (with high electron mobility) 2DES, the nonlocal features in the quantum transport has been clearly observed[8]. They are explained by the edge state conduction, whose details are discussed in the next section. The Landauer–Büttiker formula has been applied to the electronic conduction in QH regime, and successfully explain the observed resistance[8].

In this thesis, the transport property of 2DES is investigated experimentally and analyzed using the Landauer–Büttiker formula. In chapter 2, the concept of the edge state and the Landauer–Büttiker formula are reviewed as a theoretical backgrounds. In chapter 3, the sample fabrication technic, electron beam lithography system, and transport measurement system are expressed. Three kinds of samples, mesoscopic size (Sec.4.1) and macroscopic size (Sec.4.2) wires made from GaAs/AlGaAs heterostructures and Si–MOS FETs samples (Sec.4.3) are examined. The nonlocal features of the quantum transport in 2DES are discussed. The influence of the probes on the transport is investigated particularly. The width of the edge state is estimated by magnetocapacitance measurements at the QH regime. The last chapter 5 is devoted to a summary of the thesis.

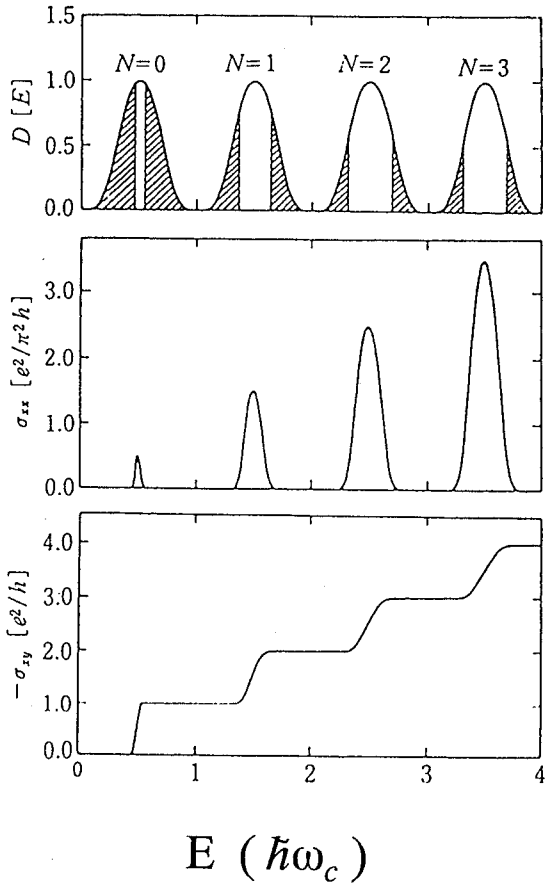

Fig. 1. The schematic illustration of the DOS *D(E)* , conductivity σ_{xx} and σ_{xy} of the 2DES at the high magnetic fields. Hatched region corresponds to the localized state.

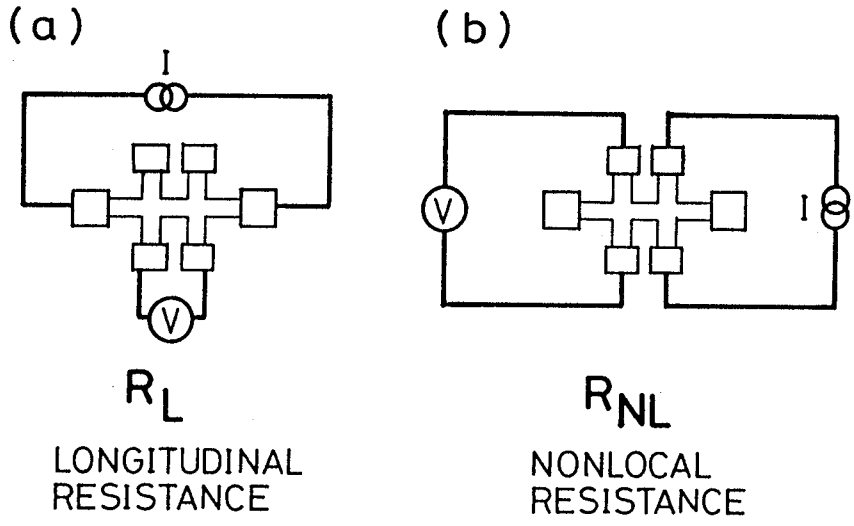

Fig. 2. Schematic layout of the four-terminal measurements. (a) Ordinary longitudinal resistance R_L. (b) The nonlocal resistance R_{NL} where the voltage probes are spatially separated from the nominal current path.

2 Theoretical background

2.1 Edge current

In the 2DES system at high magnetic fields, the electron energy band split into Landau levels. When the sample has an 'edge', the Landau levels are bent up by the confinement potential of the 2DES near the sample edge. There are two kinds of the states at the Fermi energy (E_F), '*bulk*' states in the bulk Landau level and '*edge*' states[9] at the bent up Landau levels, as shown in Fig. 3. The electrons in the edge states circulate along the sample edge as an *edge current* channels[8–10]. In the classical view, the edge electrons are moving along the skipping orbit, as shown in Fig. 3(b). The direction of the edge current is determined by the direction of the magnetic field, the edge currents go backward at the opposite side of the sample. The number of the edge channels are that of the fully occupied Landau levels. In the interior of the sample, the topmost Landau level provides a *bulk current* channel, when the E_F crosses an extended state. In this thesis, the terms 'bulk state' and 'bulk channel' are used by a current carrying topmost Landau level extending in the sample, and the 'bulk current' is denoted by a current carried through the 'bulk state'.

It is noteworthy that the electron backscattering is suppressed in the edge channels. The backscattering occurs only when electrons in a edge channel are scattered to another edge channel at the opposite side, or to the a bulk channel. The backscattering to the opposite side of the edge channel is negligible in the wide sample. The edge and bulk states are spatially separated because electrons are gently confined in the sample (see. Fig. 3) and then the overlap of the wave function between edge and bulk channels is small.

If the chemical potential of the edge state at each side of the sample is μ_L and μ_R, as shown in Fig. 4, the amount of the current I is written by;

$$I = e \int_{\mu_R}^{\mu_L} \mathrm{v}\, D(E)\, dE\,, \qquad (1)$$

where v is the group velocity of the electrons and $D(E)$ is the DOS at the energy E. The product $\mathrm{v}\, D(E)$ is equals to $2/h$, because $D(E) = \left| \pi\, \partial E / \partial k \right|^{-1}$ and $\mathrm{v} = (2\pi / \mathrm{h}) (\partial E / \partial k)$. Then the current I is given by

$$I = (2e / h)(\mu_{\mathrm{L}} - \mu_{\mathrm{R}})\,. \qquad (2)$$

The total current J is the sum of n edge currents[8],

$$J = (2e / h) \sum_{\mathrm{i}=1}^{\mathrm{n}} (\mu_{\mathrm{Li}} - \mu_{\mathrm{Ri}})\,. \qquad (3)$$

(spin degeneracy is considered)

The total current J is determined only by the chemical potential difference of the edge currents at both sides. In the quantum Hall plateau regime, the localized bulk state does not contribute to the transport; the observed phenomena can be understood by the edge current picture*. The edge channel can be regarded as the one dimensional channel, connecting the probes along the edge. Büttiker applied the Landauer formula (see sec. 2.2) to the electronic transport in the quantum Hall regime[8].

---

* Note that the expression of total current J, as shown in Eq.(3), is valid whether the fully occupied Landau levels in the interior of the sample is carrying a current or not[11]. Now, it is still important problem where is the current carrying region in the quantum Hall regime.

2.2 The Landauer–Büttiker formula

In this section, the model of the electronic transport in a mesoscopic system proposed by Landauer[12] is introduced. Consider an one dimensional conductor with probe (1) and (2). Applying the voltage difference (V) between the probes, the current I flows in the channel, as shown in Fig. 5(a). Without the scattering, the current I is expressed as;

$$I = e\, v_F \left[\int_0^{E_F+eV} D(E)\, dE - \int_0^{E_F} D(E)\, dE \right]$$
$$\approx e\, v_F D(E_F)\, e\, V = (2e^2/h)V , \qquad (4)$$

where $D(E) = \left| \pi\, \partial E / \partial k \right|^{-1}$ is DOS ,

$v_F = (2\pi / h)(\partial E / \partial k)$ is the Fermi velocity.

The conductance (I/V) of the one dimensional ideal conductor is expressed as $2e^2/h$, where the spin degeneracy is considered.

In order to take into account of the backscattering effect, the transmission probability of the electron between the probes denoted by t is considered. Since the voltage difference is written with the chemical potential difference ($\mu_1 - \mu_2 = eV$) of the probe (see Fig. 5(b)), the current in the Landauer formula is expressed as;

$$I = (2e^2/h)\, t\, (\mu_1 - \mu_2) / e . \qquad (5)$$

Büttiker extended the Landauer formula to the multi channel and multi terminal geometry[8] , as shown in Fig. 6(a). At the $i-th$ probe with the chemical potential μ_i, there are N_i current carrying channels. The transmission of the electrons from $j-th$ probe to the $i-th$ probe is denoted by T_{ij}. The probability T_{ii} represents for

coming back to the *i−th* probe. The current flowing from the *i−th* probe (I_i) is represented by;

$$I_i = (2e / h) (N_i \mu_i - \sum_j T_{ij} \mu_j) \qquad (i = 1, 2, \cdots, n), \tag{6}$$

($\sum_j T_{ij} = N_i$, for charge conservation.)

where n is the number of the probes. In Fig. 6(b), schematic view of the four-terminal resistance at QH regime is shown. In the figure, two edge channels are written, for simplicity. The notation R(ij,kl) shows the four terminal resistance where the current flows from probe i to j, and the voltage difference between probe k and l is measured. The four terminal resistance R(ij,kl) can be calculated as $R(ij,kl)=(\mu_k - \mu_l) / eI$ by solving Eq.(6). Owing to the symmetry of $T_{ij}[B]=T_{ji}[-B]$, the reciprocity of the resistance $R(ij,kl)[B] = R(kl,ij)[-B]$ is obtained, which states exchanging of the current and voltage probes and field reversing is equivalent. The edge channel picture can be applied to the Landauer–Büttiker formula[8,10,11]. The edge currents circle around the sample edge, and connect the adjacent probes without scattering.

2.3 Contact probe

In Fig. 7, the schematic illustration of the interface region between 2DES and probe is shown. The contact probe consists of the electron reserver and the disordered region at the interface of the 2DES region[8]. Suppose that the n edge currents with the chemical potential μ_i (i=0,1,··n−1) come into a probe with the transmission probability T_i , and the current I is externally injected to the probe. The chemical potential of the contact probe (electron reserver) μ_c is written as[13];

$$I = (2e / h) \sum_i [T_i (\mu_c - \mu_i)] , \tag{7}$$

thus,

$$\mu_c = \sum_i (T_i / T)\, \mu_i + (h / 2eT)\, I\,, \tag{8}$$

The chemical potential of the emitting edge currents μ'_i are also shown;

$$\mu'_i = \sum_j [\, (T_i\, T_j / T) + R_{ij}\,]\, \mu_j + (T'_i / T)(h / 2e)\, I\,, \tag{9}$$

$$T = \sum_i T_i = \sum_i T'_i\,, \tag{10}$$

$$T_i + \sum_j R_{ji} = 1 \quad \text{and} \quad T'_i + \sum_j R_{ij} = 1\,, \tag{11}$$

R_{ij} is the reflectivity of which the *i−th* edge current, incoming to the probe, is reflected to the outgoing *j−th* edge current (see Fig. 7). T_i (T'_i) is the incoming (outgoing) probability between the channels and probe, respectively. The contact resistance of the probe R_c can be written as[13];

$$R_c = [\, (n/T) - 1\,]\, (\, h / 2ne^2\,)\,. \tag{12}$$

In the ideal probe, the total transmission T=n ; the R_c becomes zero. In the real contact probe, the transmission probability of each channel is less than unity, the total transmission probability T is smaller than n.

In this thesis, the experimental results are analyzed by the Landauer−Büttiker formula, for the nonlocal resistance, longitudinal resistance, and the properties of the probes.

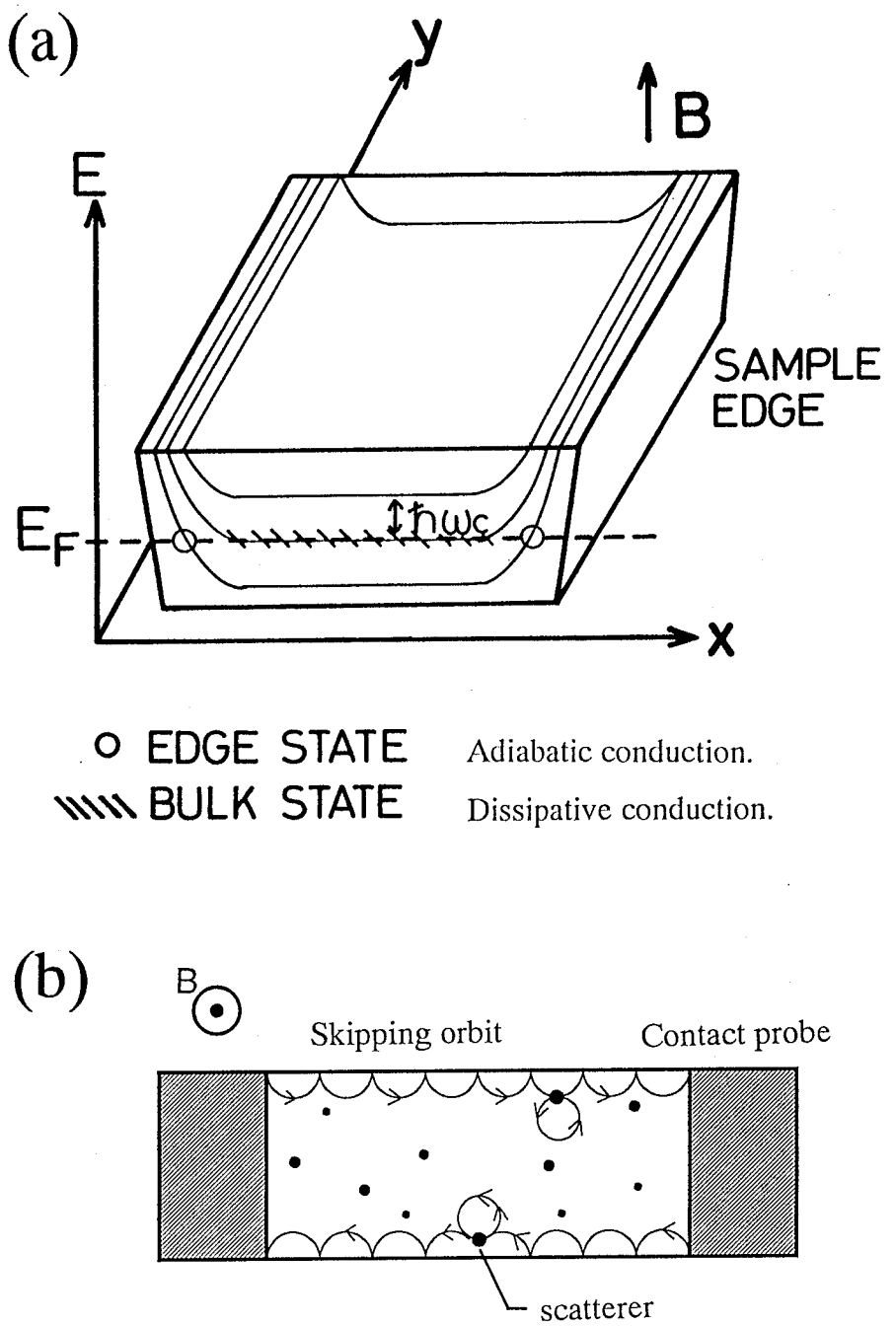

Fig. 3. (a) Schematic representation of the energy levels in 2DES at high magnetic fields. The current carrying states exist at the cross point of the Fermi level E_F and extended Landau levels. In this figure, the edge state (marked open and closed circle) and bulk state (hatched region) coexist. (b) The classical view of the edge current. The electrons move along the sample edge with skipping orbit. Closed circles are scatteres.

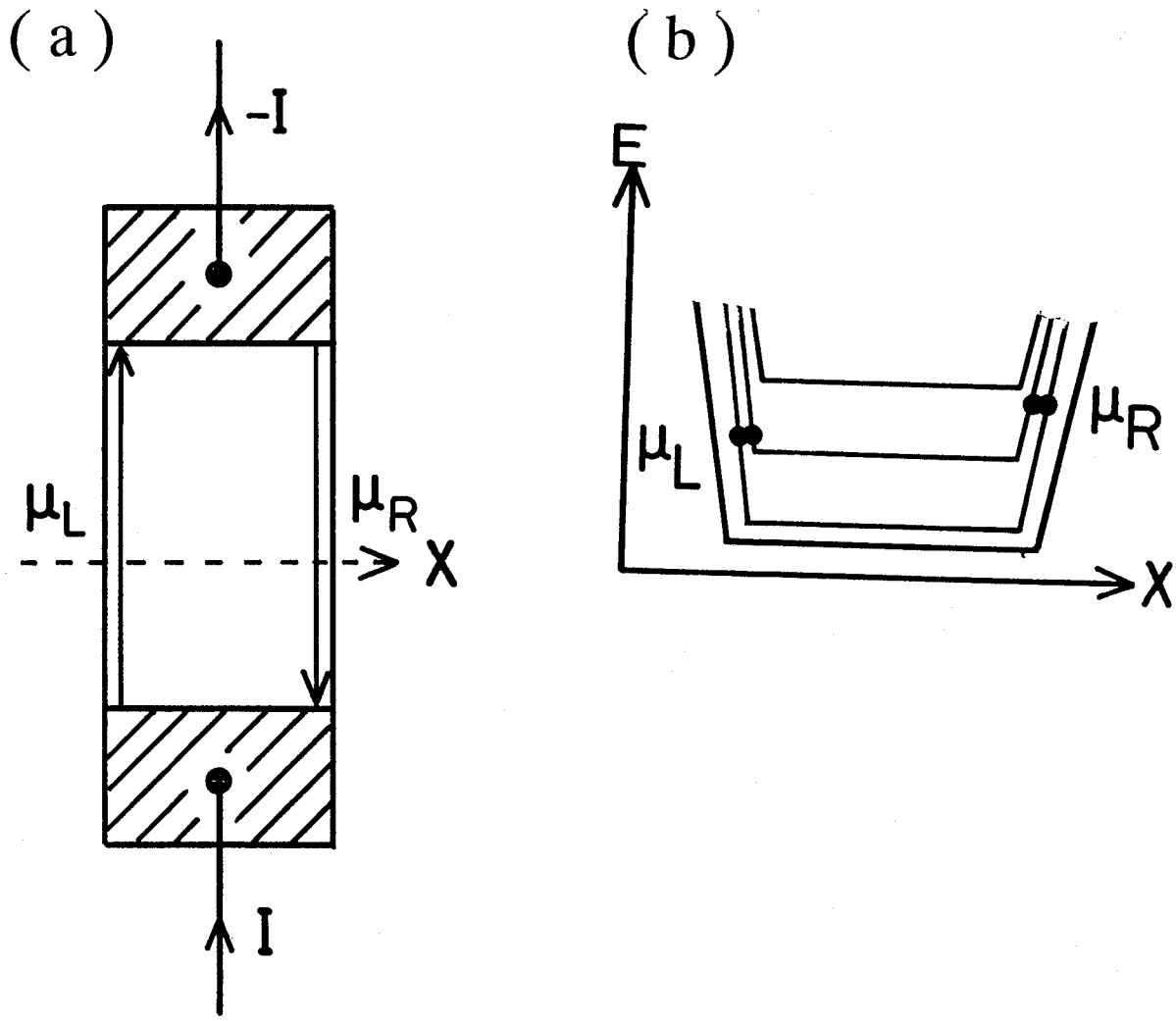

Fig. 4. The chemical potential of the edge currents at QHE regime. (a) The chemical potential of the edge current at the left (right) side is μ_L (μ_R) when the current I flows. (b) The energy level of the Landau level. The horizontal axis corresponds to the direction of the sample width (broken line in (a)).

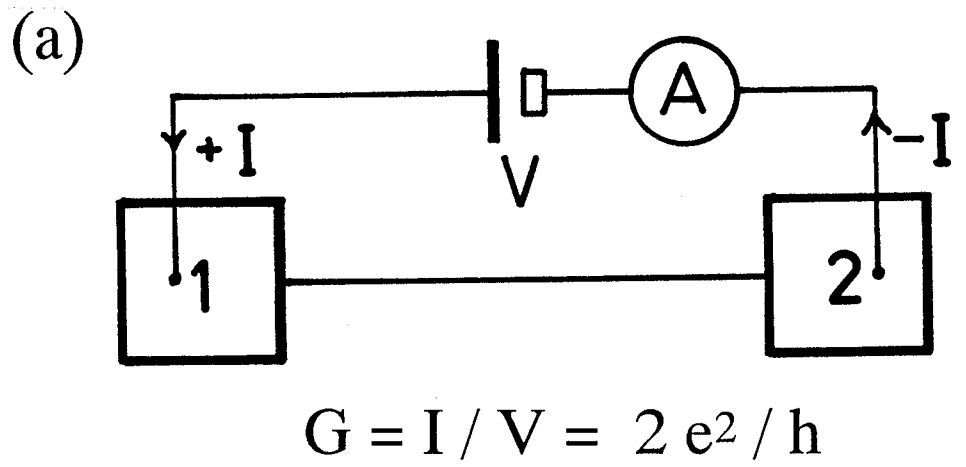

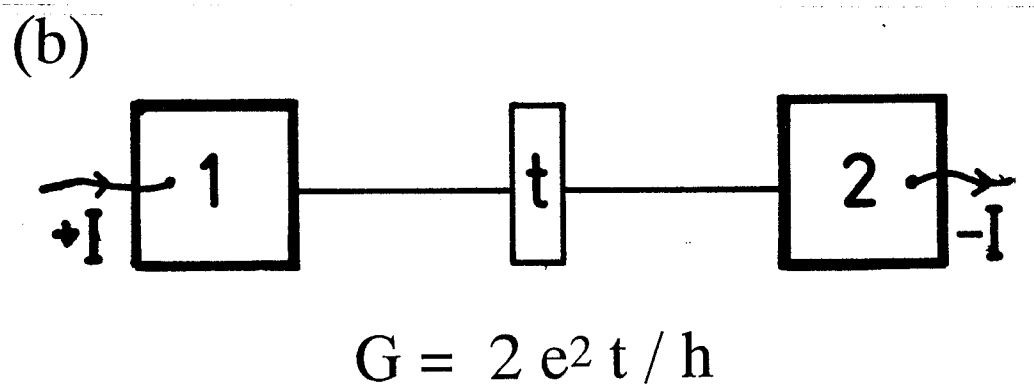

Fig. 5. (a) The dissipation–less one dimensional conductor. Note that the conductivity is $2e^2/h$. (b) The backscattering is represented with a barrier whose transmission probability is t .

(a) The Landauer–Büttiker formula

$$I_i = (e / h) [N_i \mu_i - \sum T_{ij} \mu_j]$$

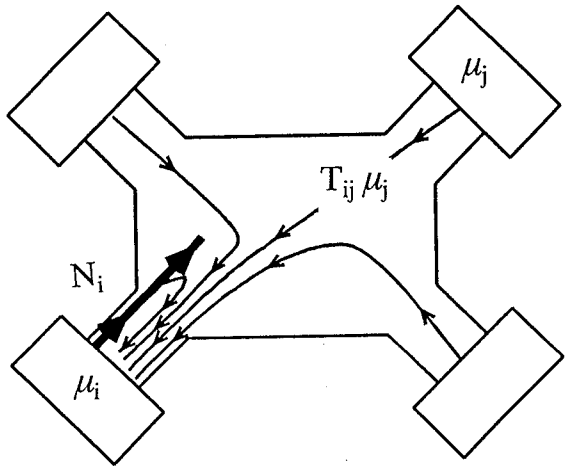

(b)

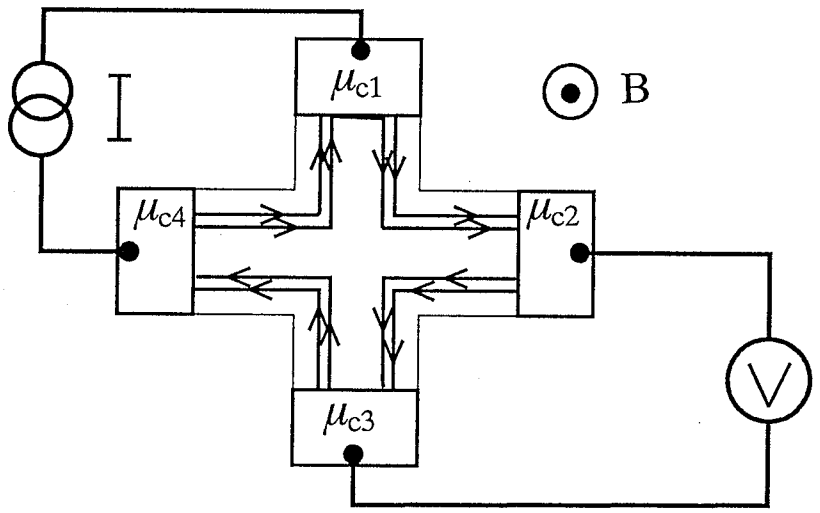

$$R(14.23) = V / I = (\mu_{c2} - \mu_{c3}) / e I$$

Fig. 6. (a) The Landauer–Büttiker formula with multi–terminal geometry. The total current I_i through the *i–th* probe is determined by the outgoing electrons through the N_i channels and incoming electrons from the probes with the transmission probability of T_{ij}. (b) The electronic transport by edge channels are shown. Two edge channels connect the adjacent probes. The direction of the current is determined by the magnetic fields.

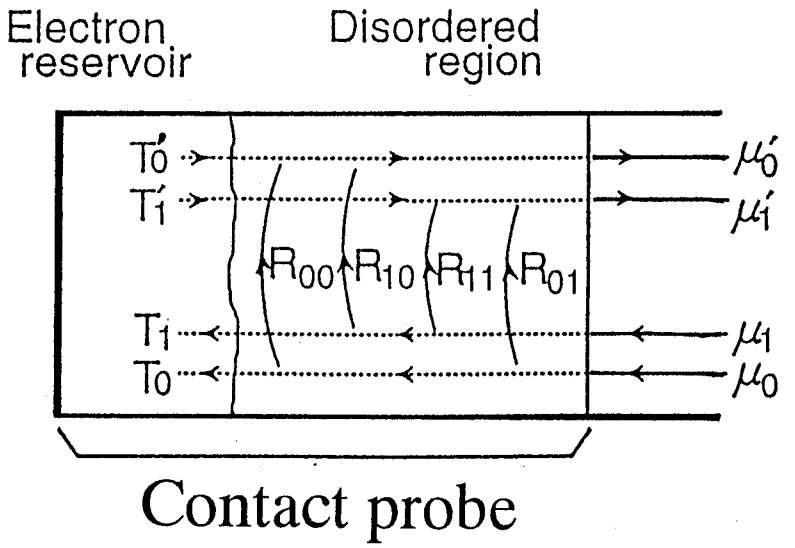

Fig. 7. The model of the disordered contact probe. T_i (R_{ij}) is a transmission probability (reflectivity) of the edge current to the probe.

3 Experimental Procedure

3.1 Sample preparation

3.1.1 GaAs/AlGaAs heterostructures

The multi-terminal wires were prepared from modulation doped GaAs / $Al_{1-x}Ga_xAs$ ($x \approx 0.3$) heterostructure wafers. In Fig. 8, a schematic cross sectional view of the wafers is shown. The GaAs and AlGaAs layers are grown by the molecular beam epitaxy technic (MBE) on a semi-insulating GaAs substrate. The two-dimensional electron system is formed at the GaAs/AlGaAs interface (Fig. 8), because the band-bending, due to the charge transfer from Si-doped AlGaAs layer to the GaAs layer, acts as a confining potential of electrons. The Si donors doped AlGaAs layer and 2DES are spatially separated by the undoped AlGaAs spacer layer. The two-dimensional electron gas has high electron mobility, because the electron scattering by impurities is decreased at low temperatures, and the interface between GaAs and AlGaAs layers is flat in an atomic scale.

3.1.2 GaAs/AlGaAs mesoscopic size wires

The mesoscopic size ($\approx \mu$m) samples were fabricated by using an electron beam lithography and Ar-ion dry etching technic. The detail of the processes is as follows; (see Fig. 9(a))

(1) As grown GaAs/AlGaAs wafer was cleaved to a 5x5 mm square piece and rinsed in trichloroethylene.
(2) Electron beam sensitive resist, PMMA (polymethylmethacrylate) was coated on the sample. Six percent solution of PMMA was dropped to

the sample spinning at 8000 rpm and then the sample was dried in air at 170 °C for 2 hours. The thickness of the PMMA resist was typically 300 nm.

(3) The resist was exposed with 50 keV electron beam using a JEOL NSF-1 electron beam lithography system at Research Center for Extreme Materials, in Osaka university. After direct writing by the electron beam, the sample was drop into developer (methylisobutylketone diluted 1/3 with isopropylalcohol).

(4) Aluminum was evaporated a thickness ≈100 nm, and then Al on the resist was removed by a liftoff technic. Then residual Al acted as an etching musk.

(5) The ohmic contact areas were also covered with photo-resist of NNR752 by photolithography (described below).

(6) The partially aluminum masked sample was exposed to 1 keV accelerated Ar-ion shower for 5 min. A shallow-mesa etching was used to avoid a damage to the narrow channels. The etching depth did not reach the 2DES layer. The electrons below the shallow etched region were fully depleted.

(7) After these processes, the ohmic contacts were formed by metal deposition and alloying. The details are described below (c)-(e).

3.1.3 GaAs/AlGaAs macroscopic size wires, ohmic contact and Schottky gate

A macroscopic size (≈mm) samples were fabricated by photolithography (see Fig. 9(b)). The wafer was prepared in the same way of (1);

(a) The negative photo-resist NNR752 was spin coated on the sample at 5000 rpm. The resist was dried at 90 °C for 5 min. By using photo-mask and aligner system, UV light was exposed. After developing,

the resist became the mask for an etching.

(b) The sample was dipped into an etching solution for 2 min. The enchant consists of the mixture H_3PO_4: H_2O_2: H_2O = 1:1:30 at room temperatures. The etching rate of this etchant is about 150 nm/min. After etching, the resist was removed.

(c) To form the ohmic contacts, the positive photo-resist AZ1350 was covered on the sample (spin coating 5000 rpm, baked 70 °C/10 min.). After UV exposure thorough the mask and developing, the areas except for contact region was covered with the resist.

(d) The contact metals were deposited by successive evaporation of Au-Ge(12%) alloy, Ni, and Au in the base pressure $\approx 2 \times 10^{-6}$ Torr. The thickness was 100, 25, and 100 nm respectively. The resist was removed with metal on the resist.

(e) The sample was annealed at 470 °C for 4 minutes to alloy the contact metals in the forming gas (Ar 90%, H_2 10%). In this way, the contact resistance was typically below 100 Ω.

Since the electrical transport properties are very much influenced by the properties of the contacts in the quantum Hall condition, the process of making contacts, material selection and annealing conditions, are very important. Details are discussed in chapter 4.2.

(f) When Schottky gates were formed on the sample, the sample surface was slightly etched with conc. HCl solution to remove an oxide layer. The same process (c) and (d) were repeated. At the metal evaporation, instead of the contact metal, the gate material of Au or Au-Al or Au-Ti was used.

3.1.4 Si-MOS FET

Si-MOS FETs were fabricated at NTT applied electronic laboratories. By using conventional photolithography and ion implantation processes, three Hall devices A, B and C of Si-MOS structures with two pairs of Hall probes were obtained. The SiO_2 layer of the samples A and B was made by thermal annealing in diluted O_2 gas, and made by using Ar/O_2 sputtering[14] for sample C. The sputtering method has an advantage that the sample is free from high temperature annealing. Details are shown in section 4.3.2.

3.2 Electron beam lithography

The photo-mask plate was made by direct electron beam lithography and wet chemical etching. In this study, many masks were needed to change the sample structures. To fabricate the masks easily, a function of electron beam lithography was added to JEOL JSM-6400 scanning electron microscope (SEM) as follows;

- An electric gun with LaB_6 cathode was used to obtain high intensity electron beam and small spot size.
- A turbo-molecular pump was used to get an oil free system.
- Beam blanking device (BBD) was installed to control the electron exposure to the sample.
- Beam scanning and blanking was externally controlled by the personal computer, and the control software was made.

This lithography system, shown in Fig. 10, enabled us to fabricate both mesoscopic ($\approx$100 nm) size and large mask ($\approx$5 mm) size sample. Since the sample could be changed quickly ($\approx$1 min.), the turn around time was much

shorter than that of the conventional electron beam exposure systems. In addition, the performance as an electron microscope was also improved.

3.3 Electron transport measurement system

The magneto-resistance up to 8 T, at temperatures below 4.2 K was studied by using superconducting magnet (SCM) and ^{3}He refrigerator. The diagram of the system is shown in Fig. 11. The cryostat and SCM were cooled by liquid ^{4}He. Temperatures 4.2 – 1.8 K were obtained to evacuate the helium gas above the liquid ^{4}He by a rotary pump. Connecting the cryostat to the ^{3}He gas handling system, shown in Fig. 12, the ^{3}He gas was liquefied, and the sample was immersed in the liquid ^{3}He. The sample was cooled below 0.5 K by pumping out the ^{3}He with sealed rotary pump. This ^{3}He refrigerator system has the following advantages:

- Easy to change a sample because of the top-loading type.
- No blockage accident has happened, since the system has no 1 K pot or capillaries.
- Temperatures below 0.5 K can be held for long time (more than one day), though the system is one-shot type refrigerator.

The sample was set in the center of the magnet, and the direction of the fields was perpendicular to the sample surface. The electrons in the edge states flow clockwise along the sample edge normally. A calibrated carbon resistor for thermometer and a GaAs light emitting diode (LED, λ=950 nm) were installed near the sample. The current level at the resistance measurement was 30 pA – 100 μA. For low level measurement, the coaxial cables and shielded cables were used to avoid noise. The ground (earth) connection was carefully done, not to make

ground loops which would be a noise source. The cryostat and pump lines (^{3}He gas handling system, and pump line from liquid He dewar) were electrically isolated to eliminate the electrical noise.

For the resistance measurement, a programmable current source (Keithley 220) as an ac current (operating at 15 Hz) source, and a high sensitive lock-in amplifier (EG&G-PAR 5210) for voltage measurement were used. These instruments have high output and input impedance ($>10^{14}$ Ω, $>10^8$ Ω respectively). They are still adequate to be used, even when the contact resistance of the samples exceeds 1 MΩ. To apply the gate voltage, a programmable voltage source (Keithley 230) was also used. For the measurement for the mesoscopic size samples and the thermometry, an automatic ac resistance bridge (RV Elektroniikka AVS-46) operating at 15 Hz was also used. In Fig. 13, the block diagram of the resistance measurement system is shown. To measure a capacitance, a ultra-precision capacitance bridge (Andeen-Hagerling 2500A) with voltage source for applying dc bias was used. This capacitance bridge is an 'actual bridge' that the measurement is not affected by the stray capacitance between a sample and the ground. Since the wiring in the cryostat should be thermally anchored well, the stray capacitance is quite large, the precise measurement is difficult without the 'actual bridge'.

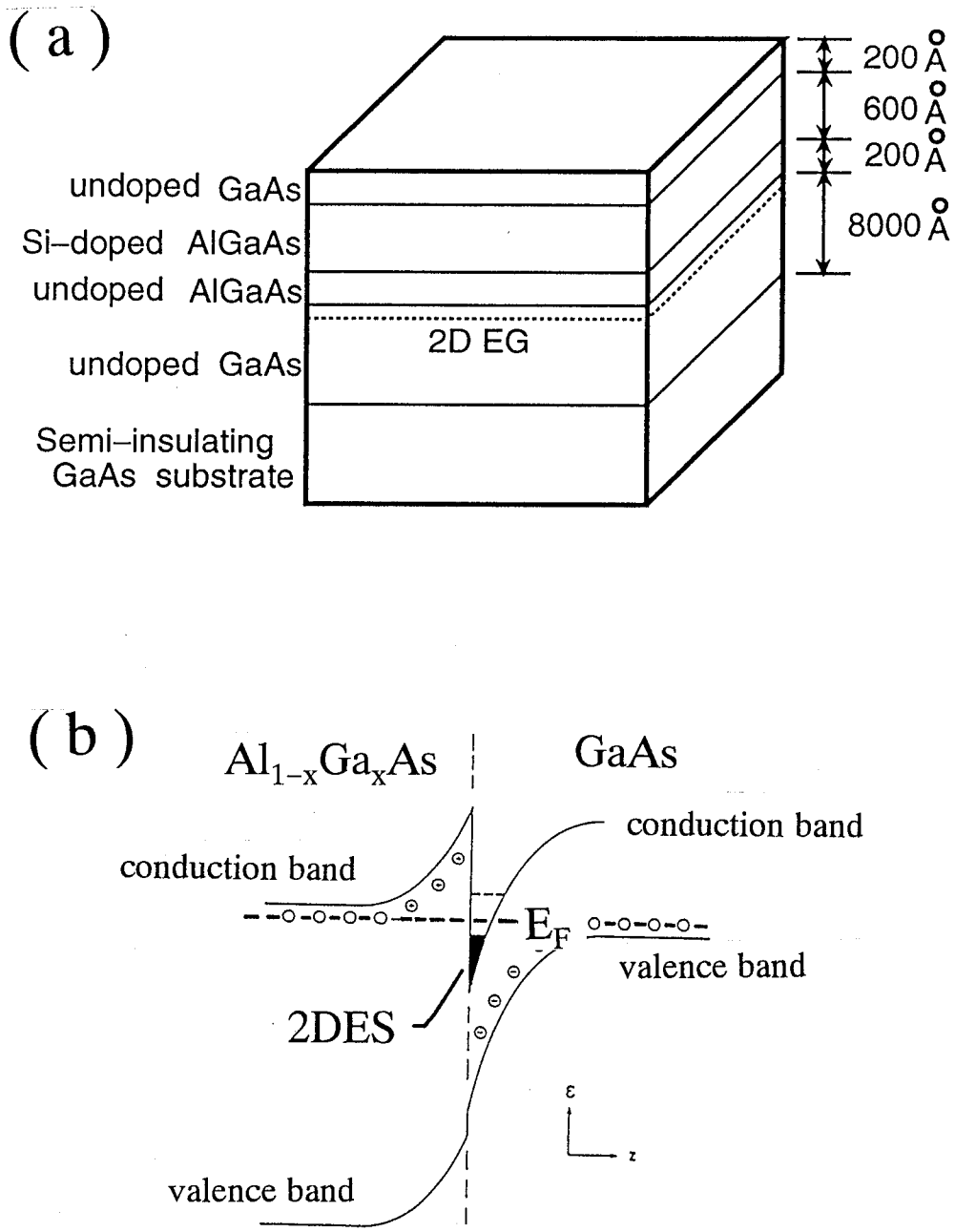

Fig. 8. The schematic cross sectional view of MBE grown GaAs / $Al_{1-x}Ga_xAs$ heterostructure and the band structure at the hetero junction of $Al_{1-x}Ga_xAs$ and GaAs.

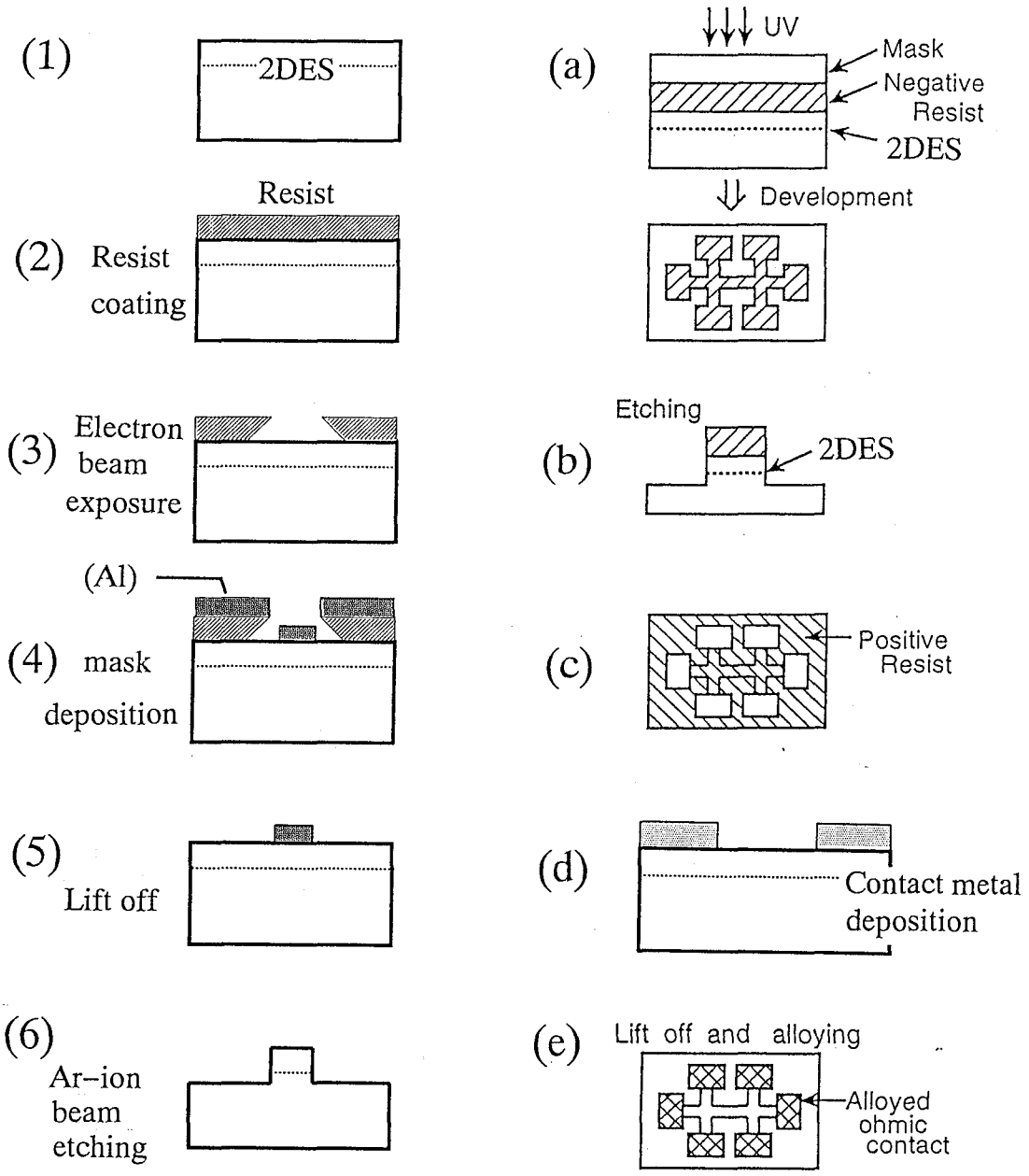

Fig. 9. (a) Process of the electron beam lithography for mesoscopic size sample fabrication. (b) Process of the UV lithography for macroscopic size sample and contact probe.

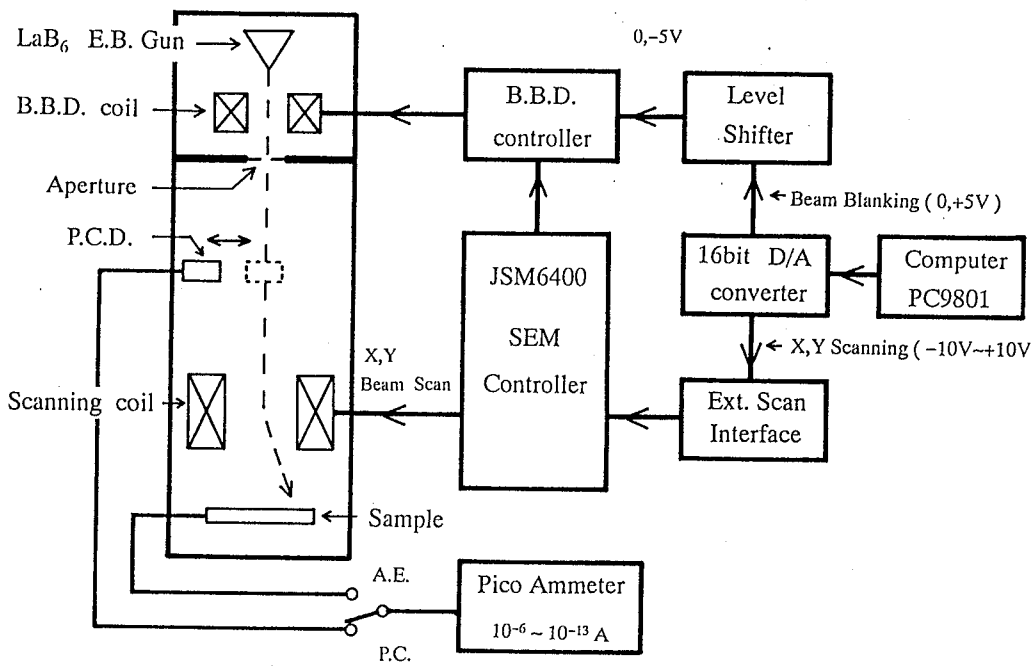

A.E.	Absorption Current
B.B.D.	Beam Blanking Device
D/A	Digital - Analog Converter
E.B.	Electron Beam
P.C.	Probe Current (Beam Current)
P.C.D.	Probe Current Detector
SEM	Scanning Electron Microscope

Fig. 10. Electron beam lithography system modified a SEM unit.

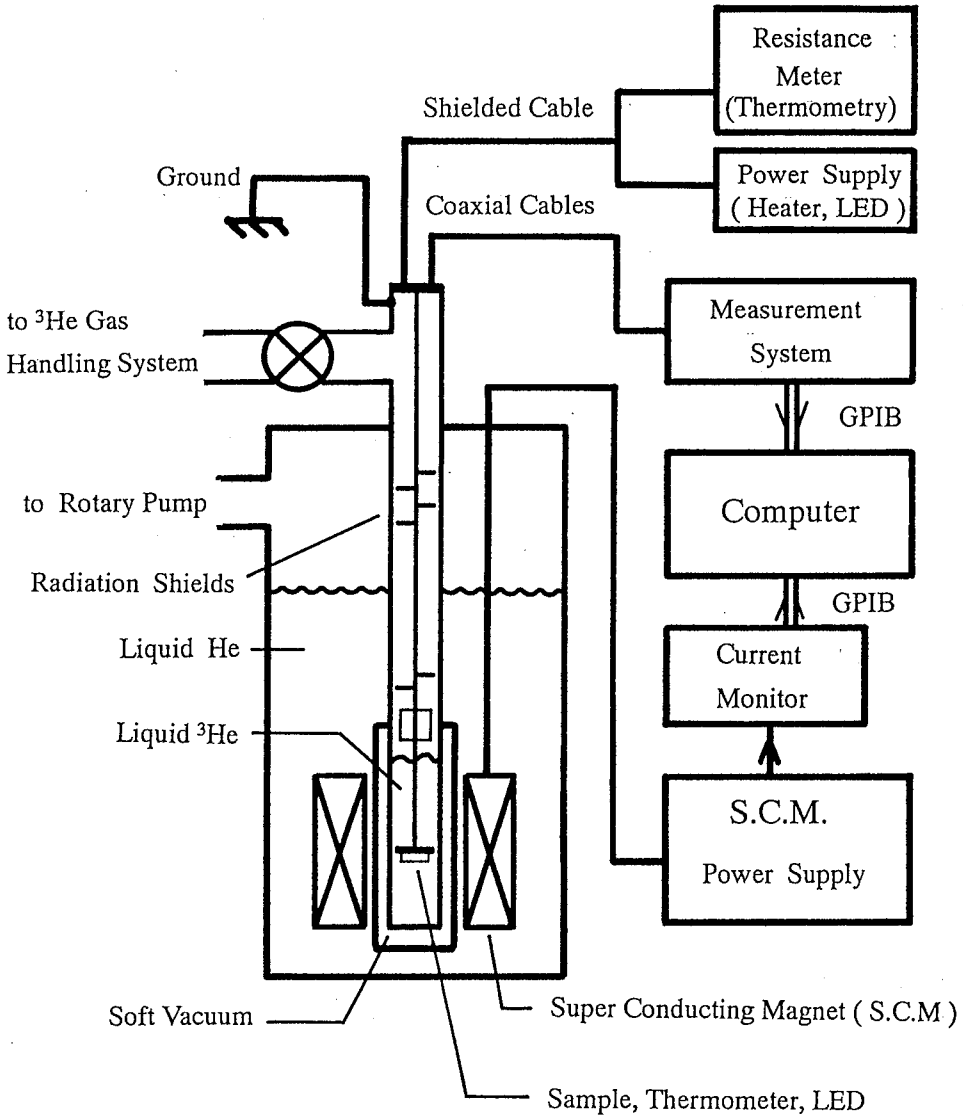

Fig. 11. Cryostat for transport measurements. A NbTi superconducting magnet (8.5 T), and ^{3}He cryostat are installed in the liquid He storage dewar of the super insulation.

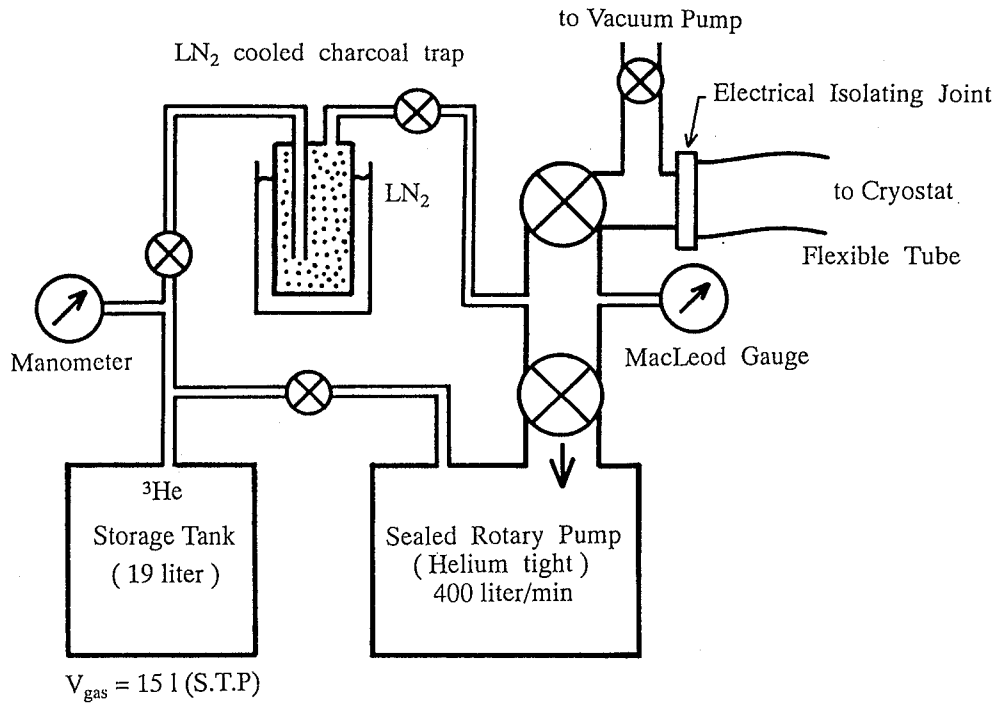

Fig. 12. Schematic of the ^{3}He gas handling system. The sample is cooled below 0.5 K and held more than a day. To avoid the noise conduction, the gas handling system and the cryostat are electrically isolated by a insulating joint.

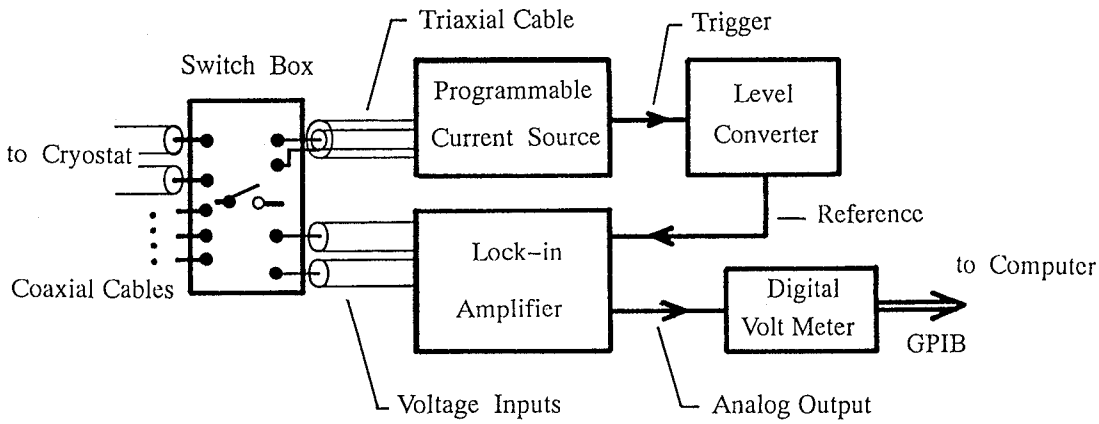

Fig. 13. Resistance measurement system.

Results and Discussion

4.1 Mesoscopic system

4.1.1 Quantum Hall effect and nonlocal resistance in mesoscopic size samples.

Three multi-terminal wires (sample A-C) of mesoscopic size were fabricated from the wafers of modulation doped GaAs/AlGaAs heterostructures. The details of the samples are shown in Table 1. Just before the resistance measurement, the wire was illuminated by a GaAs light emitting diode (LED) to increase the carrier concentration by the persistent photoconductivity. Then the effective width of the wire increased due to a reduction of the depletion region extending from the side wall. An excitation current level for the resistance measurement was limited to 30 nA or 100 nA to avoid the heating effect. The longitudinal resistance (R_L) and Hall resistance (R_H) of the sample A at 0.5 K are shown in Fig. 14(a), where the schematic view of the samples are shown in the inset. In the low field regime (B< 0.5 T), a large negative magneto-resistance in the longitudinal resistance, a quenching of the Hall resistance, and a last Hall plateau[15] are observed. These phenomena have been interpreted as a ballistic transport in the mesoscopic wires[15]. In the high field region, the QHE plateaus and the practically zero resistance of R_L appear. The Hall plateaus due to the spin splitting (filling factor of the Landau level $\nu \geq 3$) are not clearly resolved, compared to that in the macroscopic size sample which is made from the same wafer. Since the spatial expansion of the edge current is comparable to the wire width, the edge state in the opposite side is mixed. That is, the back scattering of the edge current becomes significant, and a breakdown of the quantum Hall effect occurs. Further discussion will be given in section 4.2.8.

The nonlocal resistance at several separation length ΔL measured in the sample A is shown in Fig. 14(b). The nonlocal resistance shows some peaks similar to usual SdH oscillations, and the minimum plateaus are observed when the Hall resistance is quantized at high magnetic fields. The nonlocal resistance is almost zero at low field region. Generally, the peak amplitudes of the oscillation decrease with increasing ΔL. In the cases that the extra probes are contained between the current and voltage probes, the amplitudes of the oscillations are much reduced. In the geometry with the separation length ΔL=7 μm, the oscillations almost vanish, where two pairs of the probes are contained. The similar behavior are observed in other samples B and C.

4.1.2 Model of the electric transport in a quantum Hall condition

To understand the nonlocal resistance McEuen *et al.*[6] proposed a model which treated the current carrying edge and bulk channels independently. In this model, the N–*th* (N≥1) Landau level coincides with Fermi energy. The (N–1) edge channels belonging to the fully occupied Landau levels, and the bulk channel of the topmost (N–*th*) Landau level are considered. The electrons in the edge channels are carried from probe to probe without scattering, and the conductance of each channel is e^2/h. The electrons in the bulk channel can be backscattered , because the bulk current is carried through the *extended states* in the sample. The conductance of the bulk channel is represented by a barrier in each segment in the sample (see Fig. 15). The transmission probability of j–*th* barrier t_j is expressed by using resistivity of the bulk (N–*th*) channel ρ^b, the length and width of the segment as

$$t_j = [\, 1 + (e^2/h)\, \rho^b\, (L_j/W_j)\,]^{-1} . \qquad (j = 1 \textit{ to } 5) \tag{13}$$

Each current channel is assumed to obey the Landauer–Büttiker formula[8] with the ideal probes. The scattering between edge and bulk channel is neglected. The assumption is justified at low temperatures in high magnetic fields, since the spatial separation between bulk and edge channels are large enough not to interact each other[11]. The total current I flowing from probes 2 to 3 by m edge channels and by a bulk channel is expressed as

$$I_1 = (e/h)[\, m(\mu_1-\mu_4) + \mu_1^b(\text{out}) - \mu_1^b(\text{in})\,] = 0\ , \tag{14}$$

$$I_2 = (e/h)[\, m(\mu_2-\mu_1) + \mu_2^b(\text{out}) - \mu_2^b(\text{in})\,] = I\ , \tag{15}$$

$$I_3 = (e/h)[\, m(\mu_3-\mu_2) + \mu_3^b(\text{out}) - \mu_3^b(\text{in})\,] = -I\ , \tag{16}$$

and

$$I_4 = (e/h)[\, m(\mu_4-\mu_3) + \mu_4^b(\text{out}) - \mu_4^b(\text{in})\,] = 0\ , \tag{17}$$

where μ_j is the chemical potential of j–*th* probes, and μ_j^b(in) and μ_j^b(out) are the chemical potentials of the bulk channels coming in and out of the j–*th* barrier. They are expressed as

$$\mu_1^b(\text{in}) = \mu_4^b(\text{out})\ , \tag{18}$$

$$\mu_2^b(\text{in}) = (1-t_5)\,\mu_3^b(\text{out}) + t_5\,\mu_1^b(\text{out})\ , \tag{19}$$

$$\mu_3^b(\text{in}) = \mu_2^b(\text{out})\ , \tag{20}$$

$$\mu_4^b(\text{in}) = (1-t_5)\,\mu_1^b(\text{out}) + t_5\,\mu_3^b(\text{out})\ , \tag{21}$$

and

$$\mu_j^b(\text{out}) = \mu_j\, t_j + (1-t_j)\,\mu_j^b(\text{in}), \qquad (j = 1\ to\ 4)\ . \tag{22}$$

The number of edge channels m = 2n, where n is the Landau index number (n=0, 1, 2...). When the spin–degeneracy is considered, *e/h* should be replaced by 2*e/h* and the number of the edge channels m=n. The nonlocal resistance R(23,14) is

derived analytically as

$$R(23,14) = (\mu_1 - \mu_4)/Ie$$
$$= (e/h)\, m\, t_1 t_2 r_3 r_4 t_5 E/(A+B+C), \qquad (23)$$

where

$$A = m\, r_4 D\,[\, t_2 t_5 (t_1 + m\, r_1) + m\, t_1 E\,],$$
$$B = m\,(t_1 + m\, r_1)\, r_2 t_3 r_4 t_5 F,$$
$$C = (m + t_1)\, t_4 [\,\{m E + (1 - r_2 r_5) t_3\}$$
$$\{m E + (1 - r_3 r_5) t_2\} - t_2 t_3 r_5 D\,],$$
$$D = m E + t_2 t_3, \quad E = 1 - r_2 r_3 r_5, \quad F = m E + t_2 (1 - r_3 r_5),$$
and $r_j = 1 - t_j$, $(j = 1 \text{ to } 5)$.

In this model, there is one parameter ρ^b that shows the backscattering of the bulk current. If the topmost Landau extended level is not occupied (*i.e.* quantum Hall plateau is observed), the parameters are $\rho^b=\infty$ and all $t_j=0$, and then the nonlocal resistance R(23,14)=0. When the topmost (bulk) Landau extended level is fully occupied, parameters are $\rho^b=0$ and $t_j=1$, then the bulk channel acts in similar to the edge channels and R(23,14)=0. Note that the nonlocal resistance appears when the bulk and edge currents coexists. The nonlocal resistance only appears when the Hall resistance is not quantized and the longitudinal resistance is not zero, that is, the bulk current exists. The brief description of the nonlocal resistance is shown in Fig. 16. For simplicity, one edge current and a bulk current are considered. The chemical potential of the voltage probes is determined by the chemical potential of the incoming currents (electrons). Both currents, emerging from the voltage probe, have an equal chemical potential μ_{c1} that is the chemical potential of the probe. The bulk electrons can be backscattered and the bulk chemical potential changes, but that of the edge current is conserved. The

chemical potential μ_{c2} of the next voltage probe is determined by the chemical potential of incoming edge and bulk currents, and then the voltage difference appears among the voltage probes.

The peak amplitude of the nonlocal resistance depends on the sample geometry (L_j/W_j) and the number of edge channels, but it is not influenced by ρ^b. Particularly, the transport properties are also influenced by the segment, where the *nominal current* would not flow. McEuen *et al.* pointed out that the four-terminal resistance, measured in high-mobility two-dimensional system at quantum Hall conditions, have a nonlocal behavior[6]. The resistivity tensor is not necessary to understand the observed resistance. To test the validity of the model in the mesoscopic wires, the calculated value and the measured amplitude of the nonlocal resistance are compared in the next section.

4.1.3 The amplitude of the nonlocal SdH oscillations

The solid lines in Fig. 17 are the calculated peak amplitudes of the nonlocal resistance for varying separation geometry ΔL/W (L_5/W_5 in the model. see Fig. 15) for spin split Landau level n=1↑ (the up-spin peak of the n=1 level) and for Landau level n=4 which spin degeneracy is considered. The corresponding experimental peak values of nonlocal resistance are also plotted in Fig. 17 for three samples (A, B and C) in the cases where no extra probes exist between the current and voltage probes. The ΔL/W was measured by the SEM micrographs. The conduction width reduction by the presence of the depletion layer at the side wall is neglected in this analysis. When ΔL/W is small, the experimental amplitude is larger than that of the calculated value. It is suggested in section 4.2.7 that the observed resistance is influenced by the extra probes, though they are not in between the voltage and current probes. A role of probes will be discussed in the next section. The experimental results, obtained from three

samples with different width and length, scale with ΔL/W and agree well with those of the calculated values as a whole. The sample C was made from a different wafer. The present model seems to reasonably explain the nonlocal resistance of all the sample. The nonlocal peak values at Landau number n>>4 at low magnetic fields are smaller than the calculated ones. Since the scattering between the edge and bulk channels are significant due to smaller Landau splitting at low magnetic fields, the nonlocal resistance is reduced below the predicted value from the model in which the scattering is neglected.

4.1.4 Role of the probes

Based on the previous model, the chemical potential of the edge currents are mixed up with that of the bulk current at the probes. The nonlocal resistance R(45,76) and R(45,32), where the separation length ΔL is equal to 2 μm, is shown in Fig. 18. The peaks amplitude of the nonlocal resistance R(45,76) are several times as great as that of R(45,32), as shown in Fig. 18(a). As the edge electrons, which is emitted from the current probe 5, apparently circle around via probe 6→7→8→1→2→3, the chemical potential of the edge current is mixed up with that of the bulk current at each probe. Thus the chemical potential of probes successively approaches to the value of the bulk current. In result, the potential difference between the serial probes becomes smaller. The relation R(45,76) >> R(45,32) signifies that the difference of the chemical potential between probe 7–6 is much greater than that of the probe 3–2. The schematic explanation is shown in Fig. 19. The chemical potential of the probes equilibrate with the 'bulk' one shown by the broken line in Fig. 19, the difference ($\mu_1-\mu_2$) is larger than ($\mu_2-\mu_3$). When the magnetic field direction reversed, the direction of the edge current is also reversed, and R(45,32) becomes much larger than that of R(45,76), as shown in Fig. 18(b). A suppression of the nonlocal resistance oscillations in the presence

of the extra probes within the ΔL (Fig.14(b)), is also understood by the mixing (equilibration) at the extra probes.

In Fig. 17, there is some discrepancy between experimental and calculated value, when ΔL/W is small. In this resistance measurement, the extra probes exist in the pathway of the edge currents between voltage probes, as the probe 2 in Fig. 19. The potential difference becomes larger by the existence of the extra probes. In Fig. 19, the difference ($\mu_1-\mu_3$) is larger than ($\mu_1-\mu_2$). The model of the calculation does not include the effect of extra probes, and the observed resistance is influenced by the extra probes, though they are not between the voltage and current probes.

Table 1. The device parameters of the sample A – C at 1.5 K.

sample	carrier density (cm^{-2})	mobility (cm^2/Vs)	wire width (μm)
sample A	$3.2x10^{11}$	$1.4x10^6$	0.48
sample B	$3.1x10^{11}$	$3.4x10^5$	0.57
sample C	$3.0x10^{11}$	$6.8x10^5$	0.67

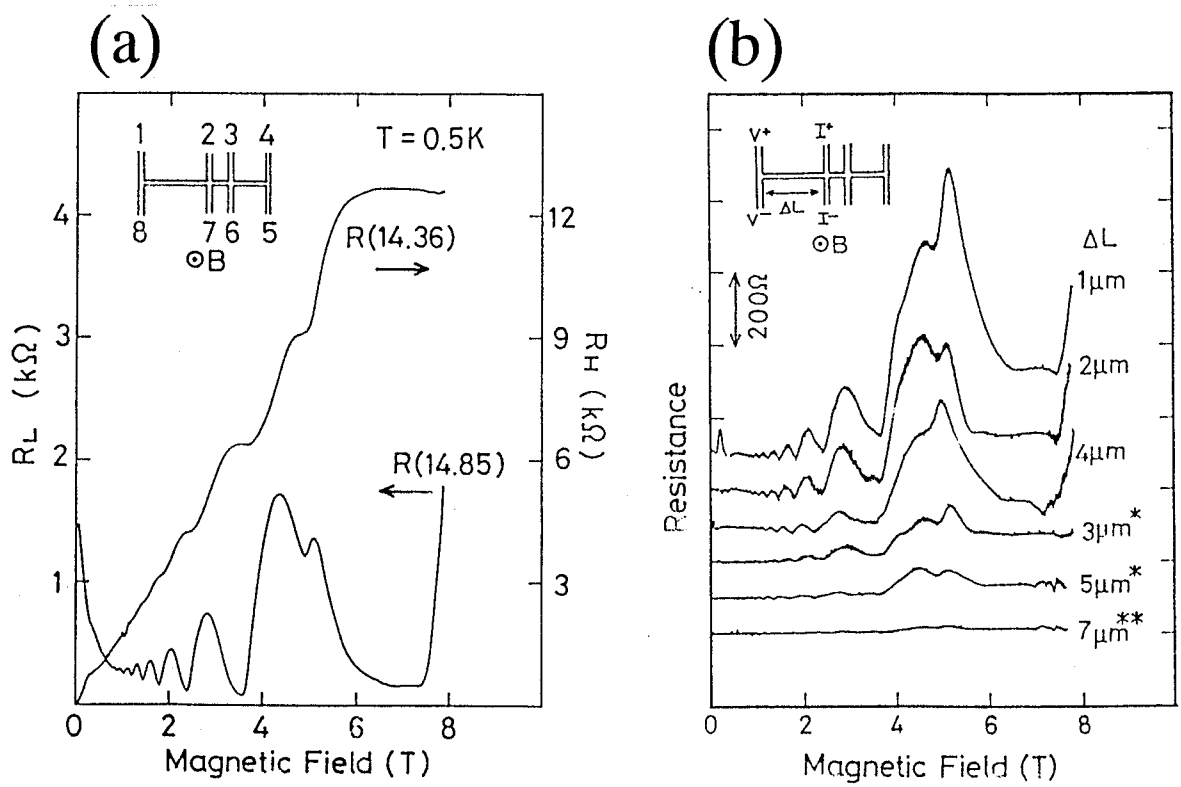

Fig. 14(a). Longitudinal resistance R(14,85) and Hall resistance R(14,36) of sample A at 0.5 K. At the low magnetic fields, a large negative resistance is observed due to the ballistic transport and magnetically reduction of backscattering in narrow wire. The SdH oscillation and quantum Hall plateaus are observed at high magnetic fields.

(b) Nonlocal SdH oscillation of sample A with various ΔL. The marks "*" ("**") denote the existence of one (two) pair of extra probes between ΔL range. The extra probes suppress the nonlocal SdH oscillation. A peak with ΔL=1 μm near zero field is caused by a electron focussing effect.

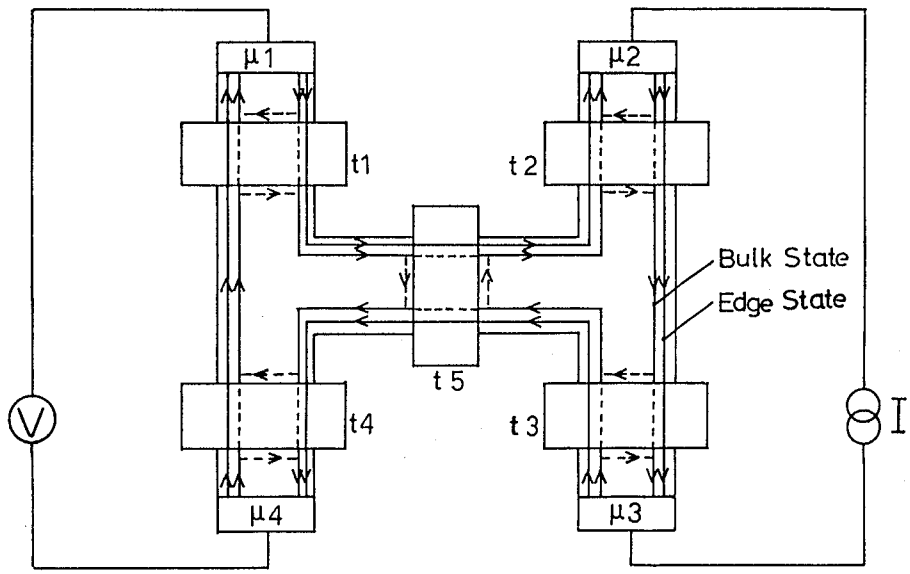

Fig. 15. Schematic illustration of a model used in the calculation of nonlocal resistance. μ_j is the chemical potential of j–*th* probe. The backscattering of the bulk current at each segment is represented by transmission probability t_j.

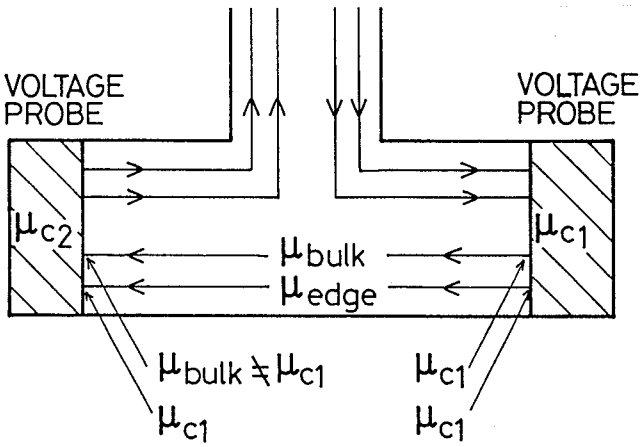

$$\mu_{c2} = \frac{\mu_{bulk}+\mu_{edge}}{2} \fallingdotseq \mu_{c1}$$

Fig. 16. Schematic illustration of a nonlocal resistance.

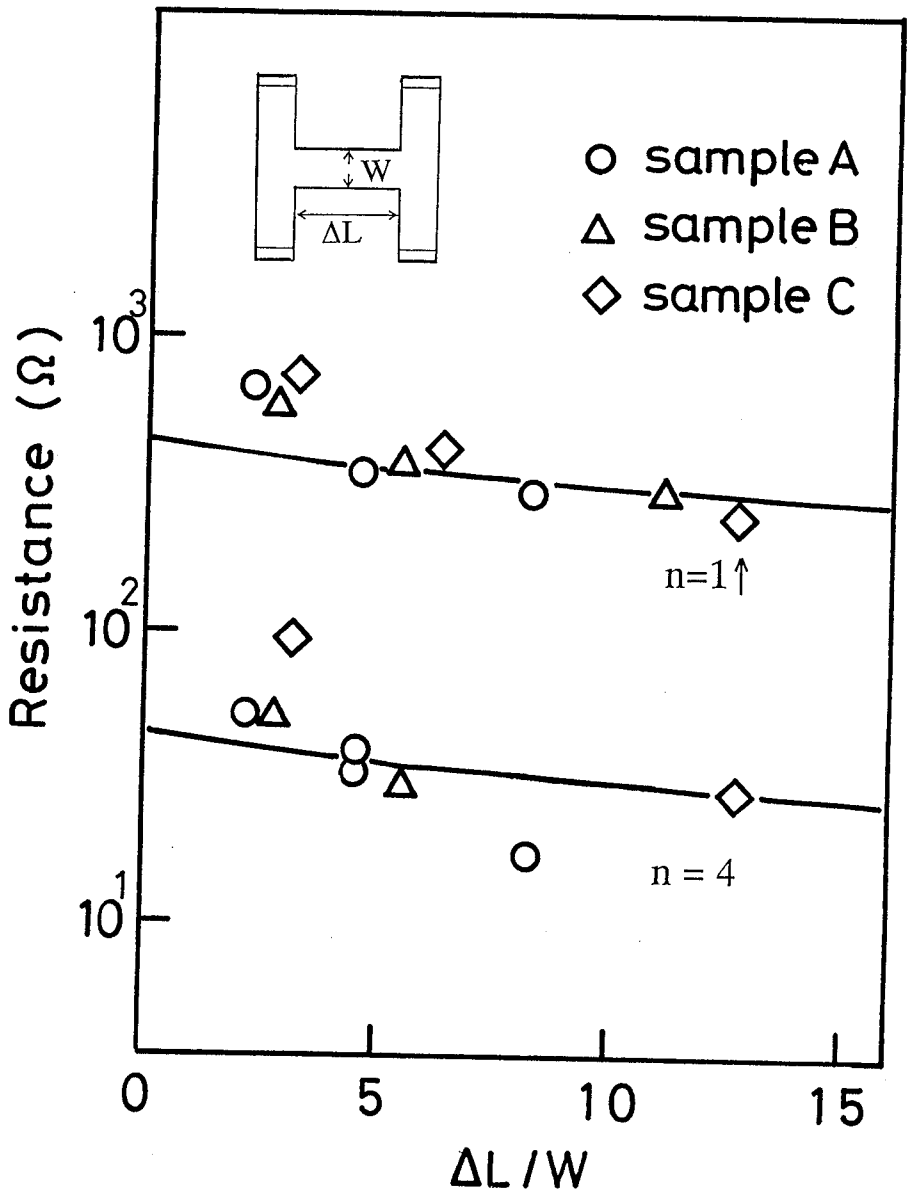

Fig. 17. Calculated (solid lines) and experimental amplitude of nonlocal SdH oscillation with Landau number n=1↑ and n=4 vs. ΔL/W, where ΔL is separation length and W is the wire width shown in the inset. In the calculation of n=4, the spin–degeneracy is taken into account.

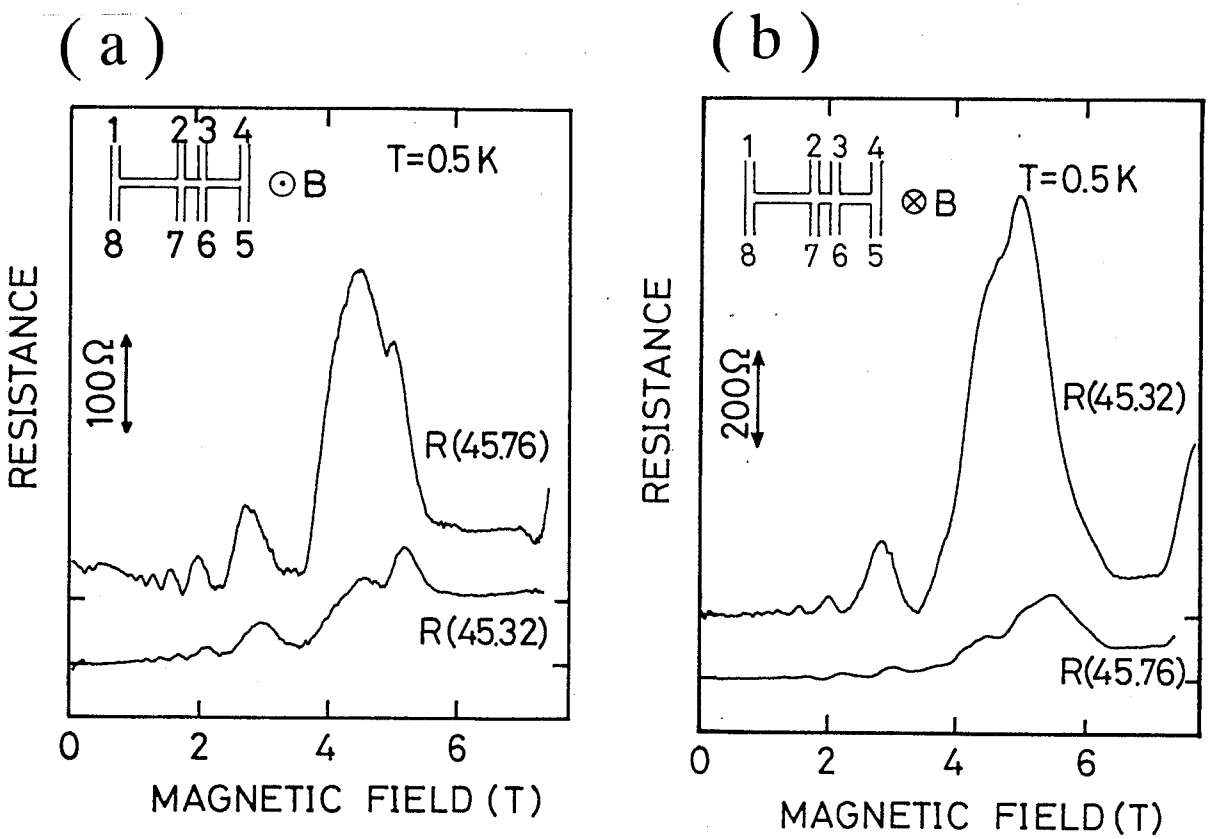

Fig. 18. Nonlocal SdH oscillation of sample A. The current flows from 4 to 5, and voltage is measured at the probes 7–6 and probes 3–2. At the forward magnetic fields, R(45,76)>> R(45,32) (a). At reverse magnetic fields, the relation also inverted (b).

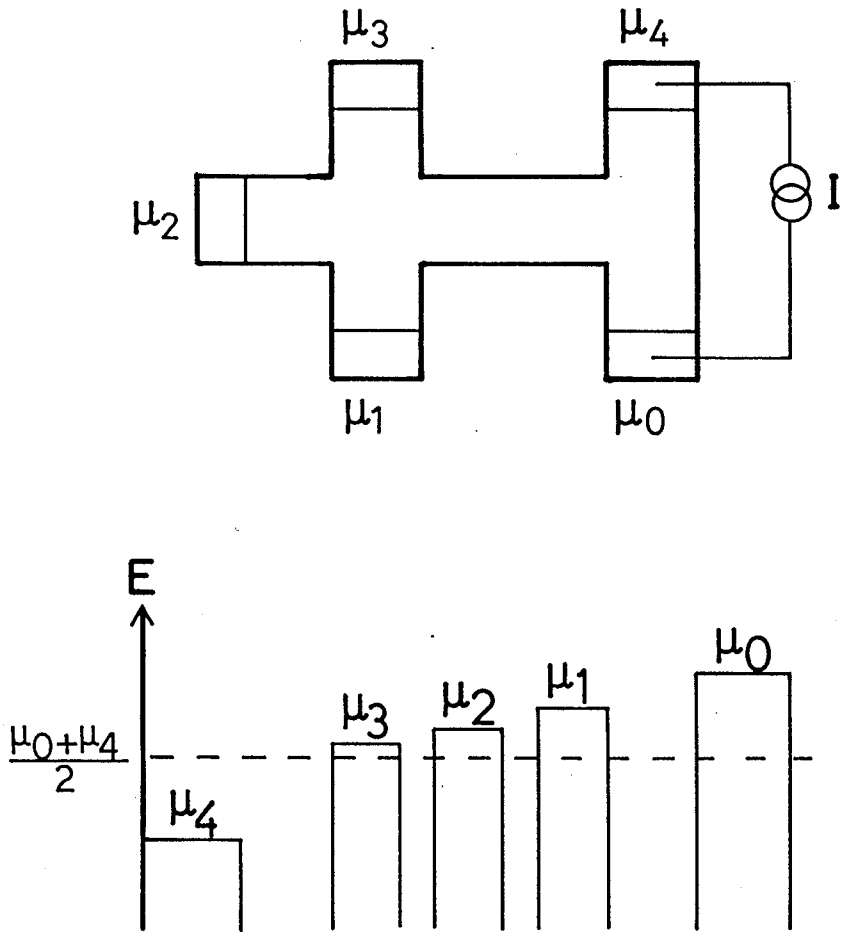

Fig. 19. Schematic illustration of the chemical potential of the probes when the nonlocal SdH oscillation is observed. One edge current and bulk current is considered for simplicity. The chemical potential of the bulk current is assumed to be $(\mu_0-\mu_4)/2=\mu_b$ near the probes 1–3. The chemical potential of the j–*th* probe μ_j, which is separated from the nominal current path, is determined by the chemical potential of incoming edge current $\mu_e=\mu_{j-1}$ and bulk current μ_b as $\mu_j\approx(\mu_{j-1}+\mu_b)/2$. The difference $(\mu_{j-1}-\mu_j)$ is reduced when j increases, that is ,the edge current path through probes.

4.2 Macroscopic system

4.2.1 Quantum Hall effect and nonlocal quantum conduction in macroscopic size samples

In macroscopic size (order of several hundred microns) samples, which were made of the high mobility GaAs/AlGaAs heterostructures, Kane *et al.*[5] reported that the resistivity in high magnetic fields was affected by the sample geometry and measuring current level. They explained that these phenomena were due to the existence of current carrying edge states. In this section, the results of resistance measurements in the order of millimeter size samples are discussed. Particularly, the nonlocal resistance is studied and analyzed with the model proposed by McEuen[6].

The millimeter size Hall bar shaped GaAs/AlGaAs wire, whose width was 20 μm, made by UV lithography and wet chemical etching technic. Schematic view of the sample is shown in Fig.20(a). The resistance measurement was made at 0.5 K with current 0.3 μA. The electron mobility and carrier concentration of the sample is $1.3\text{x}10^6$ cm^2/Vs and $3.4\text{x}10^{11}$ cm^{-2} respectively. The Hall resistance (R_H), longitudinal resistance (R_L) and nonlocal resistance (R_{NL}), where the separation length between current and voltage probes (see Fig. 2. in chapter 1) is 0.5 mm, is shown in Fig. 20(b). The QHE plateaus in the R_H clearly appear, and R_L=0 at the filling factor ν= 2 ~ 8 are also observed. Though the peak amplitude of the SdH oscillation is expected to become larger with increasing magnetic fields (*e.g.* peaks due to low index Landau level), the observed peaks of R_L is much reduced from the value estimated by the conductivity tensor which was calculated by the self consistent Born approximation theory[2]. The nonlocal resistance R_{NL} shows peaks at the magnetic fields that the R_L shows peaks, and both resistance shows minima (zero) at the QHE plateaus regime. Note that the peak values of

R_{NL} are much less (≈1/100) than those of the R_L peaks. At low magnetic fields B < 2 T, the R_{NL} is almost zero. The observed peaks of the R_{NL} and reduction of R_L SdH peaks are understood by the model[6], in which both edge and bulk channels were considered (discussed in section 4.1.2). The existence of both edge and bulk channels, and adiabatic conduction of the edge current should be needed to observe the nonlocal resistance. The appearance of the nonlocal oscillations in R_{NL} at the separation length ΔL=0.5 mm suggests that the equilibration of the chemical potential between edge and bulk currents may be suppressed during the conduction more than 0.5 mm.

The peak amplitudes of the nonlocal resistance at Landau levels n=1↑ and n=4 were calculated by the model. The spin degeneracy was considered at the n=4 Landau level, since the spin splitting was not observed in the R_{NL}. The calculated amplitude and experimental results of R_{NL}, where ΔL=0.5 and 1 mm (*i.e.* ΔL/W = 25 and 50 respectively), are shown in Fig. 21. The calculated value shows good agreement with experimental amplitude of R_{NL} for n=1↑. But the observed amplitude at n=4 is much smaller than the calculated value. The discrepancy may be attributed to the reduction of the nonequilibrium distribution of the chemical potential between edge and bulk currents for long separation length ΔL at low magnetic fields, which is neglected in the model. When the energy difference of the Landau level is small, the spatial separation between edge and bulk channels is also small. Since the scattering among channels occurs and the reduction of the nonequilibrium distribution of the chemical potential becomes significant at low magnetic fields, the nonlocal resistance is reduced.

The current dependence of the same R_L and R_{NL} with Fig. 20 is shown in Fig. 22. At the current up to 5 μA, the quantum Hall plateaus and zero resistance in R_L still appear, and QHE breakdown do not occur. With increasing current, the

longitudinal resistance increases at high magnetic fields, but no change is observed at low magnetic fields B< 1 T. In contrast with R_L behavior, the nonlocal resistance is reduced at high magnetic fields. The magnetic field (≈1 T), where the current dependence in the R_L appears, is in good agreement with that, where the R_{NL} oscillation appears. The SdH oscillations of R_L, measured with low current, are much reduced from the value expected from the conductivity σ_{xx} and σ_{xy} at the high magnetic fields. The reduction is explained as the edge currents connect between the probes without a dissipation, that is, the effect of short circuit due to the edge currents reduces the R_L.

The current dependence is understood as follows. The relaxation rate of the nonequilibrium chemical potential distribution among bulk and edge currents increases with the extent of the difference of the chemical potential among currents[11]. With increasing current, the chemical potential difference between bulk and edge currents increases in the sample, and the significant reduction of the nonequilibrium distribution occurs among currents. So, the nonlocal features, the appearance of R_{NL} and the reduction of SdH oscillation in R_L due to the existence of the edge current, are suppressed with increasing current.

The carrier concentration dependence of R_L and R_{NL} is shown in Fig. 23. The carrier was increased by using the persistent photo-conductivity by LED illumination. With increasing carrier concentrations, the peaks of R_L become larger and the R_{NL} is suppressed, though the mobility of the sample is enhanced. These phenomena suggest that when the sample is illuminated, the depletion region at the sample edge contracts, the spatial profile of the confinement potential of 2DES changes the edge and bulk channels to be close (see Fig. 24). Since the interaction (scattering) between bulk and edge channels becomes remarkable, the nonlocal features due to the edge current is extinguished with increasing carrier concentrations. The details will be discussed in section 4.2.8.

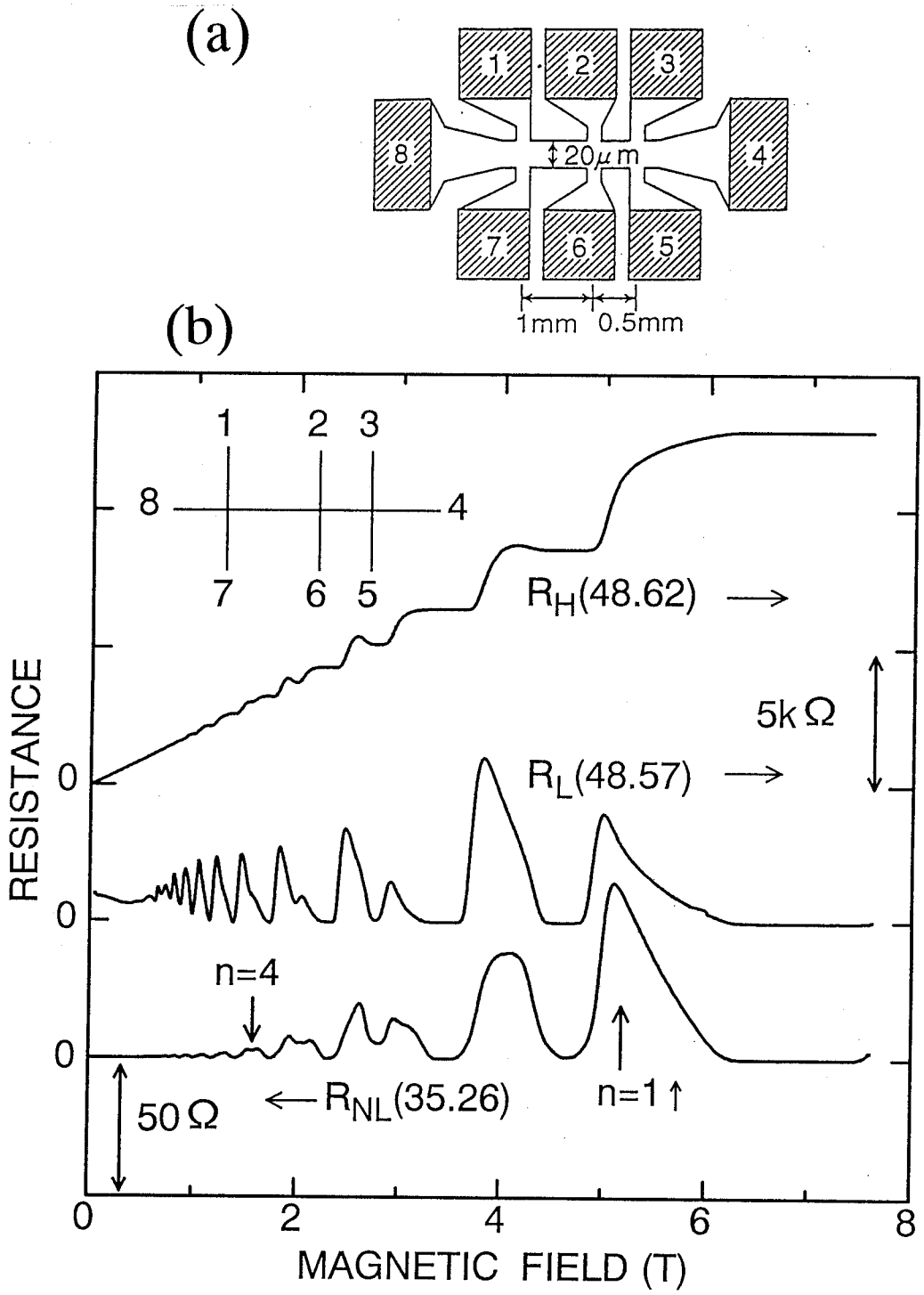

Fig. 20. (a) Schematic view of the sample. (b) Hall resistance R_H, longitudinal resistance R_L, and nonlocal resistance R_{NL} at 0.5 K with current 0.3 μA.

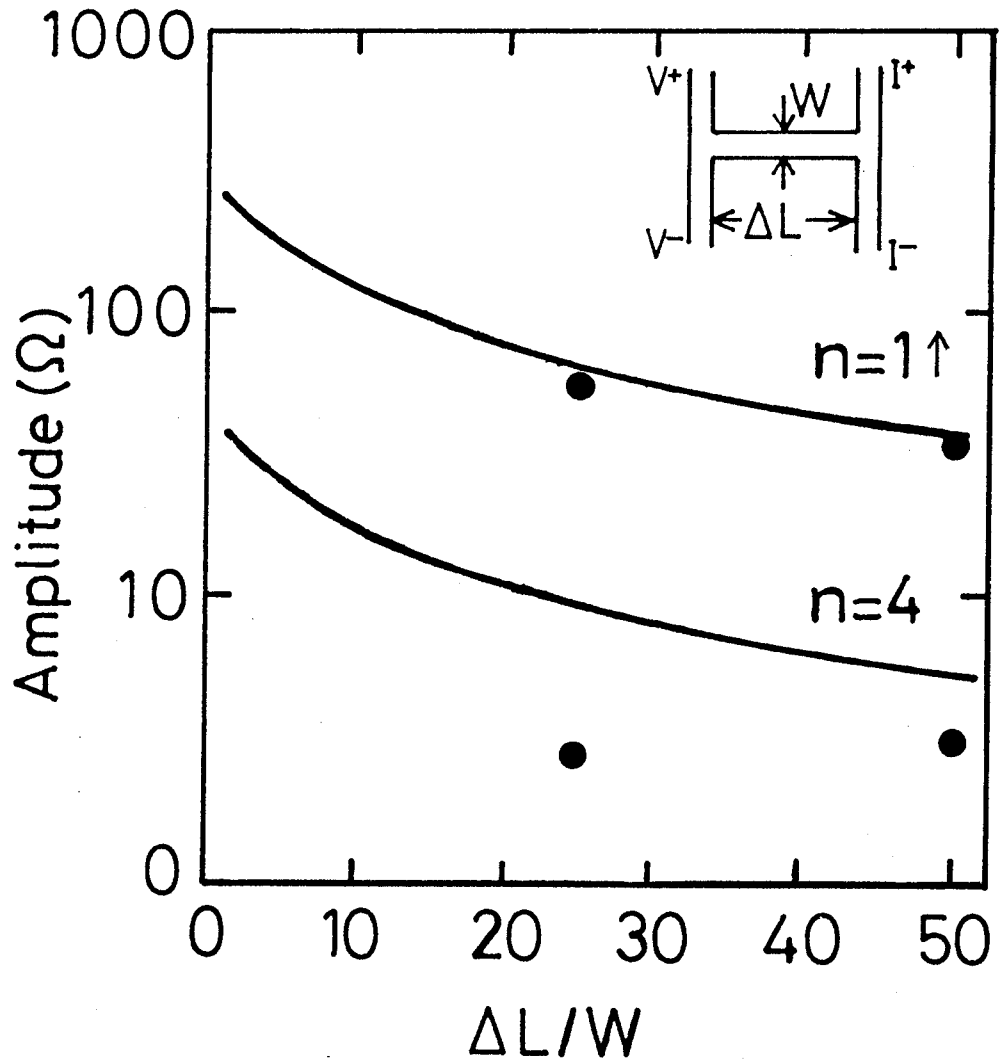

Fig. 21. Calculated (solid curves) and experimental (closed circles) amplitude of nonlocal resistance with Landau number n=1↑ and 4 vs. separation length scaled by the wire width ΔL/W as shown in the inset.

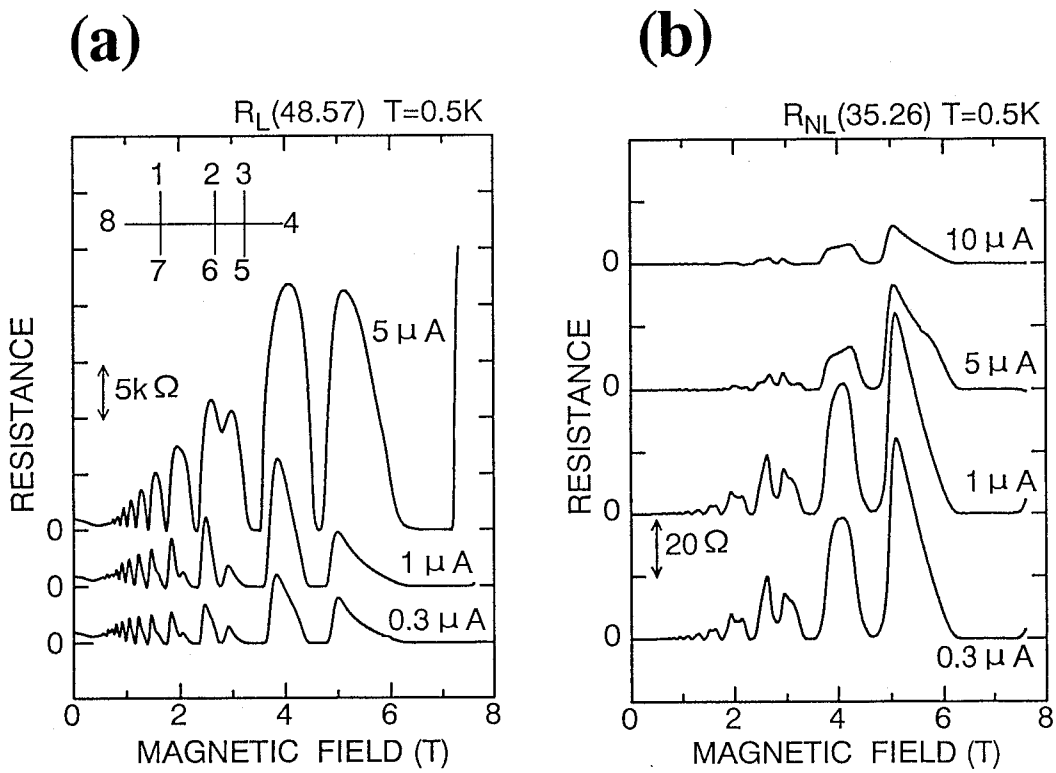

Fig. 22. Current dependence of (a) longitudinal resistance R_L and (b) nonlocal resistance R_{NL}. With increasing current, amplitude of SdH in R_L became large, in contrast with R_{NL} was reduced.

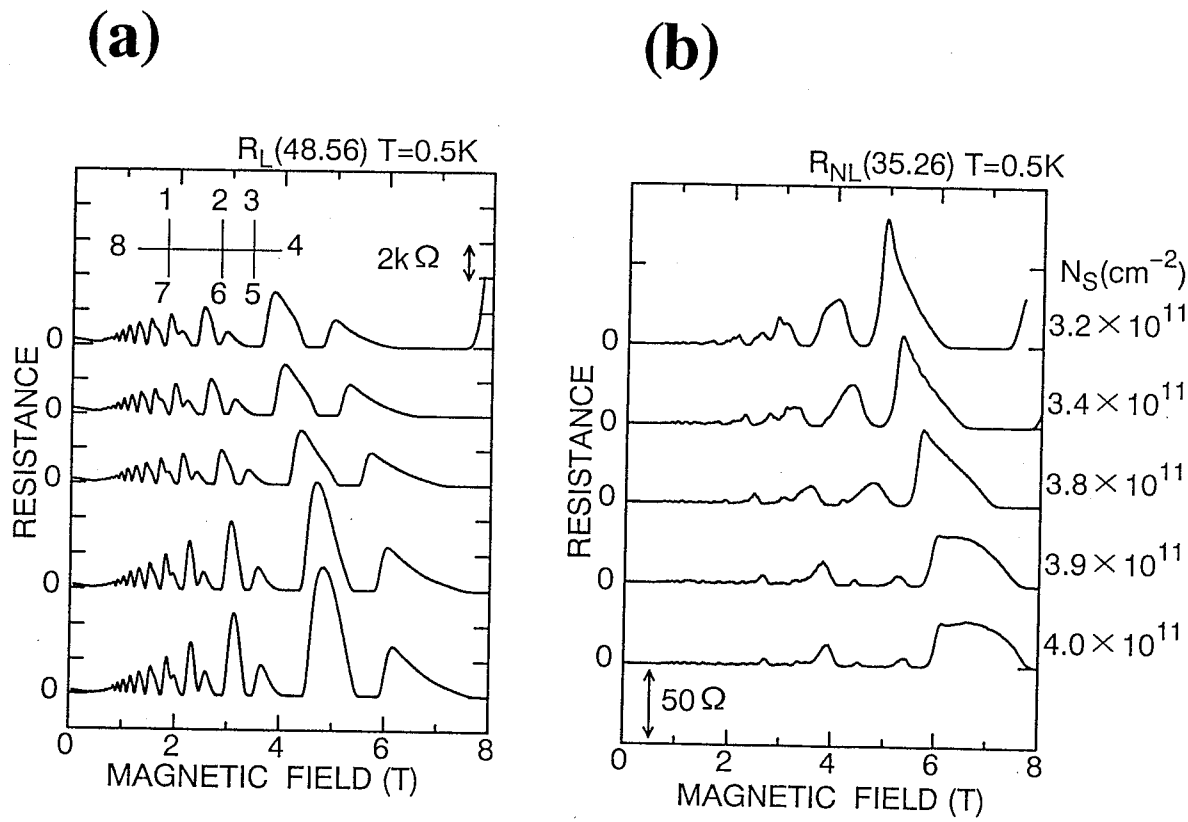

Fig. 23. Carrier concentration dependence of (a) longitudinal resistance R_L and (b) nonlocal resistance R_{NL}. The nonlocal features suppressed with increasing carrier concentration.

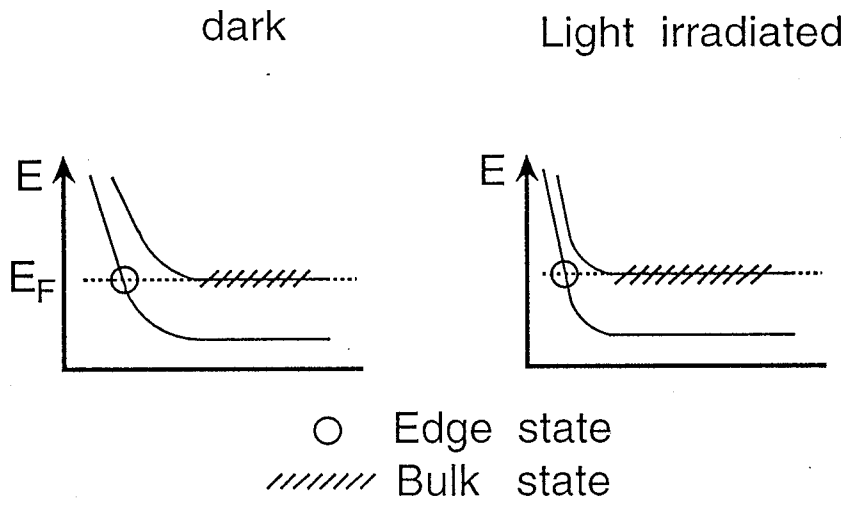

Fig. 24. Schematic illustration of the separation between edge and bulk states. When the sample was illuminated, the profile of the confinement potential changed and both edge and bulk state close together.

4.2.2 An influence of the non-ideal probe on the transport

The resistances using the probe (1) of the same sample shown in Fig. 20 exhibited anomalous behavior at high magnetic fields. The contact resistances of all the probes were lower than 50 Ω at low magnetic fields. But at magnetic fields more than 3 T, only the resistance of the probe (1) became very high (≈100 kΩ). In Fig. 25, the resistance measured at 1.7 K by using the probe (1) is shown. The three terminal resistance R(18,12) represents mainly contact resistance at the QHE plateau regime at high magnetic fields. It is found that the R_{NL} shows negative value even at relatively low magnetic fields and R_L shows negative value at high magnetic region.

In the conduction model using the analysis of the nonlocal resistance[6], the probes are assumed to be ideal, whose contact resistance is zero. To understand the observed negative resistance however, non-ideal properties of the probes should be considered by taking into account transmission probabilities of the electrons in each channel to the probe. The schematic description for the negative resistance is shown in Fig. 26. For simplicity, two edge channels are considered. The chemical potential of the edge current emitted from the current probe (2) are defined as μ_1 (outer channel) and μ_2 (inner channel). The electrons in the channels, flowing along the sample edge without equilibration, go into the voltage probe (3) with the transmission probabilities T_1 and T_2. The chemical potential of the probe (3) = μ_{c3} is given by an average of the chemical potential of incoming currents with the weight T_i. If the next voltage probe (4) is ideal, the voltage difference between probes (3) and (4) becomes $(T_1-T_2)(\mu_1-\mu_2)/2(T_1+T_2)$ as shown in Fig. 26. The voltage difference becomes negative, when $(T_1-T_2)(\mu_1-\mu_2)< 0$. Usually, the transmission probability of the channel of the lower index Landau level is larger than that of the higher index Landau level, *i.e.* $T_1 \geq T_2$ and $\mu_1 \geq \mu_2$.

So, the resistance should be positive or zero. But, using the probe (2), whose contact resistance is very high (wrong), as a current probe, there is a possibility that the reversal relation of $\mu_2 \geq \mu_1$ occurs due to possible anomalous transmission from the probe (2) to each channels. When $T_1 > T_2$ the negative resistance appears. Note that the probe (2) in Fig. 26 is non-ideal instead of the probe (1) in Fig. 25.

Above model treats only edge currents, but it can be extended to the regime, where the bulk current coexists. This situation is represented by writing a bulk current for the inner edge current. The negative resistance clearly appears at the magnetic fields, where the bulk current exists as shown in Fig. 25. At the QHE plateau regime, the nonlocal resistance is almost zero. These phenomena are understood as follows. The equilibration of the chemical potential among edge currents is much significant compared to that between edge and bulk currents, since the spatial separation among edge channels is very small[16] as shown in Fig. 27. At the QHE plateau regime, the chemical potential difference produced at the non-ideal probe $\mu_2 \geq \mu_1$ is nearly eliminated before going into the next probe. So. equilibration of the chemical potential ($\mu_2 \approx \mu_1$) reduces the negative resistance.

The current dependence of the three terminal resistance (contact resistance of the probe (1)) and R_{NL}, is shown in Fig. 28. With increasing current, the contact resistance is reduced and extent of the negative R_{NL} becomes smaller. At the current 5 μA, the R_{NL} shows positive value, and is suppressed with further increasing current. It is suggested that the extent of nonequilibrium chemical potential distribution among channels is reduced, and the total transmission probability to edge channels from the probe (1) in Figs.25 or 28 increases ($T_i \approx 1$ for all i) with increasing current.

The negative R_{NL} becomes positive when the magnetic field direction is

reversed as shown in Fig. 29(a) B⊗. At the reverse magnetic fields, the direction of the edge current is also reversed. The positive R_{NL} is observed, because the anomalous distribution of the chemical potential caused by the probe (1) is much reduced at the next probe after longer journey.

When the current and voltage probes are exchanged as shown in Fig. 29(b), the negative resistance appears at the opposite direction of magnetic fields. The profile of the resistance is noisy at the high magnetic fields, because of the high contact resistance of the voltage probe (1). In this case, the current probe (2) is ordinary, thus $\mu_1 \geq \mu_2$, but the transmission probability of the voltage probe (1) is a non-ideal one ($T_0 << T_1$). In the reversed magnetic field (Fig29(b), B⊗), the chemical potential difference $\mu_1 \geq \mu_2$ is detected by the extraordinary voltage probe (1) and the R_{NL} becomes negative. It is found that the reciprocity relations of the resistance[17] are valid even in the sample with a non-ideal probe, because the exchange of the current and voltage probes, and reversing of the magnetic field direction are equivalent. The Landauer-Büttiker formalism is available to explain the transport properties using non-ideal probes.

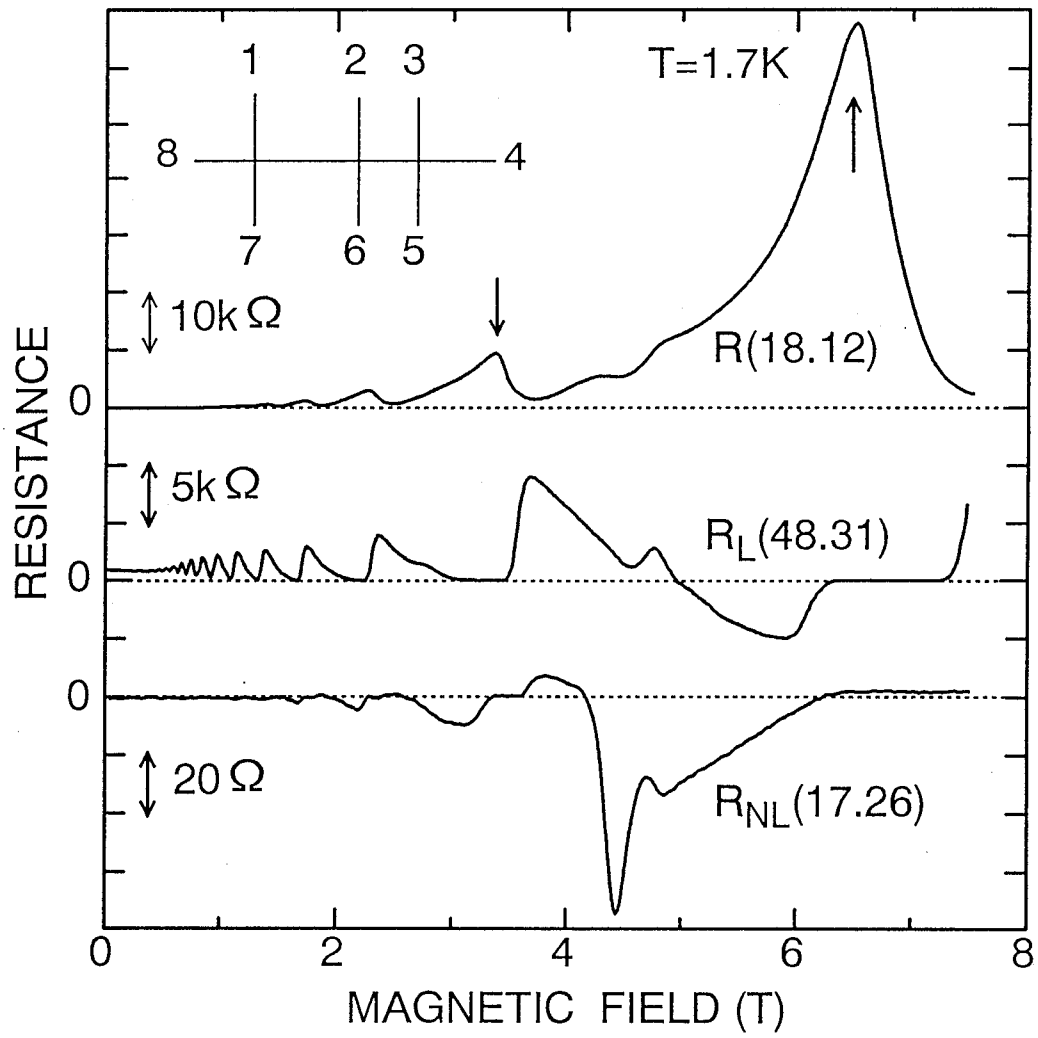

Fig. 25. (a) Three terminal resistance, (b) longitudinal resistance, and (c) nonlocal resistance using the non-ideal probe (1). The peak contact resistance estimated from (a) was ≈100 kΩ , and then R_L and R_{NL} showed negative value.

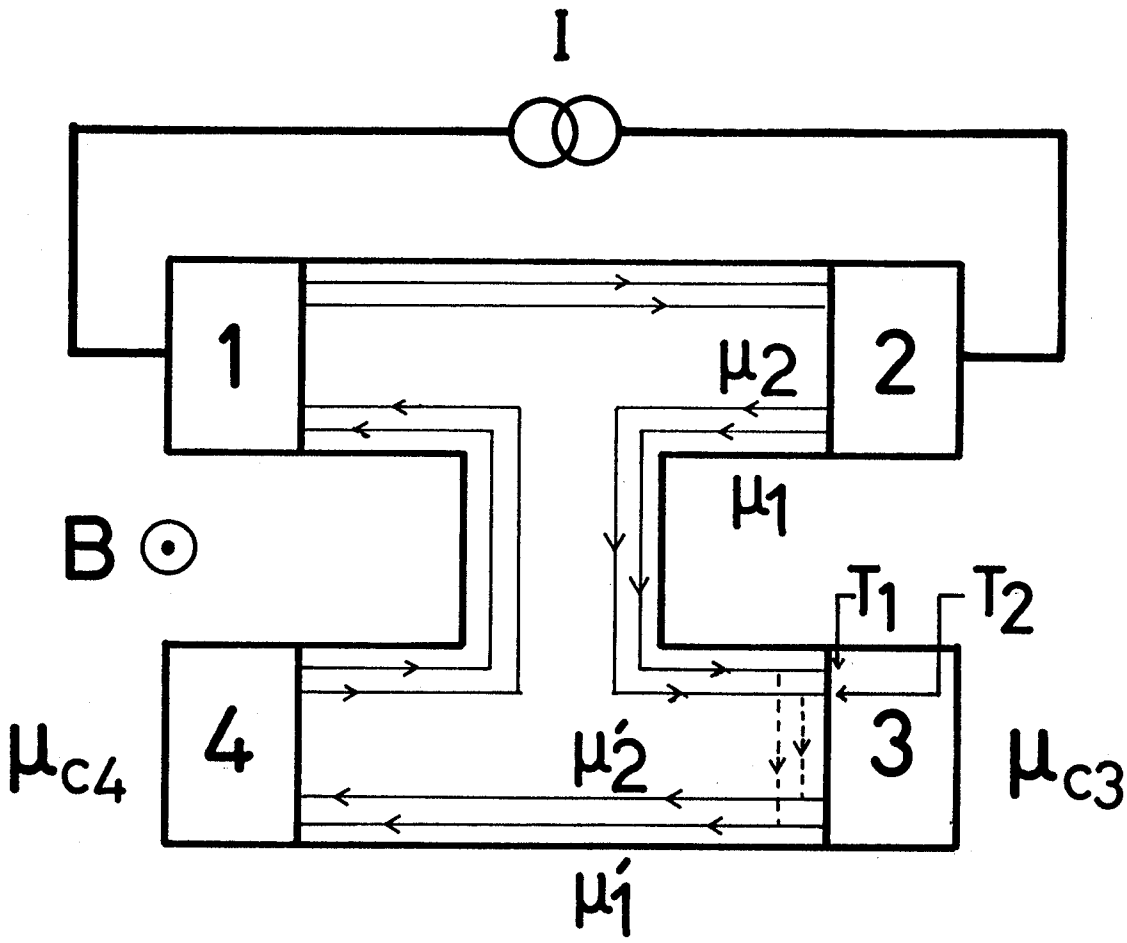

$$\mu_{c3} = \frac{T_1\mu_1 + T_2\mu_2}{T_1 + T_2}$$

$$\mu_{c4} = \frac{\mu_1' + \mu_2'}{2} = \frac{\mu_1 + \mu_2}{2}$$

$$\mu_{c3} - \mu_{c4} = \frac{(T_1 - T_2)}{2(T_1+T_2)}(\mu_1 - \mu_2)$$

Fig. 26. Schematic illustration of the negative resistance. For simplicity, only two edge channels are considered.

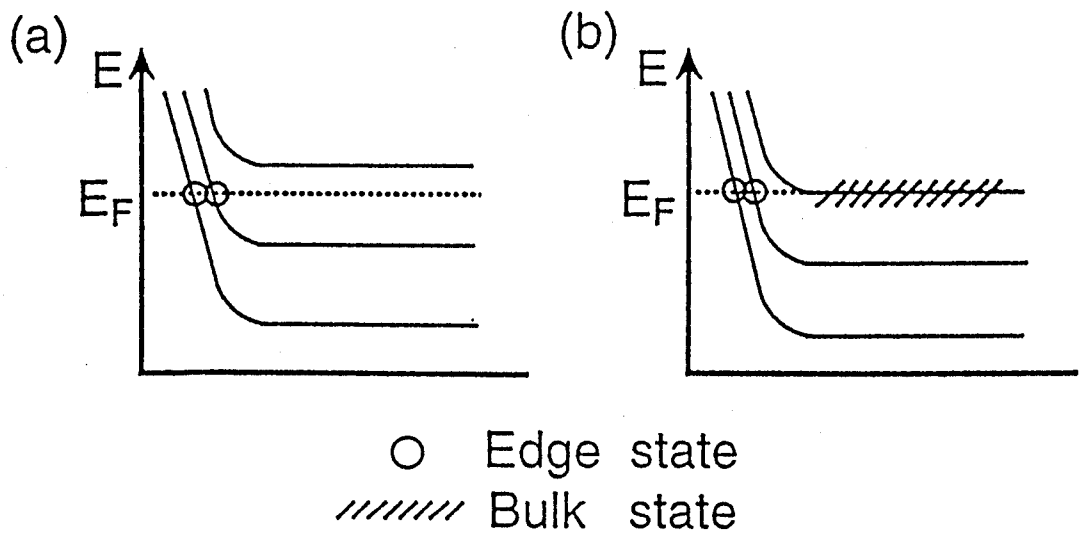

Fig. 27. The spatial separation between edge and bulk channels (b) is larger than that of among edge channels (a).

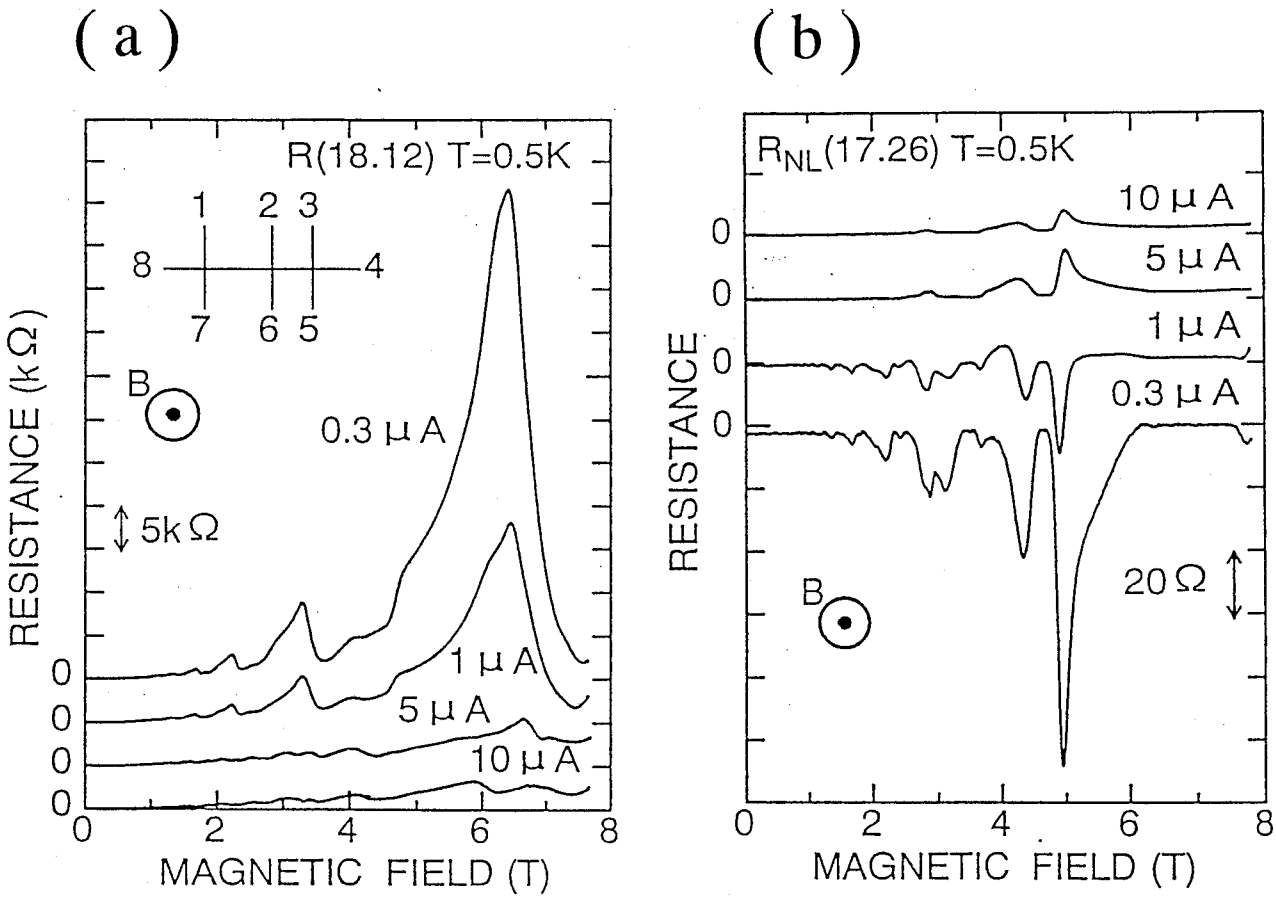

Fig. 28. Current dependence of (a) three terminal resistance, which shows the contact resistance of the probe (1), and (b) nonlocal resistance R_{NL}. With increasing current, contact resistance was drastically reduced, and the negative R_{NL} became to be positive.

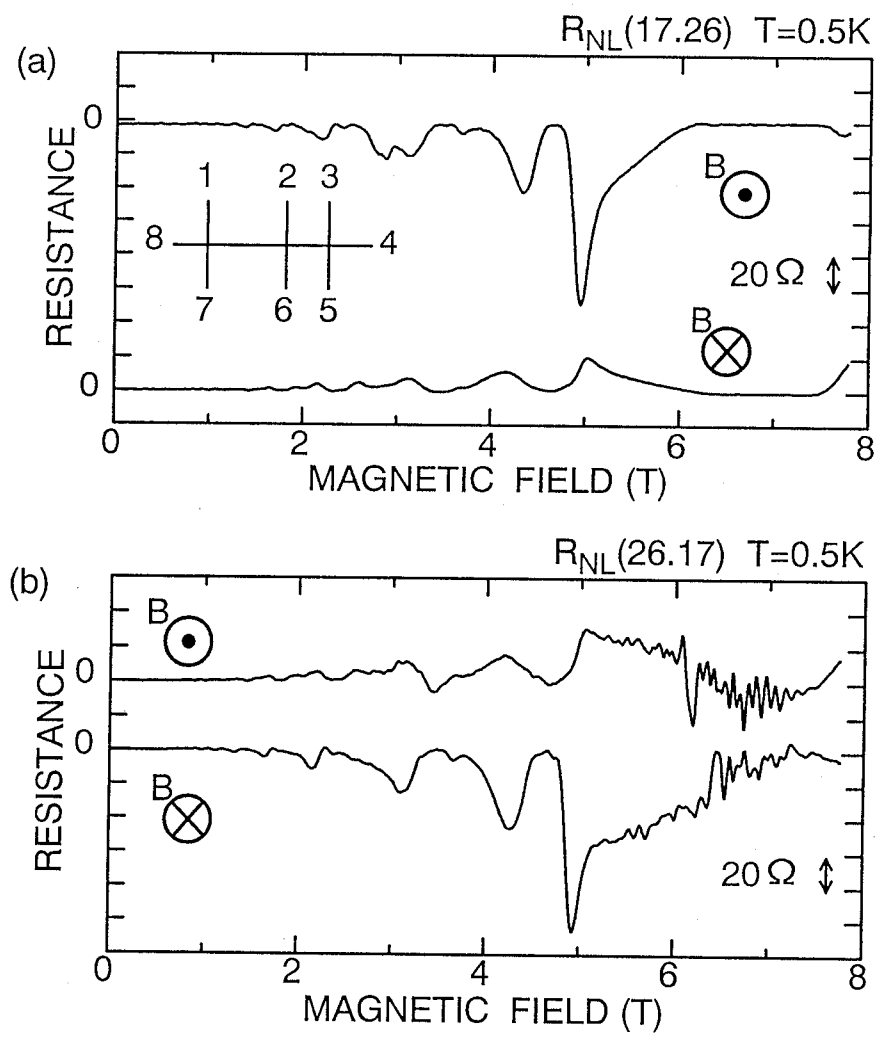

Fig. 29. The nonlocal resistance for forward and reverse magnetic fields, with the exchanged current and voltage probes.

4.2.3 Artificially fabricated non-ideal probe

In section 4.2.2, the observed negative resistance, caused by the probe whose contact resistance was happened to be very high, was explained by taking account of the selective transmission to the edge and bulk channels from the probe. In this section, the influence of the high contact resistance probe on the quantum conduction was investigated using artificially fabricated *'non-ideal'* probes[18].

Samples were made from a wafer with modulation-doped GaAs/$Al_xGa_{1-x}As$ (x=0.27) heterostructure with carrier density of $3.2x10^{11}$ cm^{-2} and mobility of $6.6x10^5$ cm^2/Vs at 1.7 K. The probes were made by alloying AuGe/Ni/Au layers. The surface of all the contact region (Fig. 30(a)) was damaged by slight etching (50 nm) before evaporating the contact metals, and alloyed at 430 °C (Fig. 30(c)). The schematic view of the sample is shown in Fig. 31. The contact resistances become high, because the carrier density of 2DES near the electrodes decreases due to the effect of the shallow etching, as shown by a dotted line in Fig. 31(b).

The longitudinal resistance R(32,41) and current dependent nonlocal resistance R(12,43) are shown in Fig. 32(a). The average contact resistance of four probes is 40 kΩ, and the resistance of the probe(3) becomes exceedingly higher with increasing magnetic fields (100 kΩ at B≈6 T). The nonlocal resistance R(12,43) measured with low current (I< 1 μA) shows negative value at high magnetic fields, while the longitudinal resistance R(32,41) shows positive value. The nonlocal resistance may be much more influenced by the properties of the probes than the longitudinal resistance is, since a large voltage drop in the nominal current path due to the bulk current does not affect the nonlocal resistance[18]. With increasing current, the negative resistance becomes smaller, and the resistance turns into positive value at I=5 μA. For comparison, the resistance measured in another

sample, whose probes were fabricated without damaged etching process, are also shown in Fig. 32(b). The contact resistance of all probes is as low as 200 Ω or less. Both nonlocal resistance and longitudinal resistance are positive value.

The negative resistance will appear in the situation that; the current probe produces the nonequilibrium distribution among the chemical potential of the edge and/or bulk currents. The chemical potential of edge currents is conserved from probe to probe, the transmission probabilities of the edge currents to the voltage probe are not even[6] (see section 4.2.2, Fig. 26). The observed negative resistance of R(12,43) in Fig. 32(a) at the quantum Hall plateau regime can be understood as the current probe (2) produces the nonequilibrium edge currents, and the next voltage probe (3) has anomalous transmission for the incoming edge currents. With increasing currents, the extent of the nonequilibrium of the edge currents decreases and the anomalous negative resistance disappears.

It is demonstrated that the negative nonlocal resistance appears due to the *non-ideal probe*. The high contact resistance probe is apt to have an anomalous transmission probability to edge and bulk channels. The fabrication process of the probes is very much important to make a *'good probe'* for electron transport measurement, such as the precision measurements of QHE.

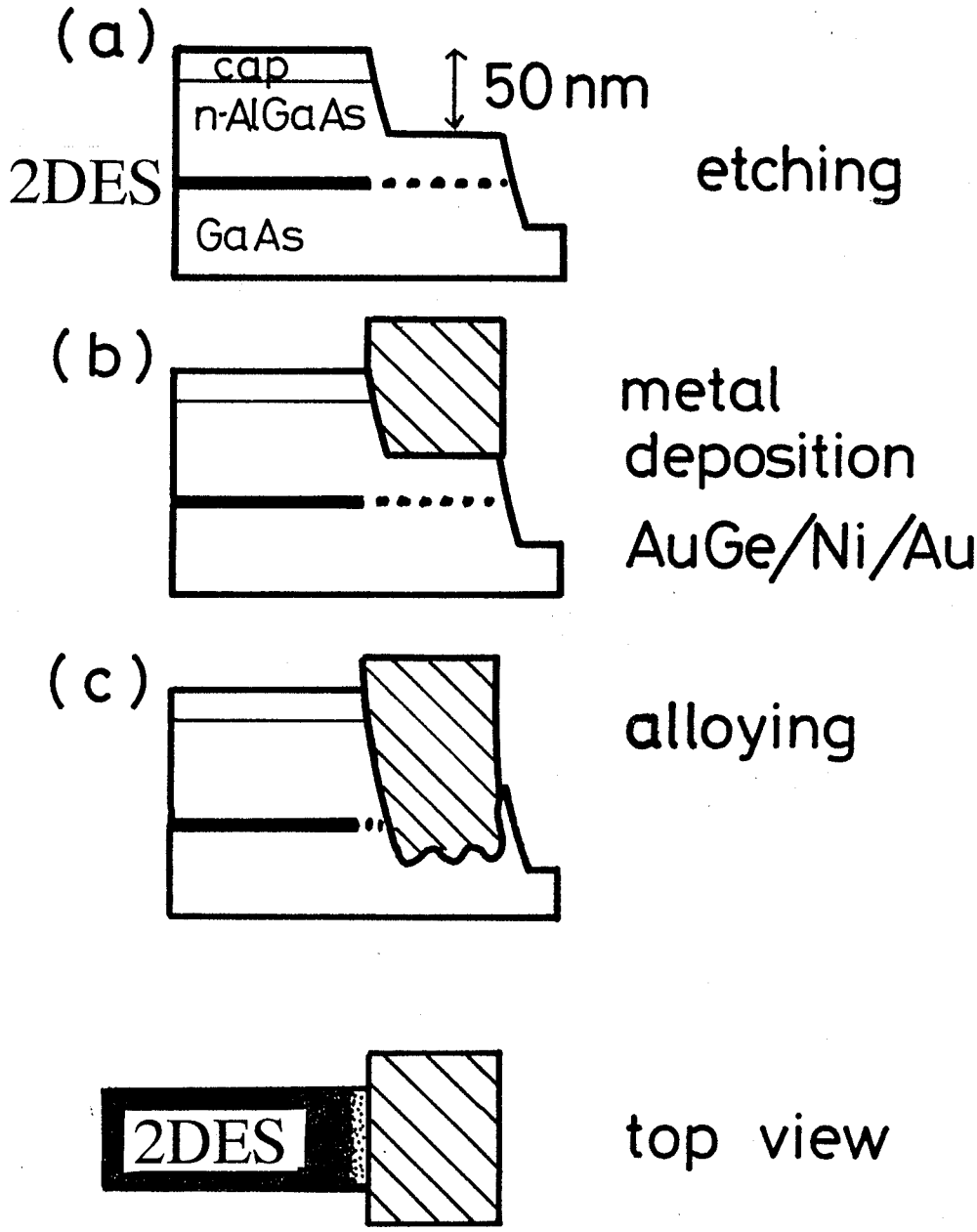

Fig. 30. Schematic illustration of the fabrication process of the non-ideal probes. The hatched region corresponds to contact probes. (a) The surface of all the contact region was etched 50 nm. (b) The metals were evaporated successively. The thickness of the materials were 100 nm of AuGe(Ge 12 at.%), 30 nm of Ni, and 50 nm of Au respectively. (c) Alloying. The carrier density of 2DES near the probes, shown by a dotted area, was decreased by the effect of the shallow etching.

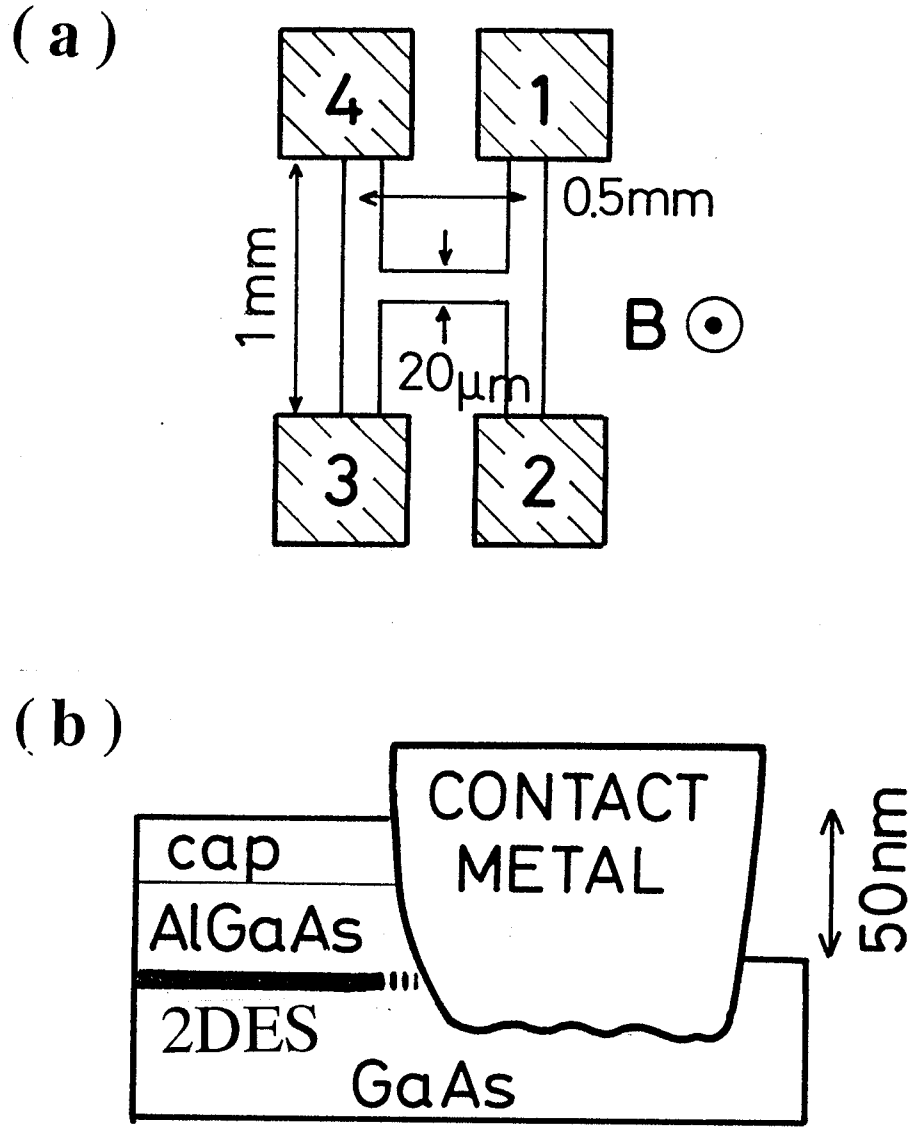

Fig. 31. (a) The view of the sample. The hatched region corresponds to contact probes. The electrons in the edge channels flow probes 1→2→3→4→1. (b) Cross sectional view of the contact probe region. The contact resistance became high, because the carrier density of 2DES near the electrodes, shown by a dotted line, was decreased by the effect of the shallow etching. The average contact resistance of four probes was 40 kΩ, and the resistance of the probe(3) became higher with increasing magnetic fields (100 kΩ at B≈6 T).

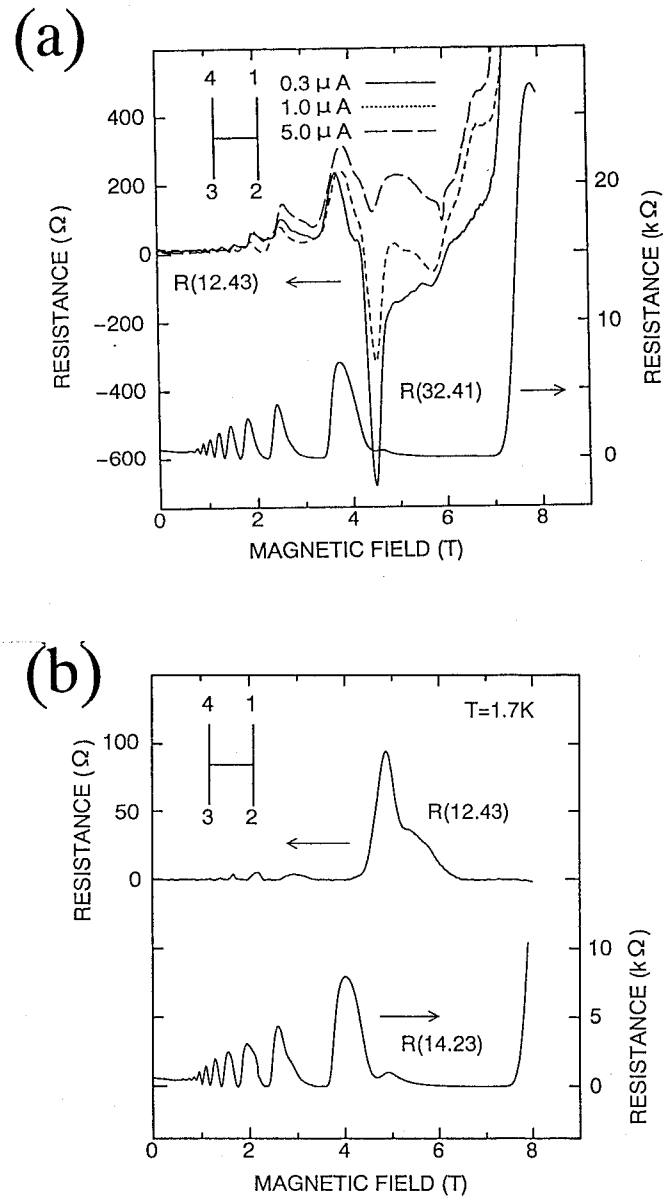

Fig. 32. (a) Current dependence of nonlocal resistance R(12,43) and longitudinal resistance R(32,41) at 1.7 K. The nonlocal resistance shows negative value at B>4 T, while the longitudinal resistance has ordinary profile. With increasing currents, the negative resistance became smaller, and the resistance turned into positive value at I=5 μA. (b) Nonlocal resistance R(12,43) and longitudinal resistance R(14,23) for another sample of the same shape, but its probes have been made without etching process. The contact resistance of the probes are about 200 Ω. Both nonlocal resistance and longitudinal resistance were positive value.

4.2.4 Gate controlled probe (1)

Wedge shaped gate controlled Corbino-like probe

In the previous sections 4.2.2 and 4.2.3, the observed negative resistance, measured with four-terminal geometry, was explained by the properties of the non-ideal probe, which showed selective transmission to the channels belonging to the higher index Landau levels. When such a probe is used as a current probe, it makes the anomalous (inverse) distribution of the chemical potential of the current to each channel. By using the non-ideal probe as a voltage probe, the chemical potential of the probe should be different from the average value of the incoming channels (see section 4.2.2, Fig. 26). In this section, the resistance measurement using the probe, whose transmission probability of the channels are controlled by a *'wedge shaped gate'*, is discussed.

In Fig. 33(a), the illustration of the sample is shown. The probe (1) is isolated 60 μm from the sample edge, and surrounded by the 2DES like a Corbino geometry. At the probe (1), the transmission probability to the inner-edge (belonging to higher index Landau level) channel is larger than that of the outer-edge channels is (see Fig. 33(b)), since the outer-edge current is much spatially isolated from the probe (1) than that of the inner-edge current. The amount of the transmission is very small at the QH plateau regime[18,19]. The wedge shaped gate was added on the 2DES region closely to the probe (1). The separation between the gate and probe was 0.5 μm. The carriers are depleted under the gate with biasing negative voltage. With increasing negative gate voltage, the edge currents can enter the probe (1), as shown in Fig. 33(c), since the depletion region extends under the gate. Note that the bulk channel, extending in the sample, is connected to the probe (1). The probe (1) acts as an ordinary probe for the bulk channel, but the edge channels are isolated from the probe. The extent of isolation can be

controlled by the wedge gate. The contact resistance of all probes was less than 100 Ω at B=0, thus, they were *'ordinary'* probes. The measurements was made after brief illumination by LED to improve the uniformity of 2DES, at temperature 1.7 K, with current 0.1 μA. The carrier concentration and mobility is N_s= 2.8×10^{11} cm^{-2}, μ=5.0×10^5 cm^2/Vs respectively.

The gate voltage V_g dependence of two-terminal resistance R(16,16) at B=5.7 T (filling factor ν=2, two edge channel exist) is shown in Fig. 34. The resistance shows a plateau of R(16,16)=12.9 kΩ (=$h/2e^2$) at V_g< −2.8 V. With decreasing negative gate voltage, the resistance increases. The two-terminal resistance at a QH plateau is the sum of the contact resistance and Hall resistance[13,17]. The observed plateau at V_g< −2.8 V is understood as the transmission probability of the edge current to the probe (1) becomes unity, since the contact resistance of the probes (≈100 Ω) is low enough. A part of the edge current, particularly the outer-edge current, is not able to enter the probe (1) at V_g>−2.8 V. The gate voltage of this wedge shaped gate affects the width of remained 2DES region between the gate and probe (1). The spatial separation between two edge channels is so small that the plateau at R=25.8 kΩ (=h/e^2), which shows only one edge current entering the probe, is not clearly resolved.

The resistance of nonlocal R_{NL}(51.42) and longitudinal R_L(36.21) geometries with gate voltage +0.2 V and −3.5 V are shown in Fig. 35. The positive gate voltage +0.2 V is needed to equalize the carrier concentrations of 2DES and under the gate, and to minimize the transmission of the edge current to the probe. At V_g=+0.2 V, both R_{NL} and R_L become negative at the same magnetic fields, where the transmission probability to the probe is very low. Note that if the other probe, (4) for R_{NL} and (6) for R_L, would be perfectly ideal probe, the negative resistance never be observed (see section 4.3.2). The observed negative resistance is one of

the evidence that the ordinary probes even have the non-equal transmission probability of incoming channels, which is $T_i > T_j$ (i<j, i and j are belonging Landau index of the channel). At V_g=-3.5 V, all channels are connected to the probe (1), the ordinary profile of both R_{NL} and R_L are observed. It is demonstrated that the anomalous selective transmission of channels can be realized with gate controlled Corbino-like probe, and negative resistance appears due to the non-ideal probe.

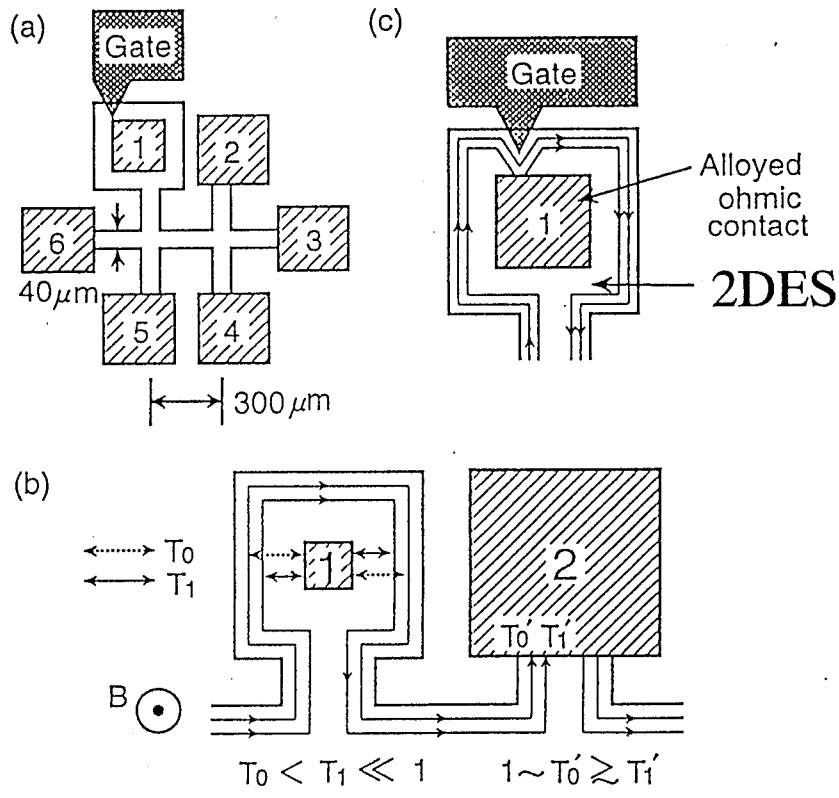

Fig. 33. (a) Schematic illustration of the sample with the probe controlled by the wedge shaped gate. The hatched region corresponds to alloyed contact probes. The probe (1) is isolated 60 μm from the sample edge. (b) The transmission of the edge current is very small when the edge current can go through under the gate. The extent of transmission of inner edge current is larger than that of the outer-edge current. (c) Expanded view of the probe (1) and the gate. The edge current transmission can be controlled by the gate.

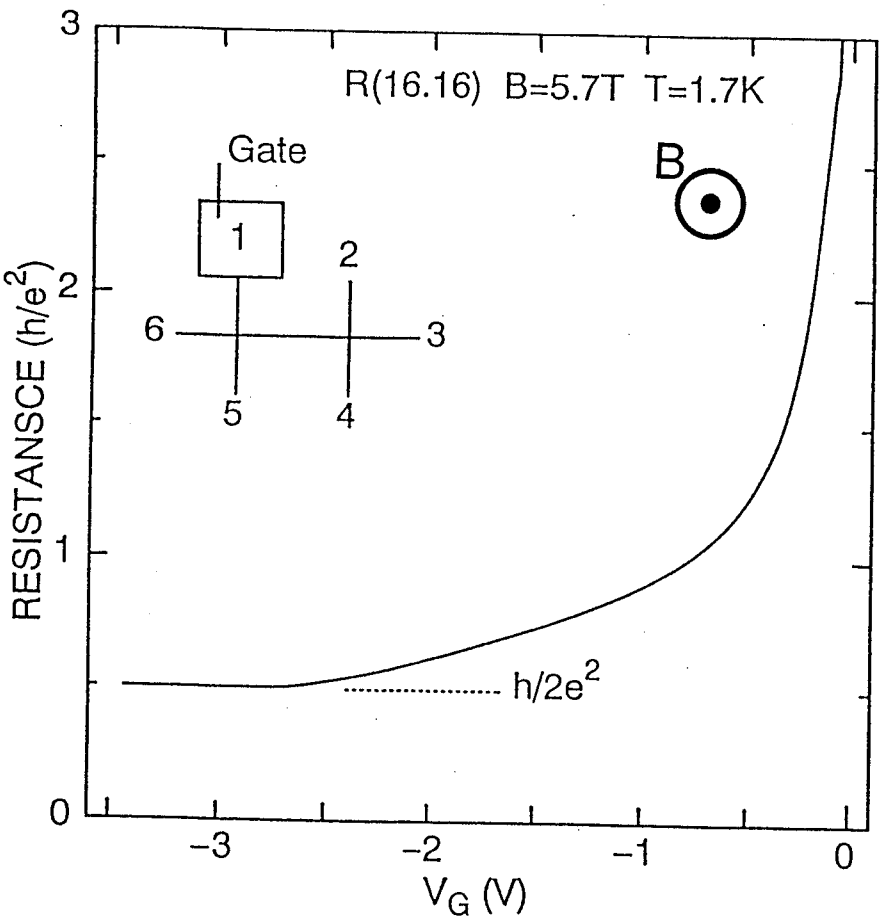

Fig. 34. The gate voltage V_g vs. two-terminal resistance R(16,16) at ν=2 (B=5.7 T). With reducing the gate voltage, the transmission probability of the edge current increase. The quantized resistance ($h/2e^2$) appears at $V_g < -2.8$ V, that is, two edge channels can enter the probe (1).

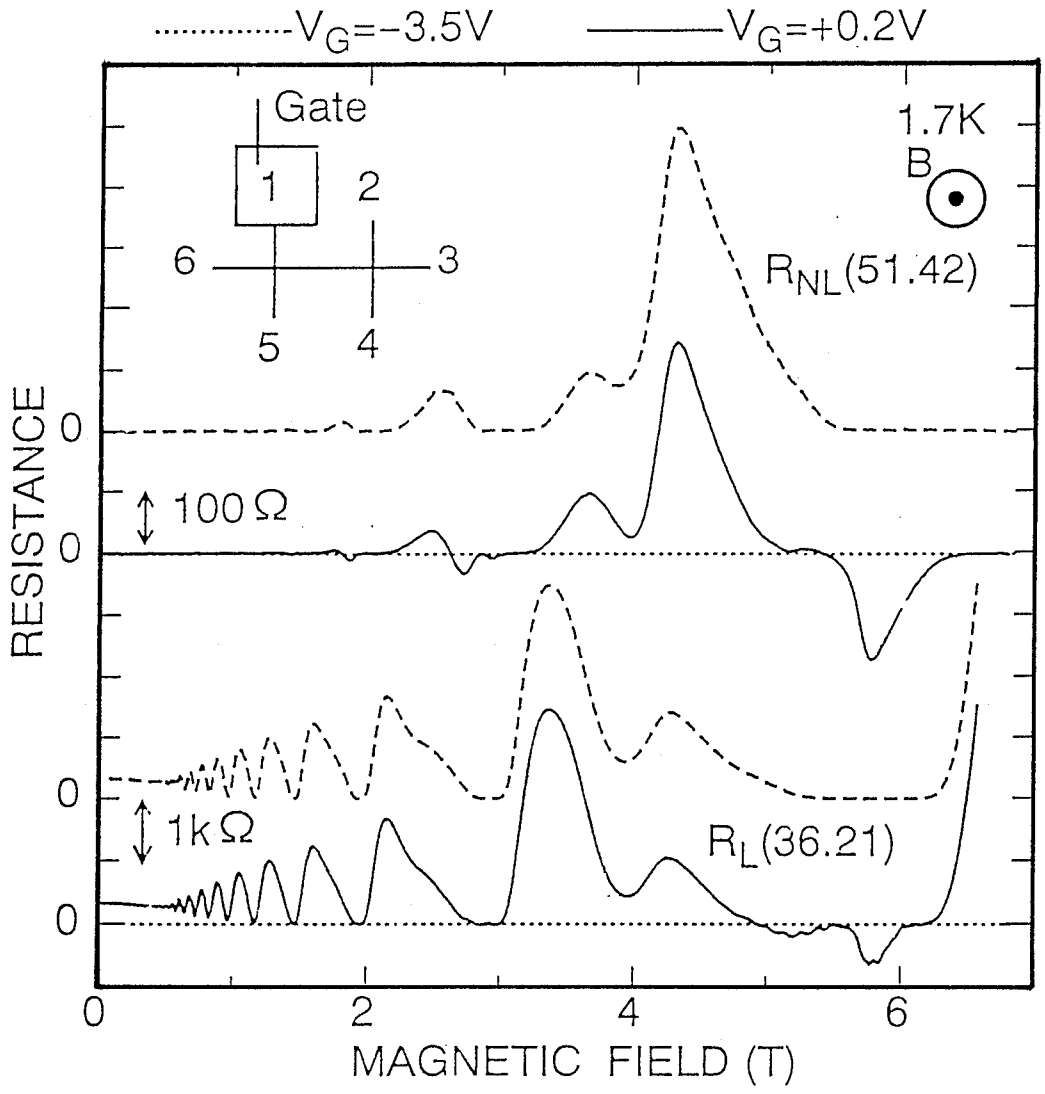

Fig. 35. The nonlocal resistance R(51,42) and longitudinal resistance R(36,21) at V_g=−3.5 V (broken curves), and V_g=+0.2 V (solid curves). At V_g=+0.2 V, the anomalous negative resistance was observed at the magnetic fields in which the edge current transmission was very small. At V_g=−3.5 V, ordinary profile of the magneto−resistance was obtained on the whole range.

4.2.5 Gate controlled probe (2)

Estimation of the energy equilibration length of edge current

In section 4.2.4, the negative resistance was reproduced by the gate controlled probe, but the transmission probability of edge channel was not separately determined. As shown in Fig. 36, a Corbino-like probe (1) controlled by Schottky gate (G_1), and a voltage probe (2) with a gate (G_2) as a detector of chemical potential distribution were used to investigate the anomalous distribution of the chemical potential of the channels and its equilibration. The probe (1) is isolated from the sample edge by 40 μm, and surrounded by the 2DES like a Corbino geometry. At the probe (1), with reducing gate voltage of G_1, the edge channel, belonging to the higher index Landau level can not go thorough under the gate, and go into the probe (see Fig. 36(b) and (c)). When the carrier is fully depleted under the gate, all edge channels are connected to the probe (1). In this way, this type of *'controlled non-ideal probe'* can tune the transmission of the edge current by using the energy difference of the Landau levels[20]. The gate near the voltage probe (G_2) was used as a detector of the chemical potential distribution among channels. The measurements was made after brief illumination by LED, at 0.5 K, with current 0.1 μA. The carrier concentration and mobility are N_s=3.3x10^{11} cm^{-2}, μ=6.2x10^5 cm^2/Vs respectively.

The two-terminal resistance R(16,16) at the gate voltage of G_1; V_{G1}=+0.1 V, is shown in Fig. 37(a). When the peaks ν= 2 and 3 were observed, the transmission of edge channels to the probe (1) was suppressed. In the gate voltage dependence of R(16,16), when the filling factor of the bulk state is ν= 2, 3 and 4, plateaus of the quantized resistance clearly appeared. In this way, the transmission of edge channels to the probe (1) was controlled one by one.

The sketch of probe (1), used as a current probe, at the filling factor ν=2 is

shown in Fig. 38. The chemical potential of two edge currents coming to the probe (1) is assumed to be μ_0. The outer-edge current (see Fig. 38) goes through under the gate and is not changed its chemical potential, while the inner-edge current can enter the probe, at which the transmission probability of t ($0< t\leq 1$). By using the Landauer-Büttiker formalism, the chemical potential of the probe (1) μ_{c1} becomes

$$\mu_{c1} = \mu_0 + \mathrm{h\,I}/t\,\mathrm{e}\ , \qquad (24)$$

where I is the current. Note that, the chemical potential μ_1 of the inner-edge current emitted from the probe (1) is expressed as $\mu_1=\mu_0$ + hI/e , and is independent of the transmission probability t. After passing the probe (1), the anomalous chemical potential difference between inner and outer edge current is made, that is $\mu_1-\mu_0$= hI/e. The extent of the difference of chemical potential is detected by using the Schottky gate[21] at next voltage probe (2).

The nonlocal resistance R(51,42), measured at the gate voltage (V_{G1}, V_{G2}), is shown in Fig. 39. When V_{G1}= −0.5 V and V_{G2}=+0.1 V, as shown in curve (a), the ordinary profile of the R_{NL} is observed, since the transmission probability of all edge currents is about unity. As shown in (b) and (c), at V_{G1}=+0.1 V and the fields that the bulk current exists, negative resistance is observed due to the very small transmission of edge currents to the probe (1). The resistance also becomes negative at the QH plateau regime (ν=2 and 4), as shown ↑ in the figure. The amplitude of negative resistance at V_{G2}= −0.24 V becomes larger (where only outer-edge channel is connected to the probe at ν=2) than that of the case V_{G1}= +0.1 V, since the chemical potential of outer-edge current is selectively detected by the voltage probe (2). The effect of the non-equal chemical potential distribution among channels is enhanced. At V_{G1}= −0.2 V (only inner-edge channel is connected to the probe (1) at ν=2), the negative resistance is observed

as shown in (d) and (e). But the negative resistance disappears at QH plateau regime. It has been mentioned that the chemical potential difference between inner and outer edge current is expressed as $\mu_1 - \mu_0 = hI/e$, which is independent of the transmission probability t. The extent of negative resistance shows that the larger chemical potential difference exists at $V_{G1} = +0.1$ V ($t \approx 0$).

The schematic illustration for explanation of the chemical potential difference of two edge currents at $\nu=2$, is shown in Fig. 40, which is corresponding to the results in Fig. 39(a) – (c).

· **(a)** (V_{G1}, V_{G2})=(−0.5 V, +0.1 V): Since all edge currents are connected to the probe (1), and the chemical potential of both edge current is equal to each other (μ_1) and the nonlocal resistance becomes zero.

· **(b)** (V_{G1}, V_{G2})=(+0.1 V, +0.1 V): The transmission of the edge channel is very small at the probe (1) and an inverse distribution of chemical potential among channels appears (μ_0, μ_1). Since the chemical potential difference is equilibrated during conduction from the probe (1) to probe (2), the chemical potential of each current becomes μ'_0 and μ'_1 just before the probe (2). The chemical potential of the probe (2) is written by using the transmission probability of each channel T_0 and T_1 as;

$$\mu_{c2} = (T_0 \mu'_0 + T_1 \mu'_1) / (T_0 + T_1) . \qquad (25)$$

The chemical potential difference of edge currents incoming to the probe (4) should be reduced. The chemical potential of the probe (4) is written as $\mu_{c4} = (\mu'_0 + \mu'_1) / 2$, and then the observed resistance is given by;

$$(\mu_{c4} - \mu_{c2}) / eI = (\mu'_0 - \mu'_1)(T_0 - T_1) / 2eI(T_0 + T_1) . \qquad (26)$$

In this case at V_{G2}=+0.1 V, both edge currents are connected to the probe (2). The observed negative resistance suggests that there is difference of the transmission probability as $1 \geq T_0 > T_1$ in the *'ordinary'* probes.

· (c) (V_{G1}, V_{G2})=(+0.1 V, −0.24 V): The negative resistance is larger than that of (b). According to Eq.(26), the extent of negative resistance is determined by the product of $(\mu'_0 - \mu'_1)$ and $(T_0 - T_1)$. In this case, T_1=0 at V_{G2}=−0.24 V. Thus $(T_0 - T_1)$ becomes nearly unity $\approx$1, the negative resistance is enhanced. It is confirmed that the inverse distribution $\mu'_0 < \mu'_1$ exists and it does not equilibrate even for millimeter distance.

The Hall resistance R_H(51.62), at the same condition of the gate voltage as in Fig. 39, is shown in Fig. 41. At the condition (b) and (c), the anomaly of the Hall plateau at ν=2 is clearly observed. The deviation of the Hall resistance from the quantized value is (b) −170 Ω and (c) −400 Ω, which are nearly equal to the negative resistance observed in the nonlocal resistance (see Fig. 39(b),(c)). The observed deviation is understood by similar explanation for negative nonlocal resistance, mentioned above. The extent of chemical potential equilibration among edge channels by the probe is estimated from the Landauer–Büttiker formalism[8,12,13]. The detail of the calculation[20] is shown in appendix 1 . The transmission probability to the probe (2) is estimated as T_0/T_1= 2.4 . If T_0 is assumed to be unity, the calculated T_0+T_1= 1.4 is much lower than the estimated value $T_0+T_1 \approx$ 2 from the contact resistance of the probe (2). The discrepancy is attributed to the chemical potential equilibration under the gate G_2. It is suggested that when the negative bias is applied to the gate (in the case of (c)), the confinement potential of the 2DES near the gate changes, and the chemical potentials between inner and outer edge channels are well equilibrated. The ratio of T_0/T_1 is overestimated by the effect of the equilibration under the gate. The

effect of the confinement potential on chemical potential equilibrium will be discussed in section 4.2.8.

The equilibration length L_e of the chemical potential of edge currents is defined as the length where the difference of the chemical potential is reduced to that of $1/e$. The calculated L_e, as shown in appendix 1, is 700 μm. But it may be overestimated by the following reason. When V_{G1}=+0.1 V, the transmission probability of the edge current to the probe (1) is very small, $t \approx 0.03$ is estimated from the observed R(16,16) in Fig. 37(a) and Eq.(24). The chemical potential of the probe (1) becomes very high value (>70 meV estimated by Eq.(24)), which exceeds several times as large as the energy separation of Landau levels at ν=2. The current is supplied to the edge channels around the probe (1), not only near the gate G_1, since the breakdown of the QHE occurs due to the large electrostatic potential of the probe (1). Then the probe (1) supplies current to the edge channels by using the bulk state. The chemical potential difference among the channels becomes larger than the estimated value from the Landauer–Büttiker formalism[22].

To reinvestigate the equilibration length L_e of the inverse chemical potential distribution of edge channels, the sample geometry is modified as shown in Fig. 42. The control gate G_1 and voltage probe (7) with a gate G_3 as a detector of the chemical potential distribution, were placed. The separation between G_1 and G_3 is 60 μm. The carrier concentration and mobility is N_s=3.4x10^{11} cm^{-2}, μ=5.9x10^5 cm^2/Vs at 0.5 K respectively.

The gate voltage V_{G3} dependence of the resistance R(51,67) at B=6.5 T (filling factor ν=2, two edge channel exist) is shown in Fig. 43. At V_{G1}= −0.4 V, all edge channels are connected to the current probe (1). The chemical potential of emitted edge current is the same value as that of the probe (1). The observed resistance is independent of V_{G3} and shows quantized resistance ($h/2e^2$= 12.9 kΩ) as shown schematically in Fig.44(a).

At the V_{G1}= −0.08 V, only inner edge current comes into the probe (1), the outer edge current goes through under the gate G_1. The resistance R(51,67) shows minimum at V_{G3}=−0.07 V, where the inner edge channel is reflected by the G_3, and it should be zero if the equilibration is absent. In this case, from the deviation from the quantized value at V_{G3}= +0.2 V and V_{G3}= −0.07 V, the property of the probe T_0/T_1= 1.08 and L_e=96 μm is obtained. If T_0 is assumed to be unity, the calculated T_0+T_1= 1.93 shows good agreement with the estimated value 1.97 from the contact resistance measurement at ν=2. The obtained L_e is comparable to the equilibration length of the normal (non−inverse) nonequilibrium distribution reported by Müller *et al.* [20]. With decreasing V_{G3} below −0.07 V, it is predicted from the Landauer−Büttiker formula that the observed resistance is constant until the G_3 completely cut off the edge current, since the chemical potential of the probe (7) becomes same value of outer edge current. But at V_{G1}= −0.08 V, the resistance increases with reducing V_{G3}. It is suggested that the mixing among channels is significant, at the gate voltage near its pinch off value, since the spatial separation of the channel is close[23].

In summary, the reciprocal symmetry is observed in the measurement with the non−ideal probe. The Landauer−Büttiker formula is valid to explain the transport property of 2DES using the non−ideal probes. By using the Landauer−Büttiker formula, the energy equilibration length of the edge currents L_e is estimated. At ν=2 , L_e=96 μm is obtained by using the probe whose transmission of the channels is artificially controlled by the gate. But the ambiguity of the estimated L_e remains, because the equilibrium by the gate is neglected.

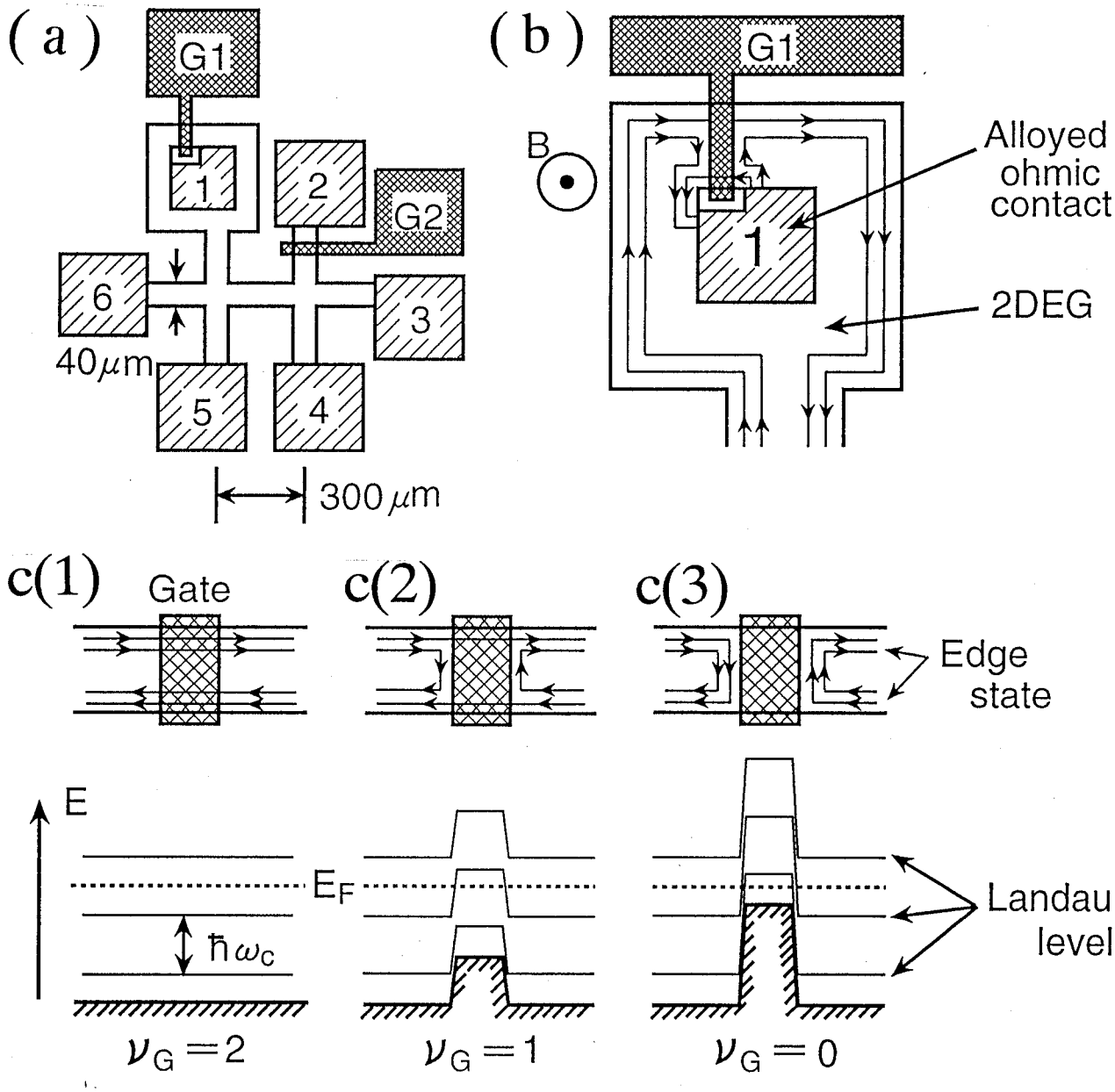

Fig. 36. (a) Schematic illustration of the sample with the probe controlled by the Schottky gate. The hatched region corresponds to alloyed contact probes. The probe (1) is isolated 40 μm from the sample edge. (b) Expanded view of the probe (1) and the gate. The edge current transmission can be controlled by the gate. The transmission of the outer-edge current is very small when the edge current can go through under the gate. The extent of transmission of inner edge current is larger than that of the outer-edge current. (c(1)-c(3)) Schematic illustration of the Schottky gate. With reducing gate bias, the edge current becomes to be reflected at the gate (c(2),c(3)). ν_G is the filling factor under the gate.

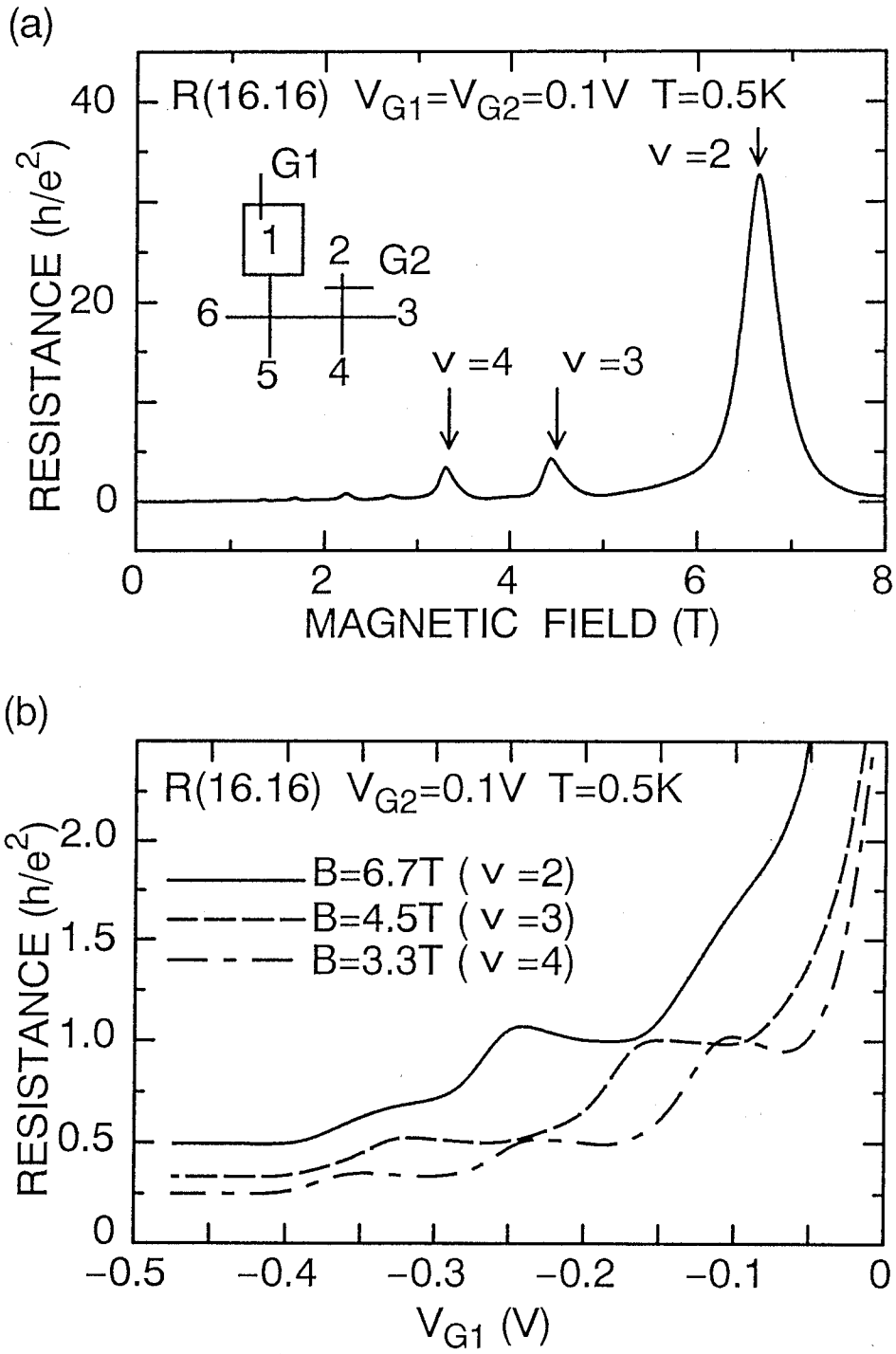

Fig. 37. (a) The two-terminal resistance R(16,16) at V_{G1}= +0.1 V. Large peaks of R(16,16) are observed at the quantum Hall plateau regime. (b) The gate voltage V_{G1} vs. R(16,16) at several magnetic fields, at which the filling factor ν=2, 3 and 4. The plateaus are clearly observed. The transmission of the edge channels are controlled one by one.

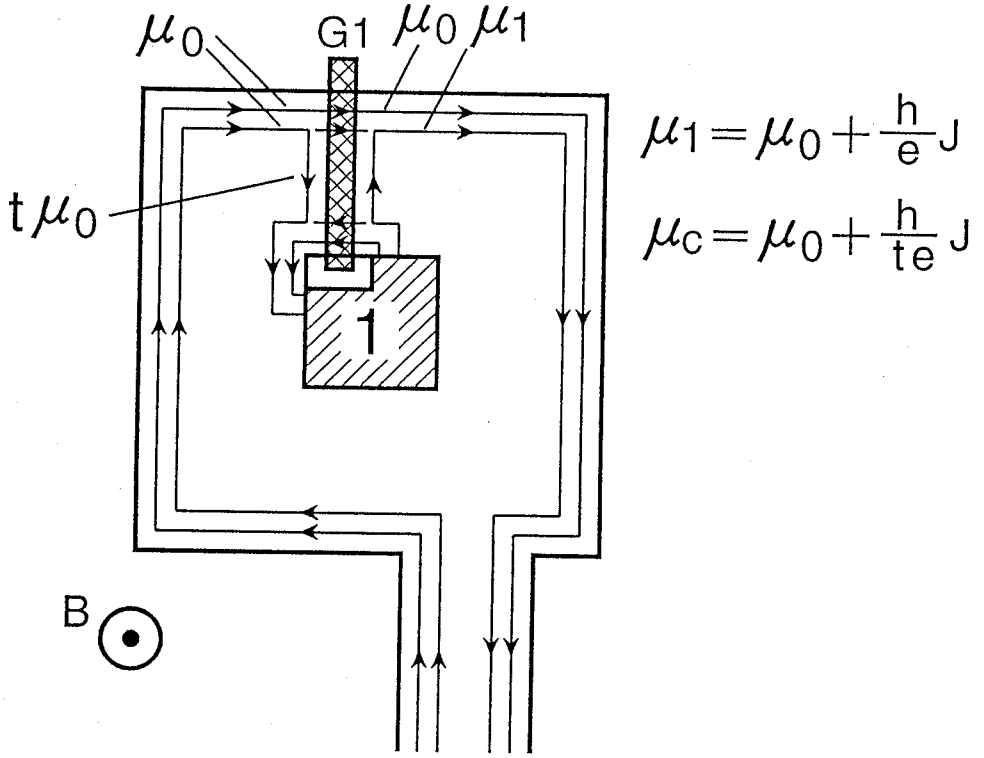

Fig. 38. Expanded view of the probe (1) and the gate. The transmission probability of the inner–edge current to the probe (1) is denoted by t. In the case that the total current I is flowing through the probe (1), the chemical potential of the probe (μ_{c1}) and emitted inner–edge current (μ_1) are shown.

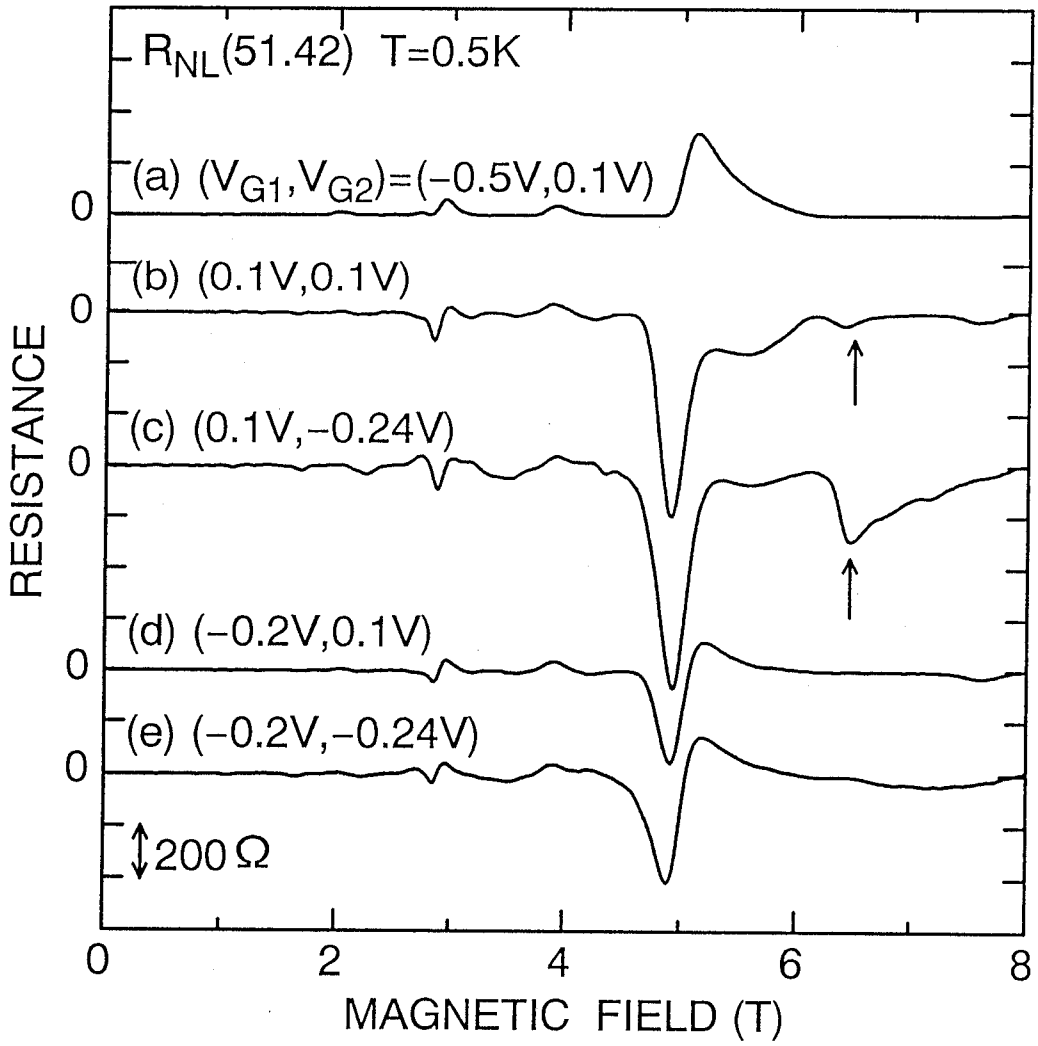

Fig.39. The nonlocal resistance R(51,42) at various sets of the gate voltage (V_{G1}, V_{G2}). (a) All the edge channels are connected to the probe (1), the ordinary profile appears. In the cases (b) – (e), the negative resistance due to the inverse chemical potential distribution of the edge currents is observed. Especially, the negative resistance at the quantum Hall plateau regime (shown ↑) is observed in the (b) and (c).

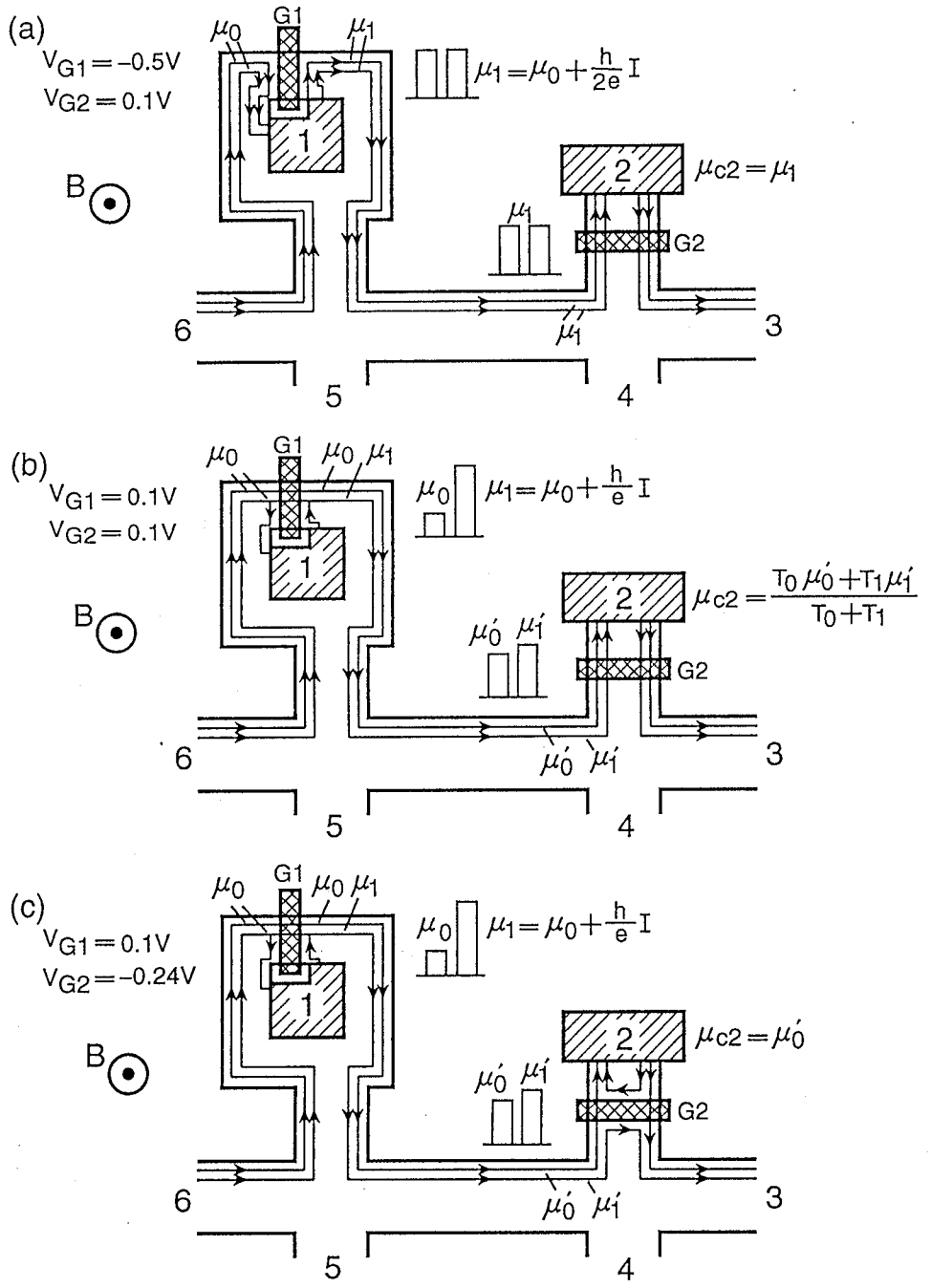

Fig. 40. Schematic representation of the chemical potential distribution. The figures (a)–(c) is correspond to the experimental condition in Fig. 39(a)–(c). The bar represents the chemical potential of each edge current.

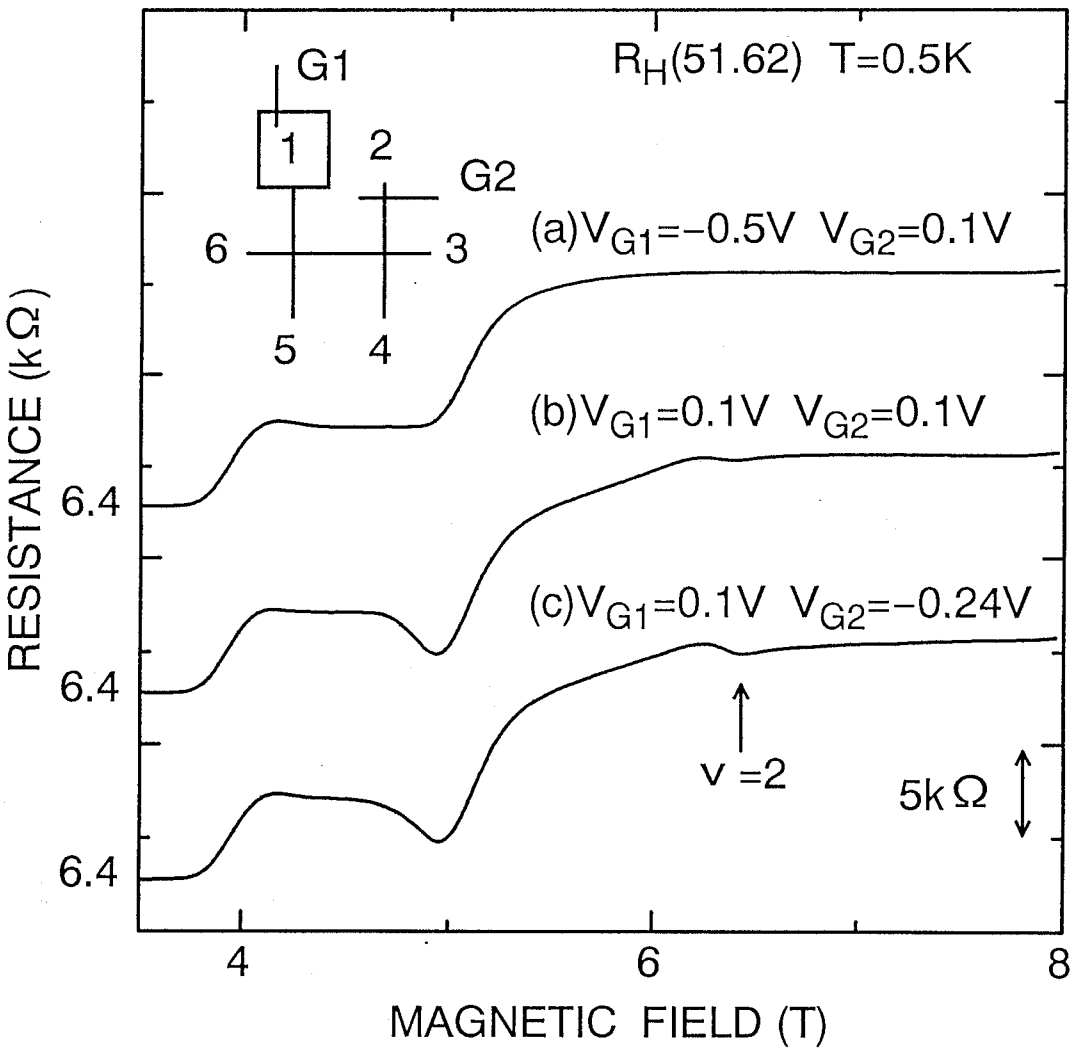

Fig. 41. The Hall resistance R(51,62) at three sets of the gate voltage (V_{G1}, V_{G2}). (a) All the edge channels are connected to the probe (1), the ordinary profile appears. In the cases (b) and (c), the anomaly due to the inverse chemical potential distribution of the edge currents is observed in the Hall plateau, as shown ↑.

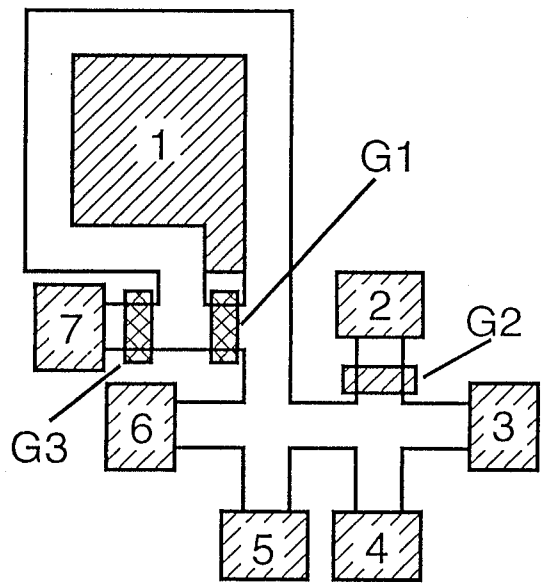

Fig. 42. Schematic illustration of the sample with the current probe control gate (G_1) and the detector probe (7) with a gate (G_3). The separation between G_1 and G_3 is 60 μm.

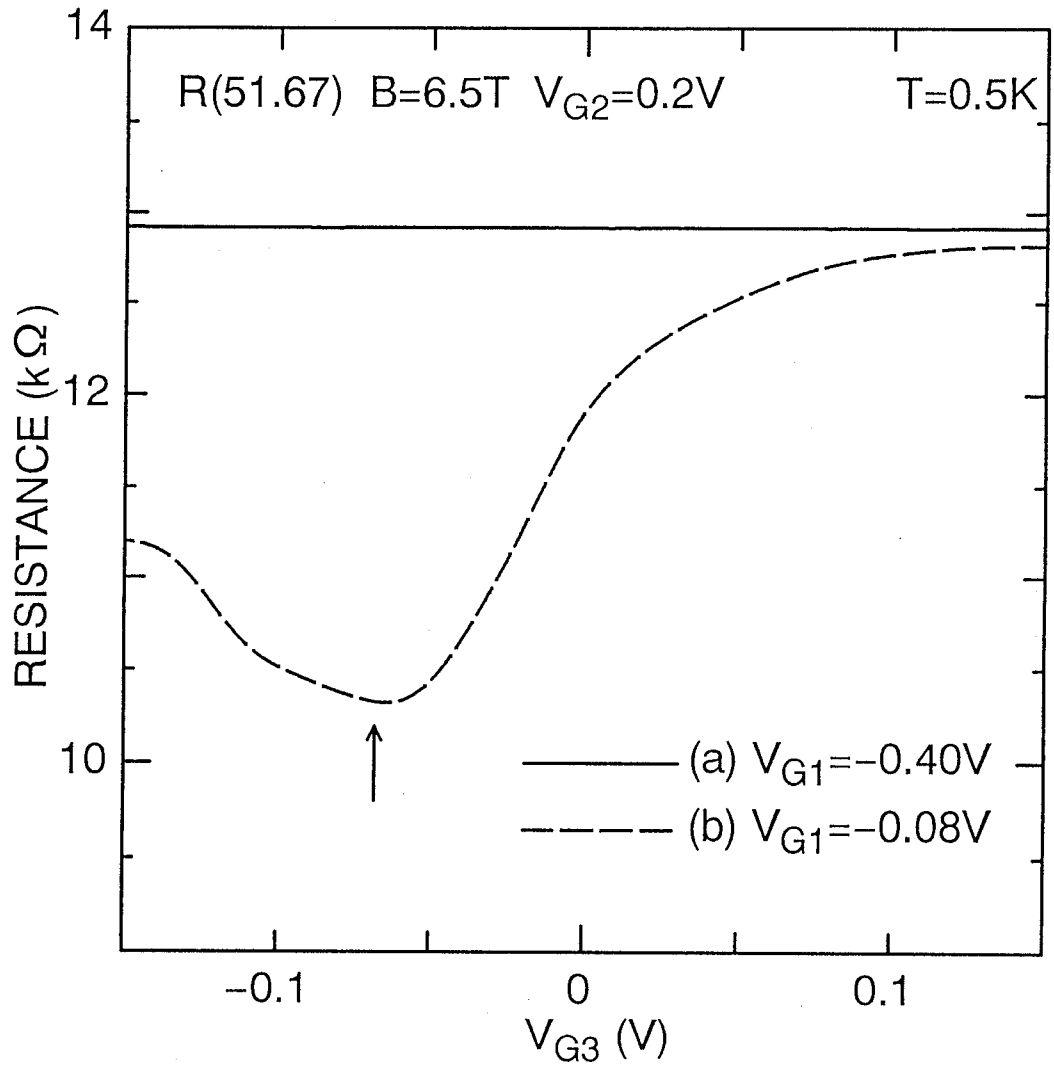

Fig. 43. The gate voltage V_{G3} vs. R(51,67) at ν=2 (B=6.5 T). (a) all edge channels are connected to the probe (1). (b) Only inner edge current enter the probe (1). The gate voltage, marked ↑ (V_{G3}=−0.08 V), only outer edge channel can enter the voltage probe (7).

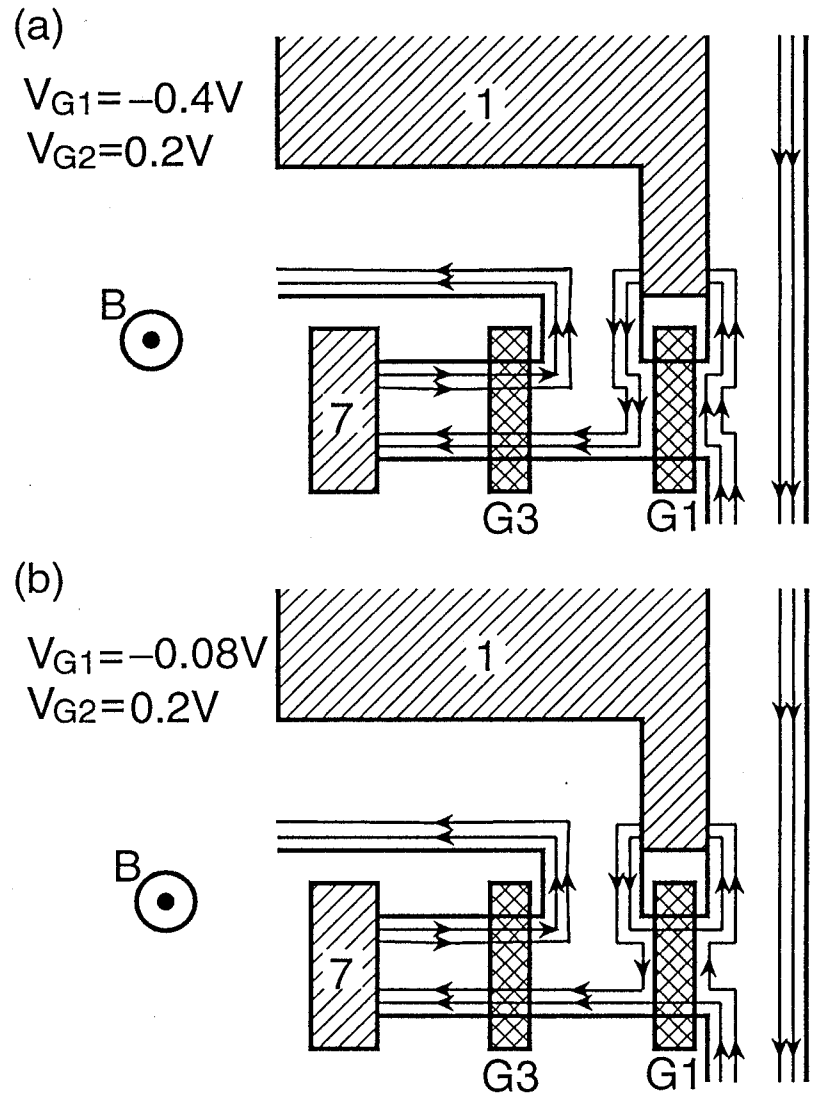

Fig. 44. Schematic representation of the electrons in the edge channels flow. The figures (a) and (b) are correspond to the experimental condition in Fig. 43(a) and (b).

4.2.6 Contribution of the edge and bulk current to the nonlocal resistance

In previous sections 4.1.1 – 4.2.1, the nonlocal SdH oscillations, observed in the mesoscopic size[7] and even macroscopic size[6,24] samples are discussed. The origin of the nonlocal resistance is interpreted by mixing of the edge channels and bulk channel at the probes[6,24]. When the nonlocal resistance shows SdH peaks, the Fermi energy level intersects with a Landau level in the sample, and both edge channels and bulk channel coexist at the Fermi level. The model proposed by McEuen *et al.*[6] explains the nonlocal SdH oscillations qualitatively by using the Landauer–Büttiker formula. The scattering of bulk electrons is represented by the transmission probability at each segment. Details are described in section 4.1.1. In order to observe the nonlocal SdH oscillations, it is necessary that both edge and bulk channels should exist and connect to the probes in 2DES, and the chemical potentials of the edge and bulk currents do not equilibrate completely at least over the nonlocal separation length ΔL. In this section, the magneto–resistance of a macroscopic size GaAs/AlGaAs wire with Schottky gates is discussed. The gate voltage dependence of the nonlocal resistance, where the gate lies across on the nonlocal path, is investigated to study the role of the edge and bulk currents[25].

A multi terminal wire with four Schottky gates[20] was fabricated as shown in Fig. 45. The contact resistance at probes is typically 100 Ω. The direction of the magnetic fields is denoted in Fig. 45, where the electrons in edge channels circle around clockwise. The measurement was made after the brief illumination by a LED light to increase the carrier density as $N_s = 3.3 \times 10^{11}$ cm^{-2}. The mobility μ is 6.0×10^5 cm^2/Vs at 4.2 K. In this experiment, only G_3 was used, and other gates G_1, G_2 and G_4 were biased at +0.1 V to compensate for reduction of the carrier

density under the gate.

The gate voltage V_{G3} dependence of the nonlocal SdH oscillations was measured with the current 0.5 μA at 0.5 K as shown in Fig. 46. With decreasing V_{G3}, the carrier density under the gate area decreased, and the peaks reduced before the gate was pinched off. The pinch-off voltage of the G_3 gate is about -0.45 V. The spin selective diminishing of the nonlocal resistance is observed at the Landau number n=1 and 2,. The peaks due to the up-spin state decreased at first, and then those due to the down-spin diminished. The peak amplitude of the nonlocal resistances at the Landau number n=1 vs. gate voltage (V_{G3}) is shown in Fig. 47. The up-spin peak and down-spin peak decreased in different manner, and completely diminished at about V_{G3}= -0.1 V. The selective diminishing of the nonlocal SdH oscillation peaks with different spin can be explained in the following way. As mentioned before, both edge and bulk current are necessary to observe the nonlocal SdH oscillations. If the bulk and/or edge currents are cut off at the gate, the nonlocal resistance can not be observed. With decreasing gate voltage, E_F crosses the bulk state and the bulk current is cut off at first. In fact, the diminishing gate voltage of all nonlocal SdH oscillations (-0.1 V) is considerably higher than the pinch-off voltage (-0.45 V), at which all current channels through the gate including the edge currents are blocked. The diminishing of nonlocal SdH oscillations is due to the cut-off of the bulk current by the gate voltage.

At the down-spin peak magnetic fields, E_F intersects with the extended Landau state of the down-spin. In this case, the down-spin and up-spin states were overlapped (Fig.48(a)) in 2DES region, since the spin splitting energy in the bulk GaAs sample, is much smaller than $\hbar\,\omega_c$ (Landau level separation energy). The chemical potentials of both states are in equilibrium and the 'bulk current' consists

of the two states. With decreasing gate voltage, E_F comes between two states, because the spin-splitting is enhanced due to the exchange interactions of electrons under the gate area (Fig.48(b))[26]. Even in such a case (b), the bulk current can flow under the gate through the up-spin state, and the nonlocal resistance can be observed. With reducing gate voltage, E_F crosses the up-spin state under the gate and the bulk current is completely cut off, and then the peak of the nonlocal resistance diminished (Fig.48(c)).

On the other hand, at the up-spin peak magnetic fields, E_F intersects with the up-spin state and only the up-spin state exists mainly as the 'bulk current' in 2DES region (Fig.48(d)). With decreasing gate voltage, E_F is below the up-spin state and the 'bulk current' from the up-spin state can not go through the gate (Fig.48(e)). The cut-off gate voltage of the up-spin peak is higher than that of the down-spin peak, since the amount of E_F reduction to cut the 'bulk current' from mostly one state (the up-spin state) is smaller than that of two states (the up-spin and down-spin states).

In summary, the influence of the bulk and edge states on the nonlocal resistance is investigated by cutting the bulk and edge current at the gate. With decreasing gate voltage and carrier density under the gate, the SdH oscillation peaks of the down-spin Landau levels diminish at lower gate voltage than those of the up-spin levels. This could be explained as the 'bulk current' corresponding to the down-spin Landau level peak of the SdH oscillations comes from the overlapping down-spin and up-spin states, while the up-spin Landau level peak comes from mostly the up-spin state.

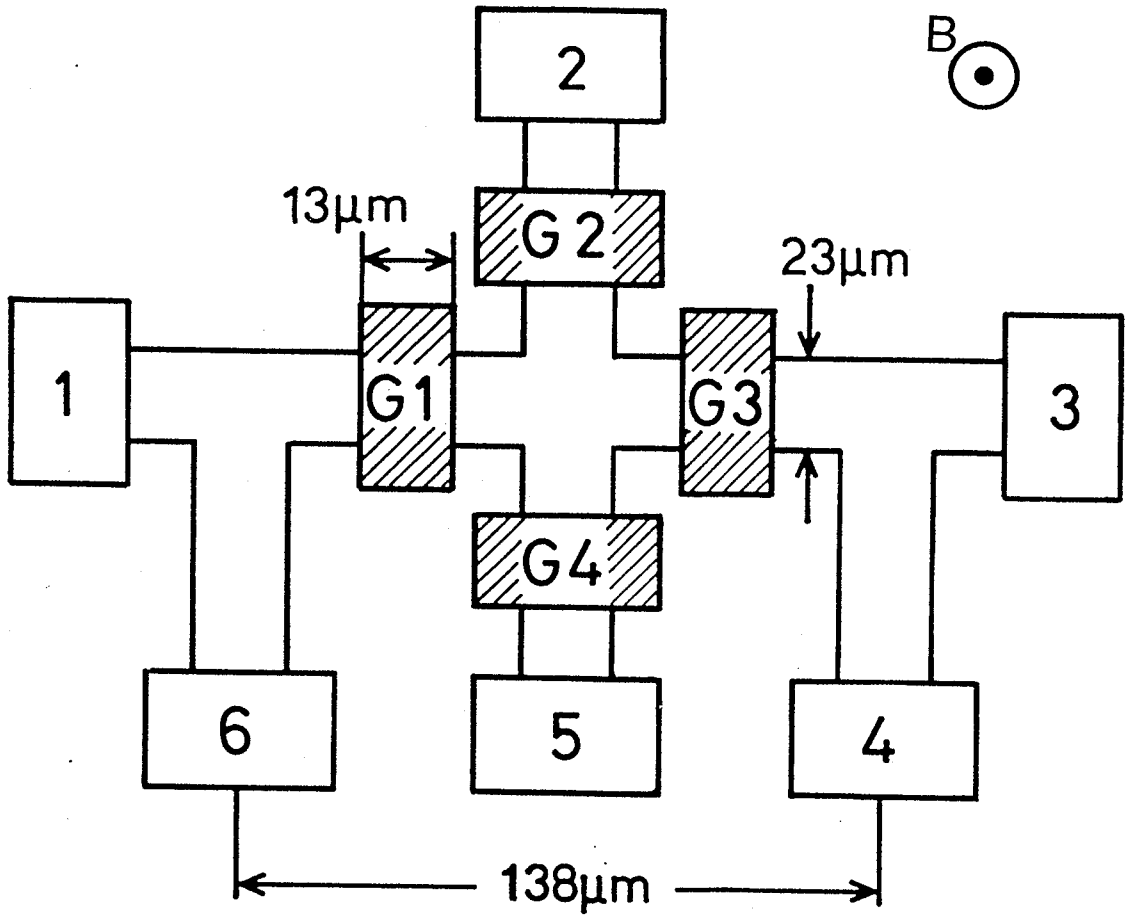

Fig. 45. Schematic view of the sample. The notation G_i(i=1 – 4) and number denotes Schottky gate and probes, respectively. At denoted magnetic fields, electrons in the edge channels circulate clockwise along the sample edge.

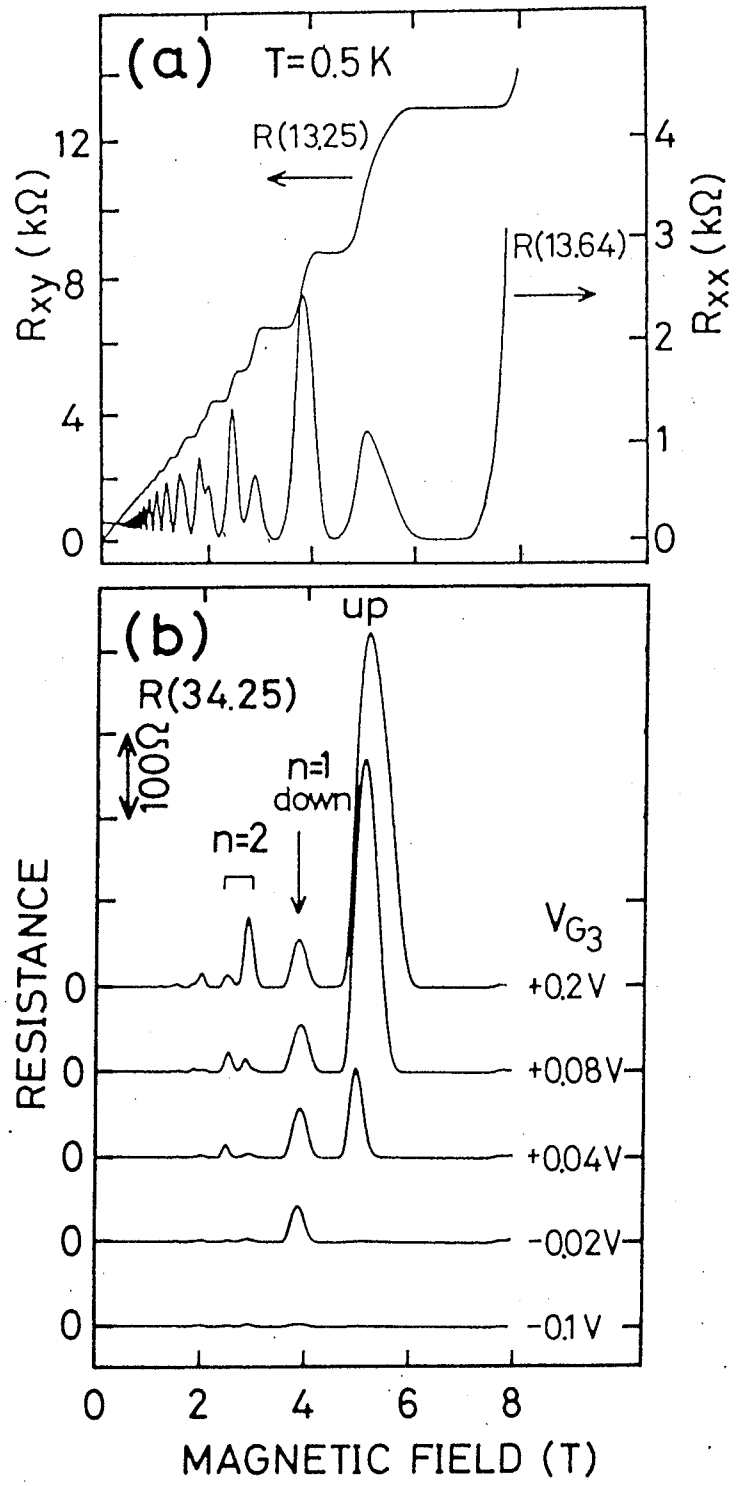

Fig. 46. (a) Longitudinal resistance $R_{xx}(13,64)$ and Hall resistance $R_{xy}(13,25)$. (b) Nonlocal resistance R(34,25) with various gate voltages (V_{G3}). The number denoted n is Landau index number. Up and down represent the spin state of Landau levels.

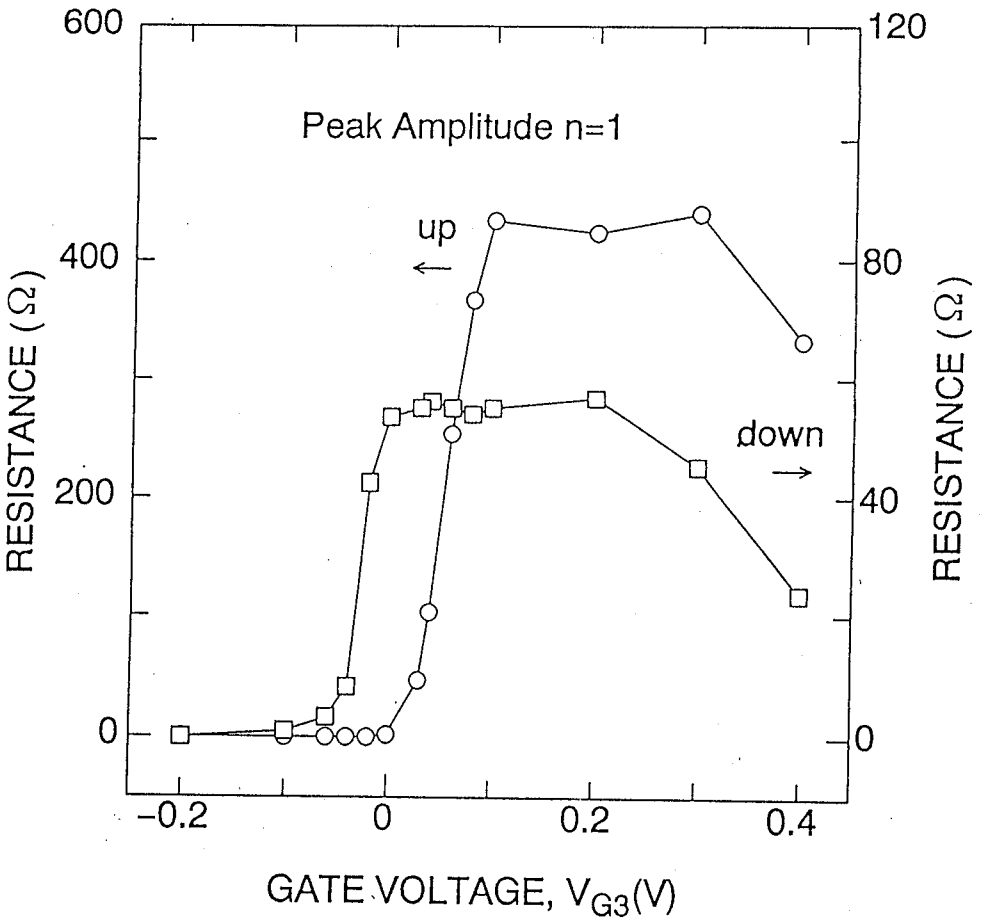

Fig. 47. Peak amplitude of nonlocal resistance of up-spin state and down-spin state of Landau level number 1. The diminishing voltage of the down-spin state is smaller than that of the up-spin state.

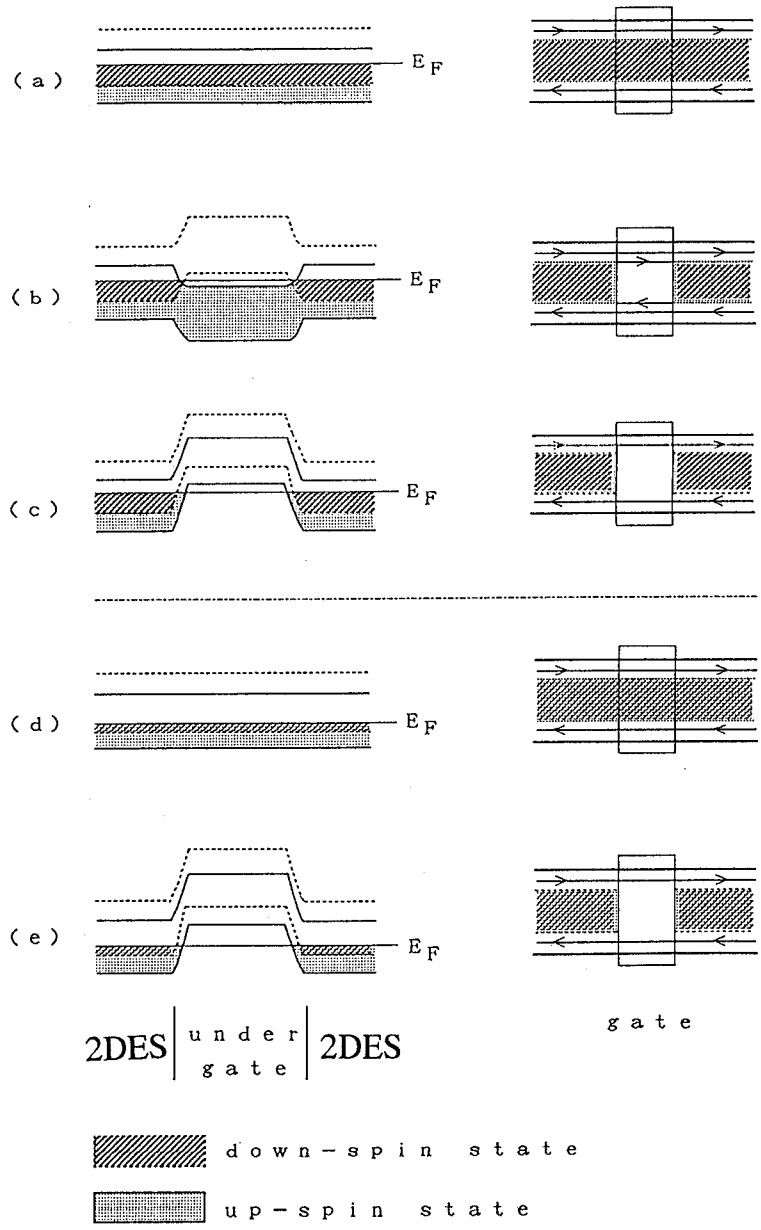

Fig. 48. Schematic cross section of electron energy levels in a magnetic fields parallel to nonlocal path of 'bulk current'. The broadening of each state is the energy width of extended zone of Landau level. The hatched region represents occupied down-spin state and shaded region shows occupied up-spin state. When the Fermi level comes between these states by applying the gate voltage, the spin splitting is enhanced. Fermi level intersects with down-spin state in 2DES region (a) – (c), intersects with up-spin state in 2DES region (d) and (e).

4.2.7 Influence of the extra probe on the quantum transport

In section 4.1.4, the role of a probe was discussed. It was suggested that the chemical potential of the edge and bulk currents are equilibrated in the probe. The influence of extra probes on the transport have been examined by cutting the bulk and edge currents in the extra-terminals by the gate voltage[20,27]. These extra probes have apparently no effect on the measurement. The same sample section 4.2.6 was used (Fig. 49). The configuration of the measurement was the same as described in section 4.2.6. The gate voltage -0.5 V was applied to electrically disconnect the extra probe. The gate was biased at +0.1 V, when the extra probe was connected.

When the extra probe is disconnected, both normal and nonlocal SdH oscillation peaks at high magnetic fields are altered as shown in Fig. 49. The influence of extra probe on the edge and bulk currents is considered as follows[20,27]. When the extra probe is connected, the bulk and edge currents go through the gate, and the mixing of the edge and the bulk currents occurs in the extra probe, as shown in Fig. 50(a). Then the chemical potential of the emitting edge and bulk currents is equilibrated. As a result, the chemical potential of the edge current outgoing from the probe μ'_e changes from the incoming one μ_e, since chemical potential of the incoming bulk current μ_b is not equal to μ_e. On the other hand, when the extra probe is disconnected, the bulk and edge currents, incoming to the extra probe, are reflected at the gate. In this case, the mixing does not occur, and the chemical potential of edge current does not change, as shown in Fig. 50(b). The SdH oscillation peaks of the longitudinal resistance should become larger, when the extra probes between the voltage probes are connected, since the change of chemical potential of the edge current at the extra probe results in a larger voltage difference. As shown in Fig. 49(a), the peaks of normal SdH oscillations

R(13,64) become smaller, when the extra probes 2 and/or 5 are disconnected by the gates G_2 and/or G_4.

The nonlocal SdH oscillations are also affected by the extra probes. As shown in Fig.50(b), the nonlocal SdH oscillations R(34,26) become smaller when the extra probe 5 in between the separation path is connected by the gate G_4. In the case that the extra probe is attached to the separation path, this extra probe causes a larger voltage difference in the separation path. The voltage difference between the current probes (the two terminal resistance) is hardly affected by the other probes. Thus the voltage difference between the voltage probes (the nonlocal resistance) becomes smaller when the extra probe is connected. This is consistent with the previous experimental result, where the nonlocal SdH oscillations in the mesoscopic multi-terminal wire diminish greatly, when there exist extra probes in the separation path[28].

On the contrary, the nonlocal SdH oscillations R(34,25), as shown in Fig.50(c), become larger when the extra probes 1 and 6 between the voltage probes are connected by the gate G_1. These experimental results can be also explained as the extra probes attached to the path between the voltage probes causes a larger voltage difference. The nonlocal resistance becomes larger when the extra probes between the voltage probes are connected.

In summary, it is found that the normal and nonlocal SdH oscillations at high magnetic fields alter by disconnecting the extra probes electrically. These changes can be understood by the result that the mixing of edge and bulk currents at the electrode of the extra probe is interrupted, when the extra probe is disconnected. The magneto-transport properties of a 2DES at high magnetic fields are governed by the edge and bulk currents and the effect of all probes linked to the sample should be considered.

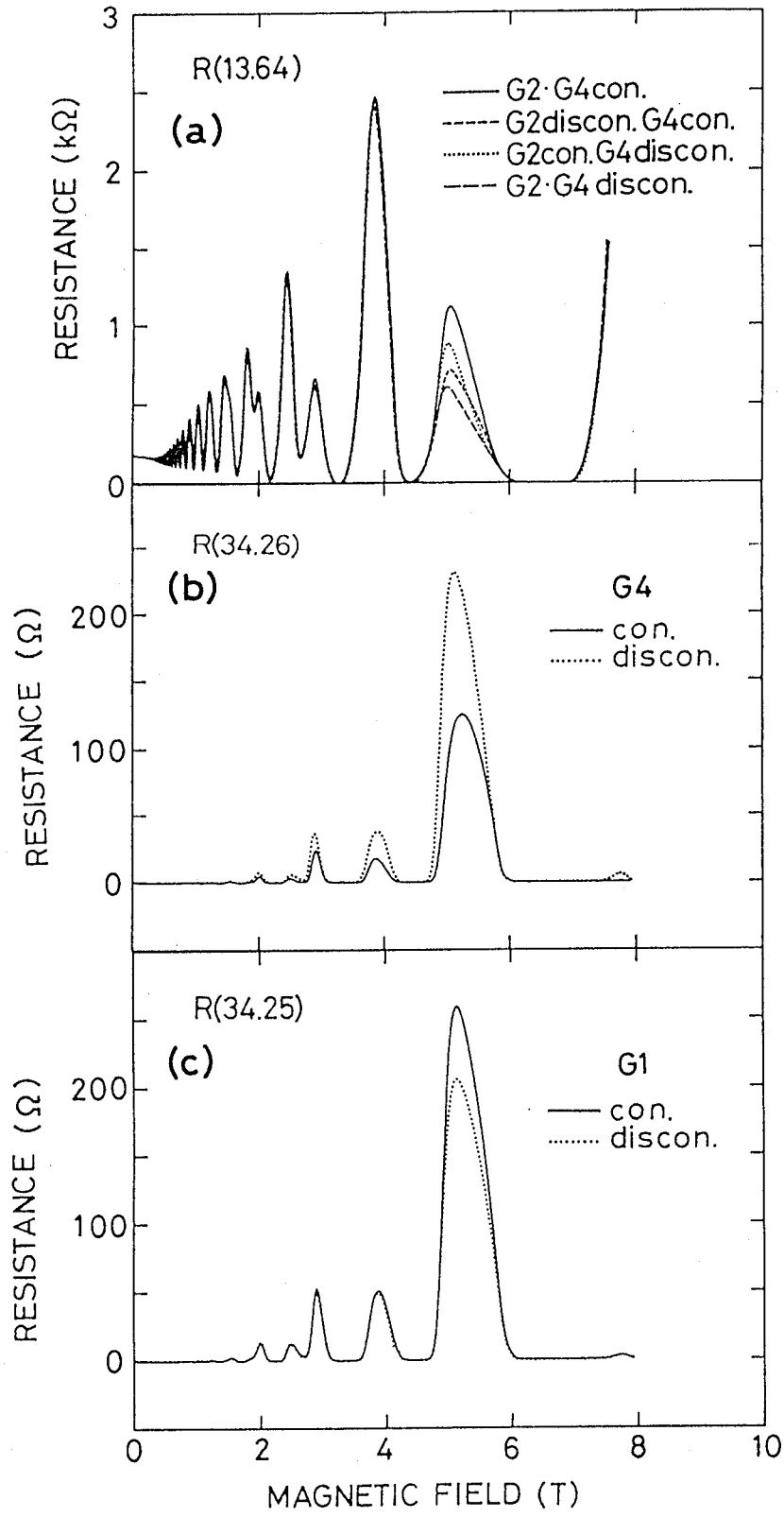

Fig. 49. Normal and nonlocal SdH oscillations with connecting (con.) and/or disconnecting (discon.) extra probes by the gates. (a) Normal SdH oscillations. (b) and (c) Nonlocal SdH oscillations.

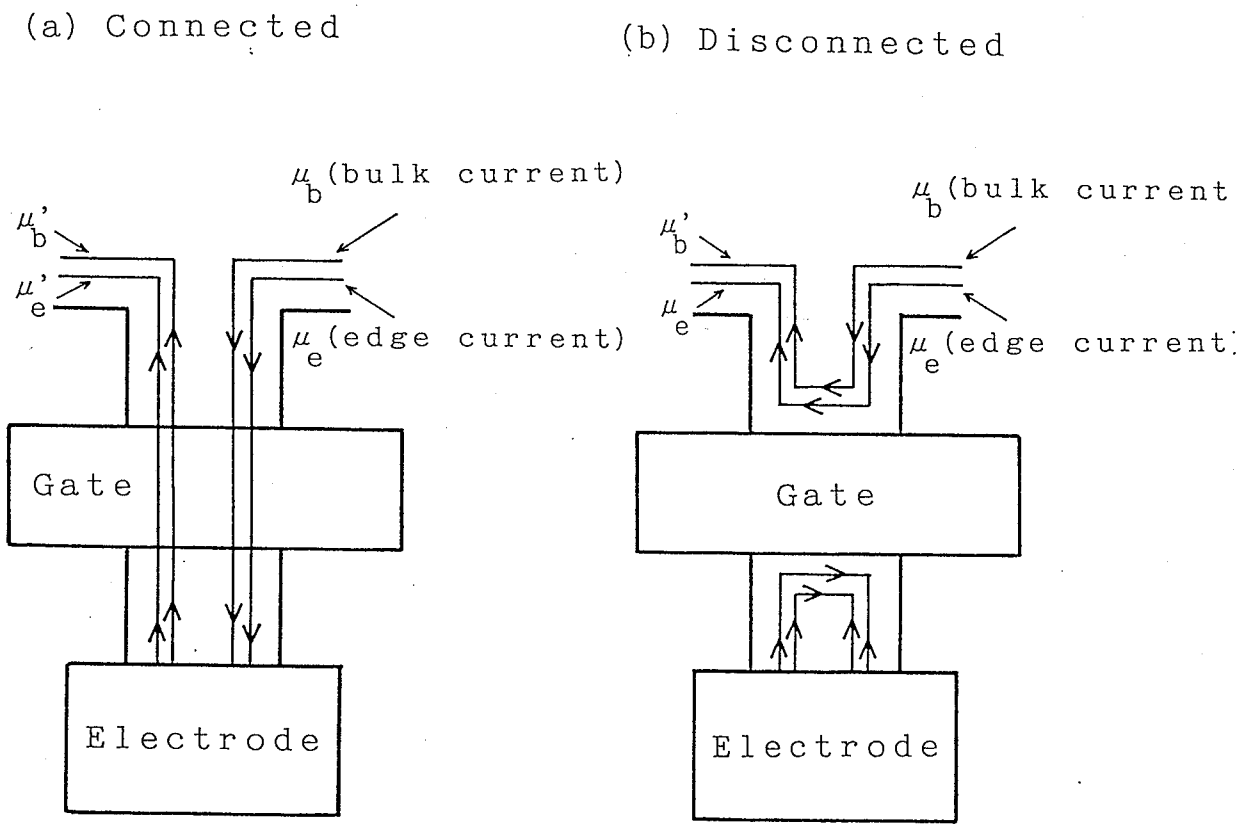

Fig. 50. Influence of an extra probe on the chemical potentials of the edge and bulk currents. (a) Extra probe is connected, (b) extra probe is disconnected. When the extra probe is connected, the chemical potential of the edge current changes.

4.2.8 Nonlocal quantum transport controlled by tunable confinement potential of 2DES

The electronic transport of the two-dimensional electron system (2DES) in a quantum Hall regime is understood by considering both edge channels and bulk channels [6,11] (see section 4.1.2). The nonlocal features of the quantum transport, such as nonlocal SdH oscillations[6,7], non-scale resistance[5], appear when the adiabatic edge channels and dissipative bulk channels coexist and they are well *decoupled*. The extent of decoupling between edge and bulk channels may be influenced by the profile of the confinement potential of the 2DES. The magneto-resistance of the GaAs/AlGaAs wires, whose brinks are covered with Schottky gates, was measured to investigate the influence of the confinement potential of the 2DES on the quantum transport.

The sample was made of modulation doped GaAs/AlGaAs heterostructure, with carrier density $3x10^{11}$ cm^{-2} and mobility $7x10^5$ cm^2/Vs at 4.2 K. It was shaped by photo lithography and wet chemical etching technic. The schematic view of the sample is shown in Fig. 51. The width of the mesa-etched wire is 120 μm, the edge of the wire is covered with the Schottky gate (G1 – G4 in Fig. 51, made from Au) of width 20 μm, except for the ohmic contact region. The 2DES under the gates is depleted with the gate voltage lower than the threshold value V_{th}= –0.55 V. The extent of the depletion region from the edge of the gate was estimated to be 0.5 μm at V_g= –2 V from the resistance at the zero field. The effective confinement potential of the 2DES can be controlled with the applied gate voltage which is lower than V_{th}. The magnetoresistance up to 8 T was measured at 0.5 K with a current 0.3 μA. In this experiment, the same voltage was applied to all gates G1 – G4, otherwise noticed.

The nonlocal resistance R(14,23) at different gate voltage is shown in Fig. 52. In the peaks corresponding to the spin split Landau level n=1, the amplitude of the up-spin peak changed very little, while that of the down spin peak was much affected by the gate voltage (see Fig. 52(a)). The peak amplitudes corresponding to $n \geq 2$, became larger with reducing gate voltage. At the low field region ($n \geq 3$), as shown in Fig. 52(b), the down-spin peaks developed with decreasing gate voltage, while these were almost extinct at $V_g \geq -1.2$ V.

In Fig. 53, the gate voltage dependence of the longitudinal resistance R(34,21) is shown. The peak resistance of SdH oscillations was much reduced with lowering gate voltage. The up-spin peak of n=1 Landau level is not much changed by the gate voltage, which is similar to the behavior observed in the nonlocal resistance.

The gate voltage dependence of the longitudinal resistance at the peak of n=4 Landau level is shown in Fig. 54(a). Four dips of the resistance, in the gate voltage range of $V_{th} < V_g < 0$, were observed when the region under the gate is in quantum Hall plateau regime, where the bulk states and edge states were separated spatially by the gate (see Fig. 54(b)). With lowering gate voltage below V_{th}, the longitudinal resistance decreases drastically. By using the model, proposed by McEuen *et al.*[6], the peak amplitude of the longitudinal resistance can be calculated. But the model does not contain the equilibration of the chemical potential among channels, thus the observed longitudinal resistance should be larger in the case that the equilibration among channels occurs. Since the separation between bulk and edge channels is large enough to decouple each other at $\nu=8$ dip ($V_g \geq 0$ V) and $V_g = -2$ V, the resistance reduces to the value (134 Ω), as is predicted by the model. The detail of the calculation is shown in appendix 2.

The enhancement of the nonlocal magneto-resistance and reduction of the longitudinal resistance with decreasing gate voltage are understood by considering

nonequilibrium conduction and decoupling among edge and bulk states. The schematic expression of the decoupling is shown in Fig. 55. With reducing gate voltage, the depleted region of 2DES expands under the gate, the spatial profile of the effective confinement potential near the Fermi energy becomes gentle, the edge channels and bulk channels are spatially separated well, and their chemical potential is not equilibrated. Recently, Chklovskii *et al.* reported[29] the calculation that the spatial separation between edge and bulk states scales with the width of the depletion layer that extends under the gate to the boundary of the 2DES. Their theoretical prediction is qualitatively consistent with our results. In this Schottky-gated sample, when $V_g<V_{th}$, the impurities and/or defects due to the sample fabrication process are well separated ($\approx$20 μm) from the edge and bulk channels, they may not affect the mixing among channels, in contrast to the experiment which is measured in the in-plane-gate sample fabricated by focused-ion-beam[17].

The nonlocal resistance R(14,23), when one gate voltage (shown G_i, (i=1 - 4) in Fig. 56) is applied -2 V and other gate voltage is -0.4 V, is shown in Fig. 56. When G_1 is applied -2 V, the observed amplitude of nonlocal resistance becomes larger than that in other cases. At V_g=-2 V, the equilibrium of the chemical potential among channels are much reduced. On the other hand, a significant mixing among channels occurs at the V_g=-0.4 V. To appear the nonlocal resistance, the edge current emitted from the current probe, should arrive at the voltage probe without equilibration of its chemical potential between the bulk current. In this measurement, the edge current is transported from the current probe (1) to the voltage probe (2) along G_1. Since the equilibrium of the chemical potential between bulk and edge currents is reduced at G_1= -2 V, the nonlocal resistance R(14,23) is enhanced.

In summary, the peak amplitudes of nonlocal resistance become larger with decreasing gate voltage, while the amplitude of the normal SdH oscillations in the longitudinal resistance is reduced. These phenomena are interpreted in terms of the enhancement of the decoupling between edge and bulk channels. The nonequilibrium between edge and bulk currents becomes marked by the gate induced *gentle* confinement potential. It is demonstrated that the energy equilibration length of the current carrying edge states varies with the profile of the confinement potential.

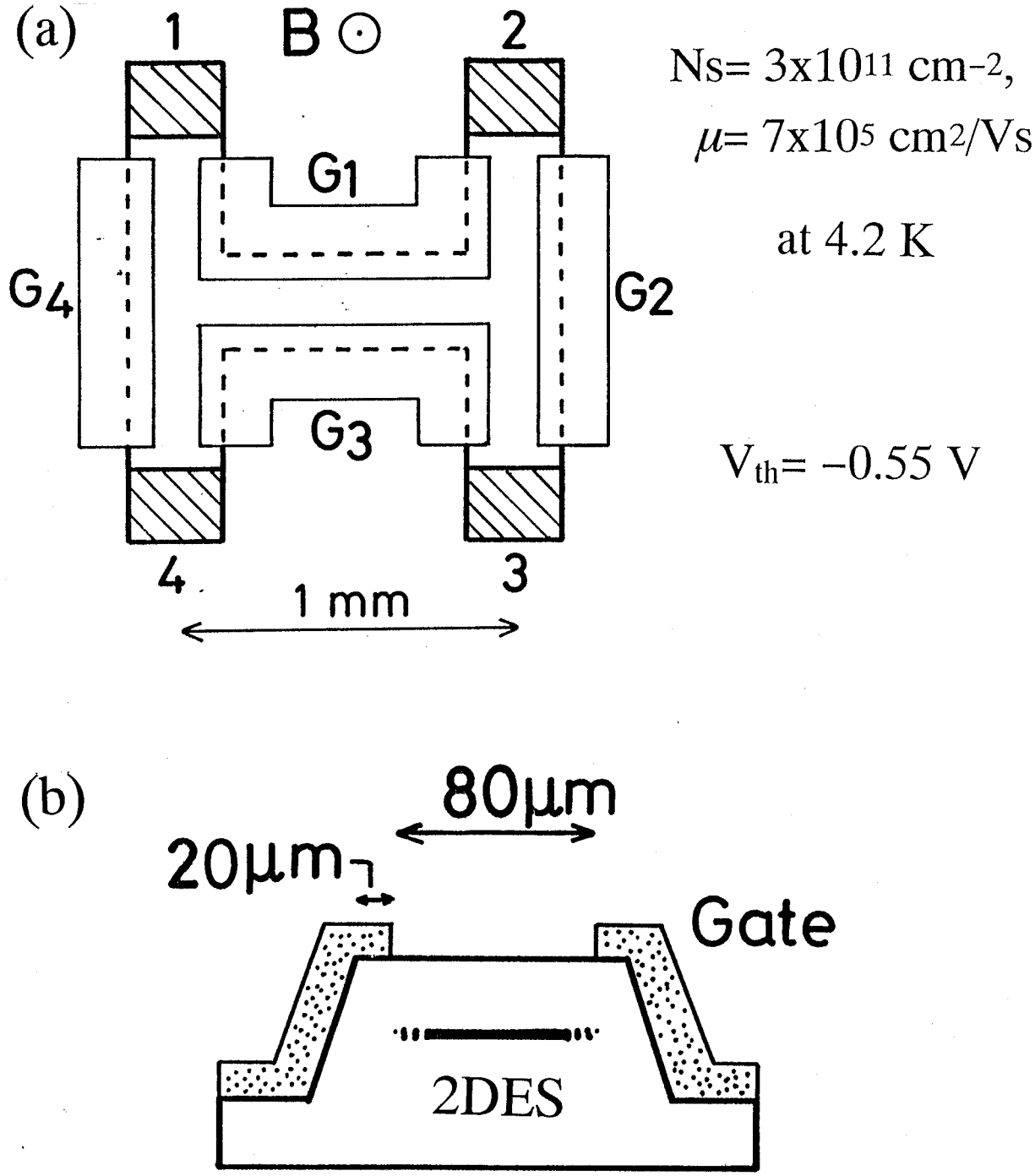

Fig. 51. Schematic view of the sample. (a) G_1 – G_4 are Schottky gates. The hatched region (1 – 4) corresponds to ohmic contact. (b) The cross sectional view of the sample across the channel. The Schottky gates covered 20 μm of the sample edge. The 80 μm width of the center of the sample is not covered with gate metal.

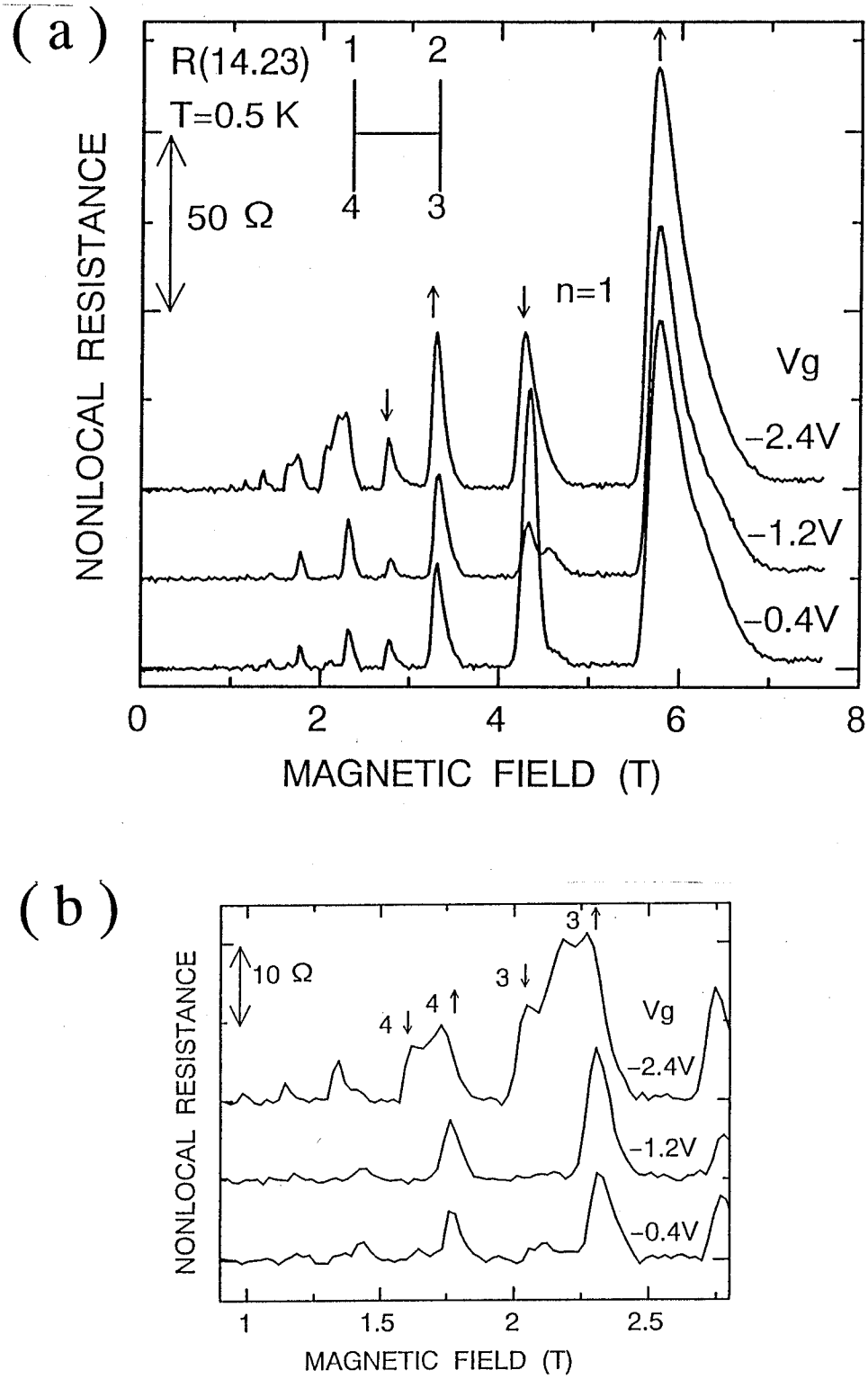

Fig. 52. (a) Gate voltage dependence of the nonlocal resistance R(14,23). Arrows show the spin state of Landau levels (n). (b) Expanded view of the low-field regime.

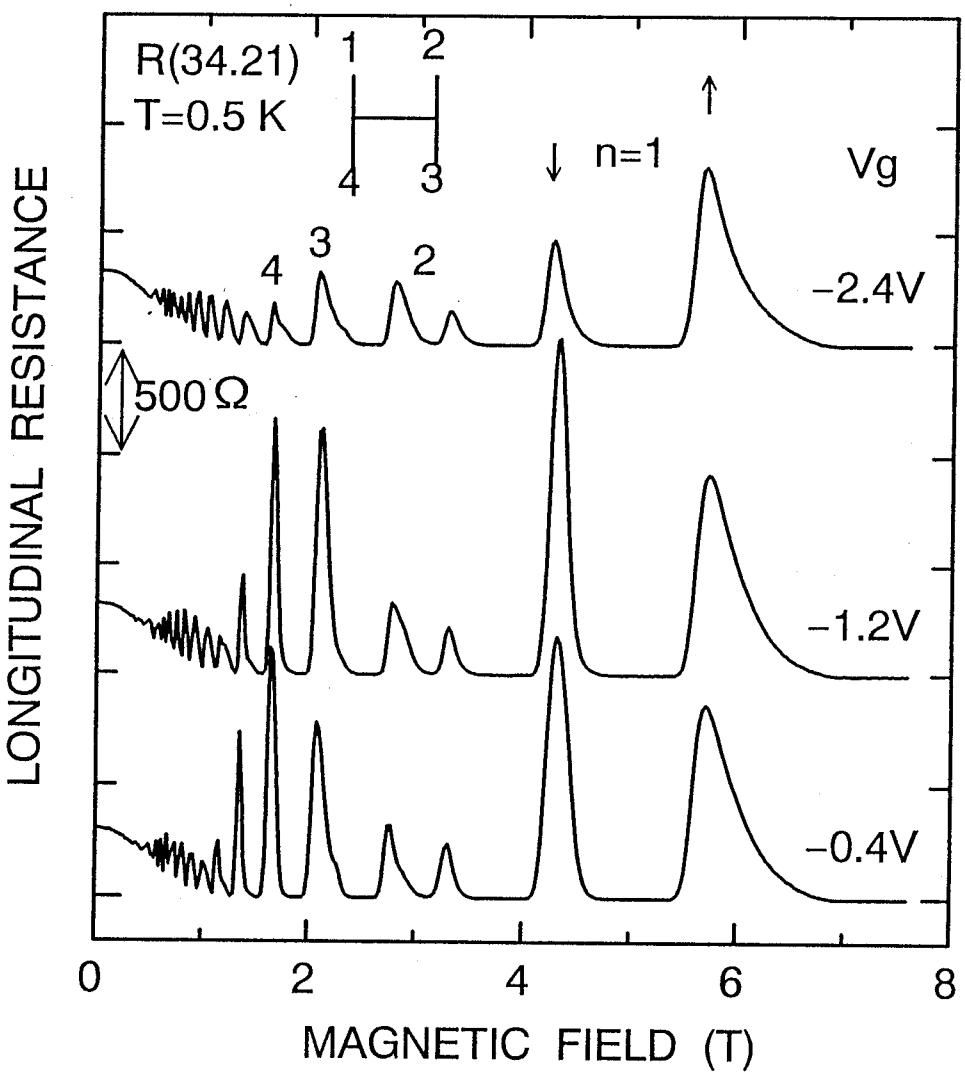

Fig. 53. Longitudinal resistance R(34,21) for various gate voltage. Arrows show the spin state of Landau levels (n).

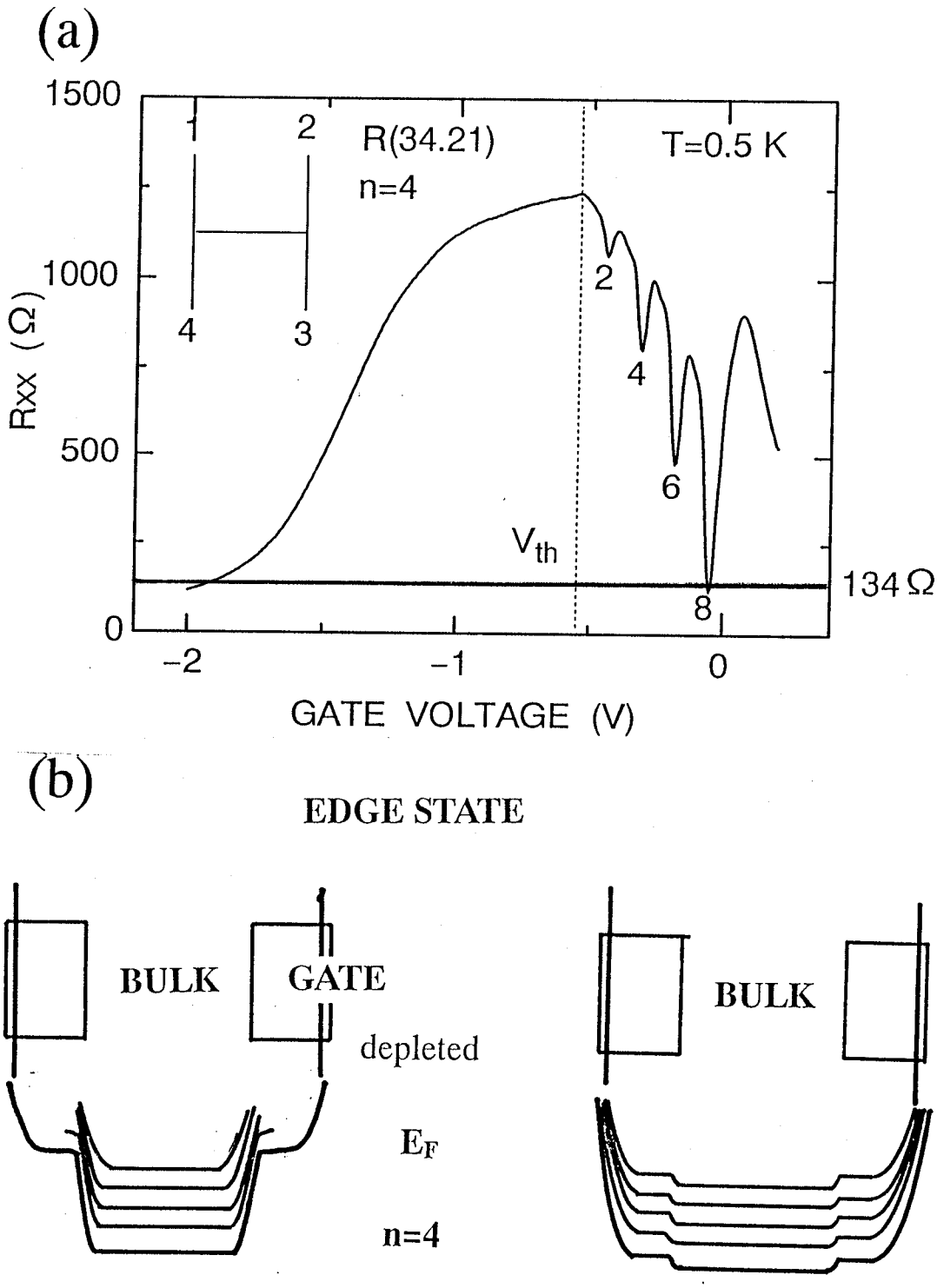

Fig. 54. (a) Longitudinal resistance R(34,21) vs. gate voltage at B=1.6 T. The Landau level n=4 is occupied as bulk states. (b) Schematic illustration of the confinement potential of 2DES and Landau levels at $V_g < V_{th}$ (left) and $V_{th} < V_g < 0$ V (right).

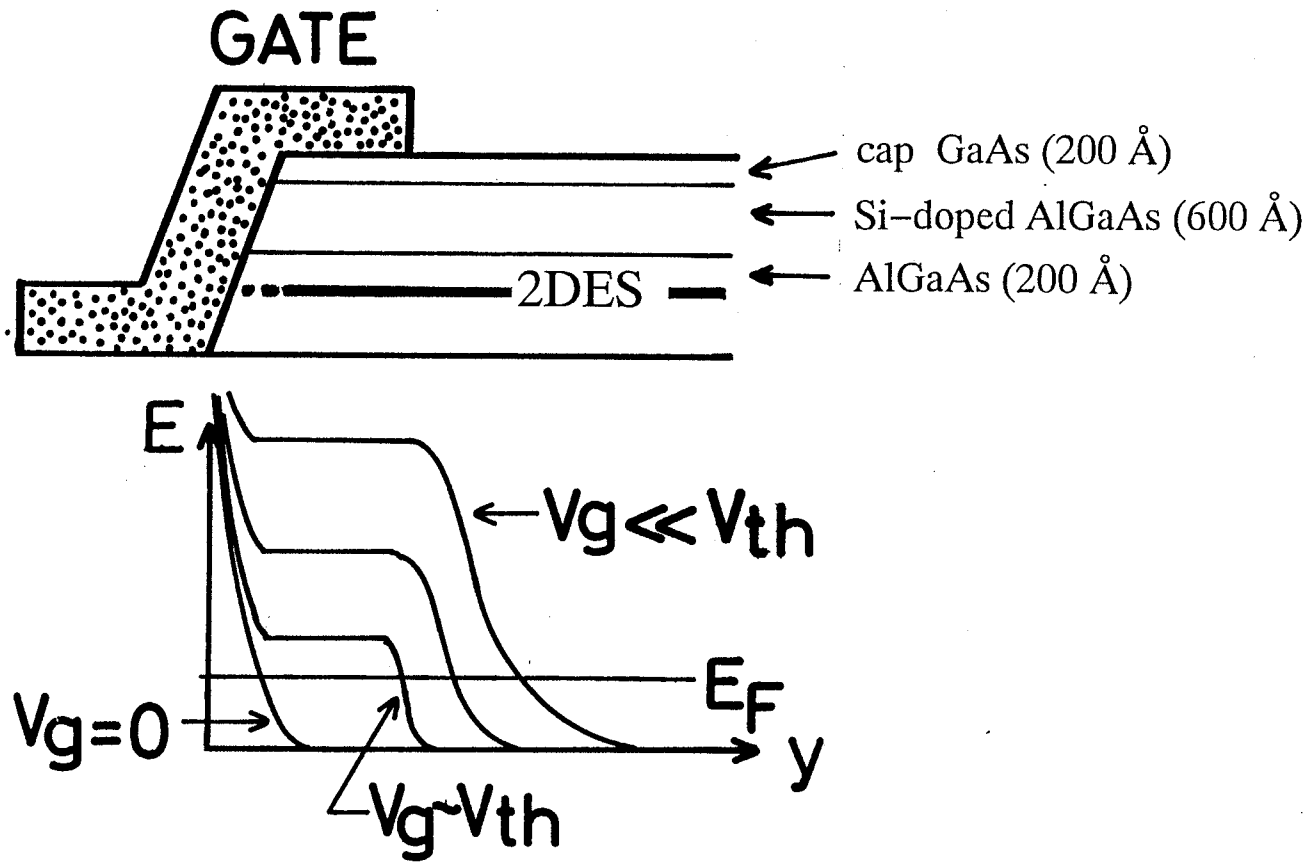

Fig. 55. Schematic representation of the electrostatic confinement potential. Lowering V_g, the depletion region expands from the edge of the gate, the spatial profile of the potential at E_F changes.

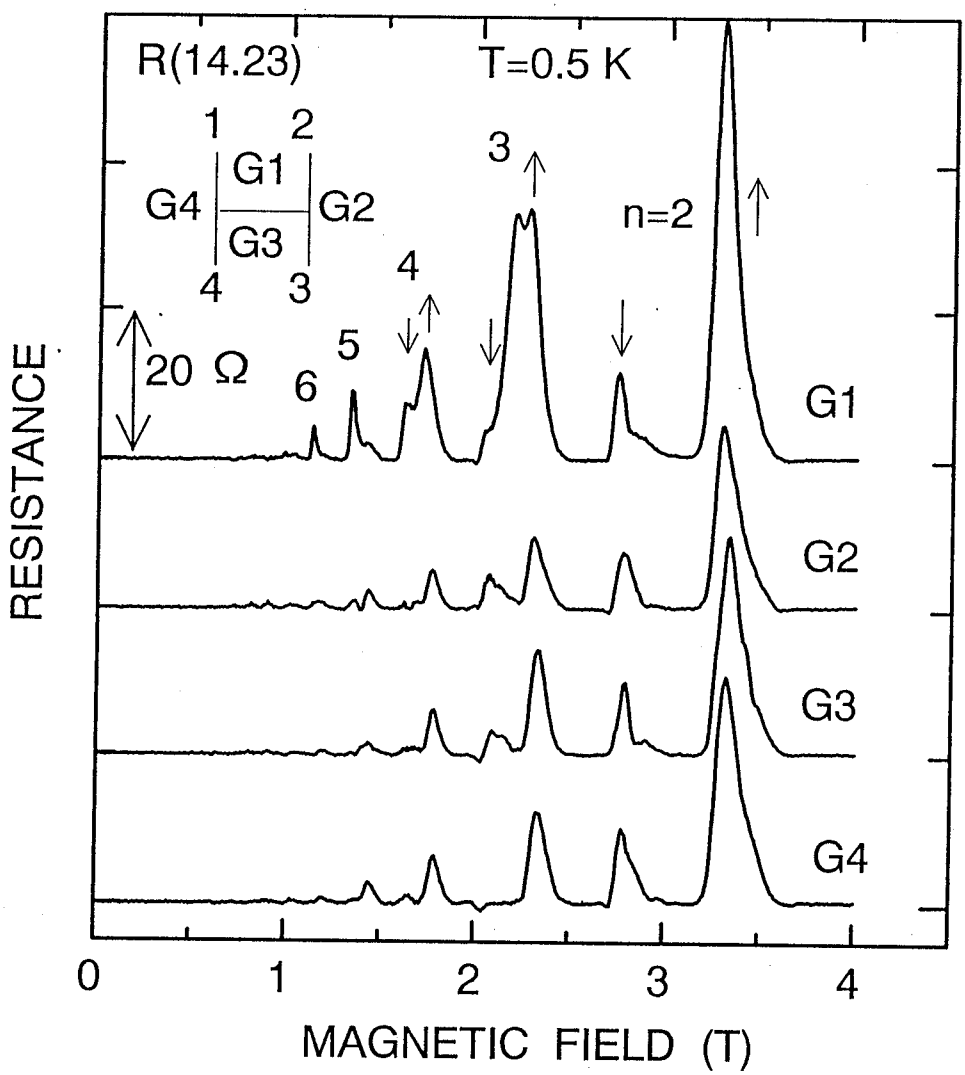

Fig. 56. Nonlocal resistance R(14,23). One gate G_i is applied −2.0 V, and others are biased at −0.4 V. The gate G_1, along the pathway from the current probe (1) to the voltage probe (2) affect the observed resistance.

4.2.9 Magnetocapacitance and edge state in quantum Hall regime

Magnetocapacitance in a two dimensional electron system (2DES) showed the quantum oscillations and minima at the quantum Hall plateaus[30–34]. There were two kinds of interpretation about the origin of the quantum oscillations; a 'DOS (density of states) model' and a 'resistive plate model'. In the DOS model[32,33], the measured capacitance consists of series capacitance of the barrier layer capacitance between 2DES and the metal gate (C_b), and the channel capacitance, which is proportional to DOS of 2DES at the Fermi level (E_F). When E_F is in the localized state between the Landau levels, DOS becomes small and the minima of measured capacitance would be observed. In the resistive plate model[31], the total capacitance is determined by the distributed system of C_b and the resistive plate with σ_{xx}. The minima of the capacitance is due to the minima of σ_{xx}, when E_F is between the Landau levels. Since the samples with the Corbino geometry are used in the resistive plate model, there is no influence of the edge channels on the measured capacitance. In this section, the influence of the edge channels on magnetocapacitance is discussed.

The samples were made of the GaAs/AlGaAs heterostructure wafers. The thickness of non-doped AlGaAs, doped AlGaAs and non-doped GaAs cap layer is 200Å, 600Å and 200Å, respectively. The carrier density N_s= 2.8x10^{11} cm^{-2}, and the mobility μ= 3.7x10^5 cm^2/Vs at 0.5 K, respectively. The Schottky gate was formed by evaporating Au on the GaAs cap layer. Schematic view of the sample is shown in Fig. 57(a). The differential capacitance with respect to the gate voltage between the probe and gate was measured by a capacitance bridge with a modulation frequency of 1 kHz. After this, differential capacitance was abbreviated to capacitance and the gate area (S) was defined as the area of 2DES which is covered with the Schottky gate, as shown hatched region in Fig. 57(a).

The modulation voltage (1 mV) is so small that further reduction did not influence the results.

In Fig. 57(b), a typical magnetocapacitance is shown, with the Hall resistance which was measured in a Hall bar sample made from the same wafer. The capacitance shows minima at the Hall plateaus. The measured capacitance at zero magnetic field agrees very much with the calculated value of a two-plate capacitor (C_b) in the measured geometry. The capacitance shown is the corrected one, after the stray capacitance is subtracted from the measured one, The stray capacitance ($\approx$2 pF) was estimated from the capacitance at the negative gate voltage enough to deplete 2DES under the gate.

To examine whether the magnetocapacitance is related to the DOS of 2DES as predicted from the DOS model, the capacitance is measured with various gate areas, and same longitudinal edge length of the gated area as shown in Fig. 58. The capacitance at zero magnetic field is proportional to the gated area, while the bottom values of capacitances are almost same. In Fig. 59, the bottom values at various filling factor of the Landau levels ν are plotted with respect to the gated area. This result can not be understood by the DOS model, where the minima of the capacitance must be proportional to the gate area.

To investigate the origin of the bottom value of magnetocapacitance, the samples, with different edge lengths and nearly same gate area, are used, as shown in Fig. 60. The bottom values become larger with the edge length, although the capacitance at zero magnetic field is nearly same. The slight capacitance difference at zero field is due to the slight gated area difference. In Fig. 61, the bottom values at various ν are plotted with the edge lengths. The bottom values are nearly proportional to the edge lengths. The capacitance at the quantum Hall plateaus (at least its bottom values) is determined by the edge length. From these

experimental results, it is deduced that the capacitance at the quantum Hall plateaus is governed by the edge channels.

At an ideal quantum Hall plateau (σ_{xx}=0), the bulk state is fully localized and the electron conduction occurs only through the edge state at E_F. The induced charge caused by change of V_g in 2DES is not supplied to the bulk area but to the edge state region from the probe. At the quantum Hall plateaus, the effective area of the capacitor should be reduced from the total gated area to the edge region and then the capacitance shows minima. By this model, the widths of edge channels are estimated from the bottom values of the capacitance. The capacitance between a strip line (whose area is S^*) and an infinite metal plate is approximately given as;

$$C^* = \pi \varepsilon_b S^* / 2 d_b , \qquad (27)$$

d_b : the thickness of the barrier layer (1000 Å in this study),
ε_b : the effective dielectric constant of the barrier layer
(ε_b= 12.3 ε_0 in this study).

By substituting the observed bottom values for C^* in Eq.(27), the total widths of edge channels (W(ν)) are estimated by assuming that $S^* = W(\nu) L_e$, where L_e is the length of the edge channels under the gate. In Table 2, the estimated W(ν) with various filling factor is listed. The width W(ν) becomes larger with ν. The estimated W(ν) is much larger than the magnetic length ($\lambda=(\hbar / eB)^{1/2}$) and the cyclotron radius ($r_c = \hbar (2\pi N_s)^{1/2} / eB$) at E_F. For example, λ=110 Å and r_c=160 Å at ν=2 in this sample. In a qualitative picture of edge state considering the screening effect[35], it has been pointed out that the edge state is expressed as the compressible liquid in 2DES. Chklovskii *et al.*[29] calculated the self-consistent electrostatic potential near the edge and showed that the electrostatic potential and

the Landau levels become flat in the compressible liquid (the edge state) and the width of edge state broadens. The total width of edge state(W(ν)) is given approximately as $4\ L_d\ \nu^2 / (2\nu+0.5)$, where L_b is the width of the depletion layer at the sample boundary. Since L_b is estimated as 0.2 – 0.5 μm, the calculated W(ν) is an order of microns and comparable to the measured W(ν). However, in this calculation the spin degeneracy effect is not considered. The effect of finite σ_{xx} at higher ν (lower magnetic fields) should cause the overestimation of W(ν) in Table 2. The more quantitative discussion should be given in future.

The measured W(ν) at V_g=+0.1 V is narrower than that at V_g=0 V, as shown in Table 2. With increasing V_g, N_s in 2DES increases and L_d becomes narrower due to the screening effect. The calculation of Chklovskii *et al.* showed that W(ν) is proportional to L_d and W(ν) decreases with increasing N_S. As shown in section 4.2.8, the nonlocal resistance in a sample surrounded by the Schottky gates becomes stronger by reducing the gate voltage[23]. This is explained by the enhancement of decoupling of the edge and bulk states due to the increase of L_d. This trend is consistent with the present experiment.

In summary, the bottom values of the magnetocapacitance at the quantum Hall plateaus is not proportional to the gate area but the edge length. These results can not be explained by the conventional interpretation of magnetocapacitance , where the capacitance is directly related to the density of states of a two dimensional electron system. The bottom values of the magnetocapacitance is decided by the effective area of edge states, where the carrier can be supplied from the electrode. From this model, the total width of edge states was estimated, which is much larger than the magnetic length and the cyclotron radius. This estimated value is compared with the calculated one from an electrostatic theory considering the screening effect. The influence of the gate voltage on the edge states was also examined.

TABLE 2. Estimated total width of edge states W(ν) at V_g=0 and 0.1V.

filling factor (ν)	2	4	6	8	
W(ν) (μm)	0.9	3.5	8.0	21	at V_g= 0 V
	0.3	2.9	4.8	10	at V_g= 0.1 V

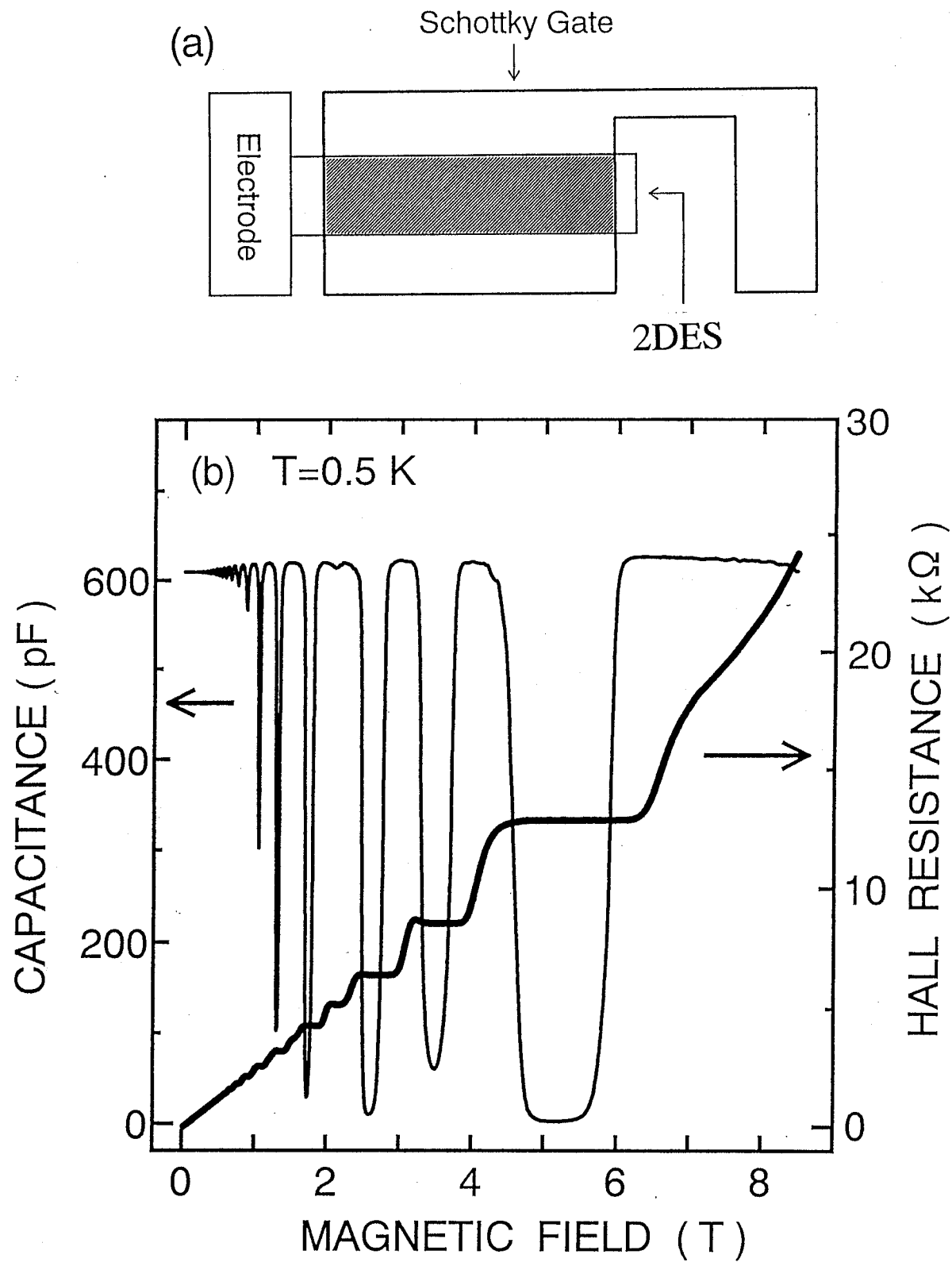

Fig. 57. (a) Schematic view of sample used in magnetocapacitance measurement. (b) Magnetocapacitance and Hall resistance measured from the same wafer.

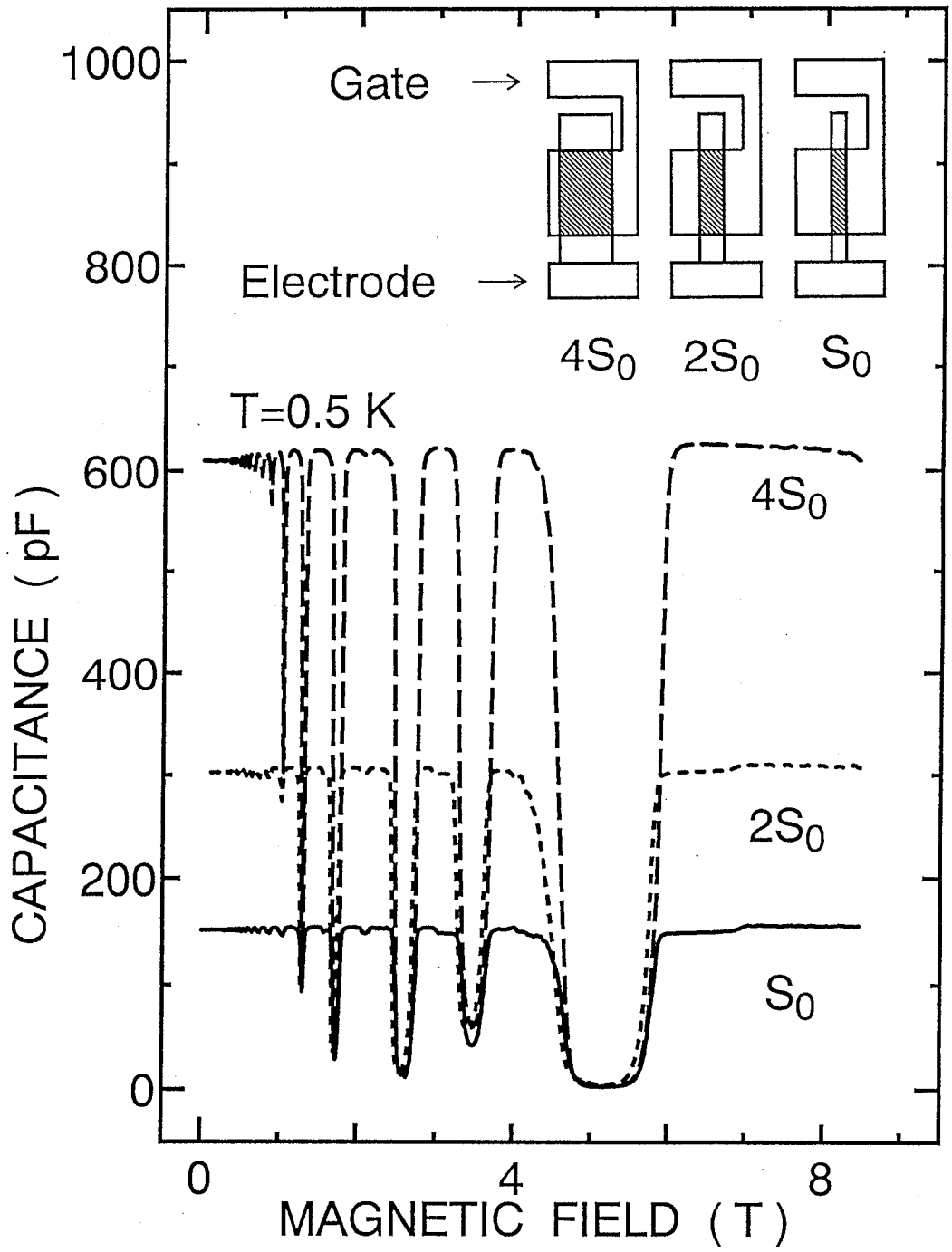

Fig.58. Magnetocapacitance of the samples with various gate areas and same edge length of the gate as shown schematically in the inset.

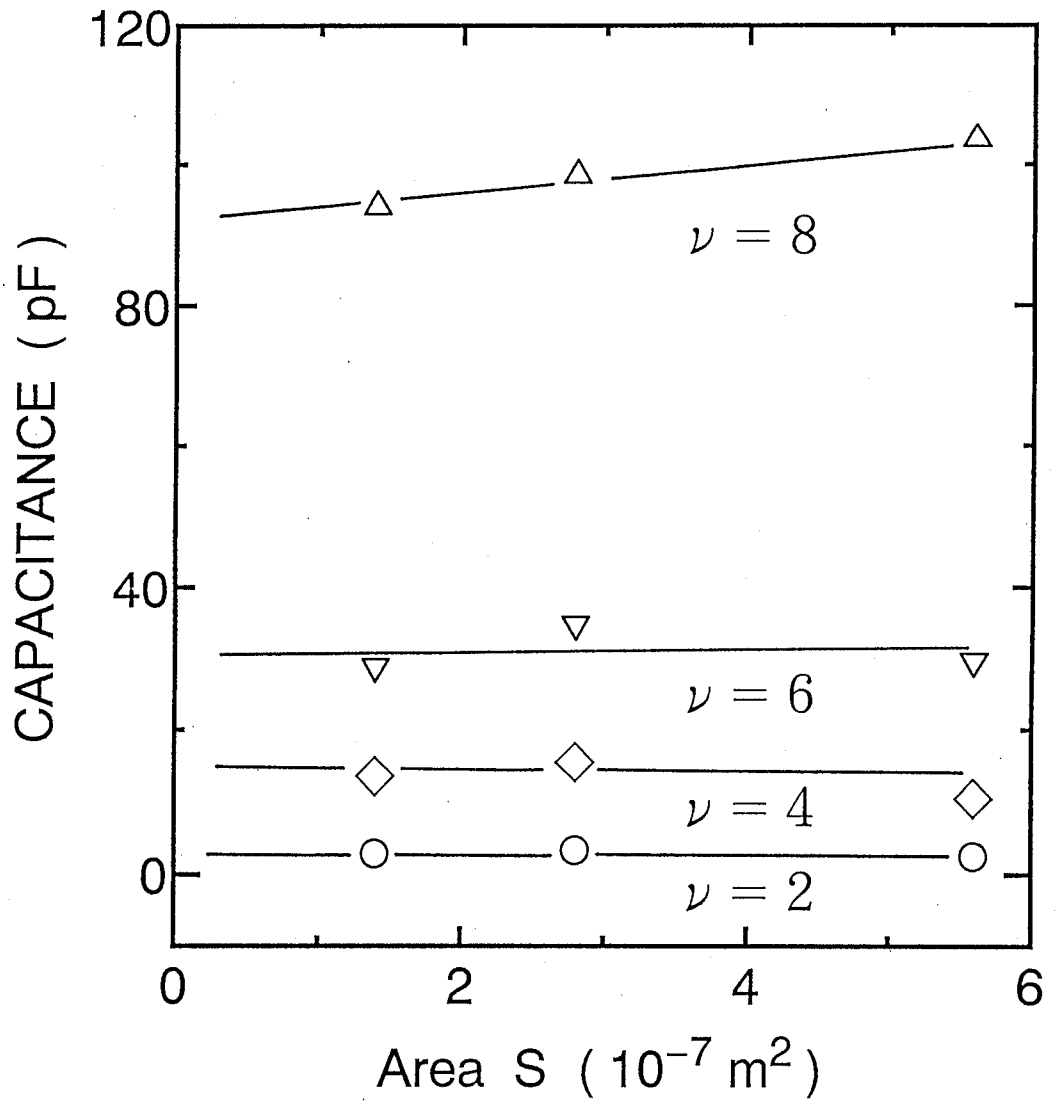

Fig. 59. Bottom values of magnetocapacitance at various filling factor (ν) are plotted with respect to the gate area. Bottom values are nearly independent of the gate area. Solid lines are provided to a guide to the eye.

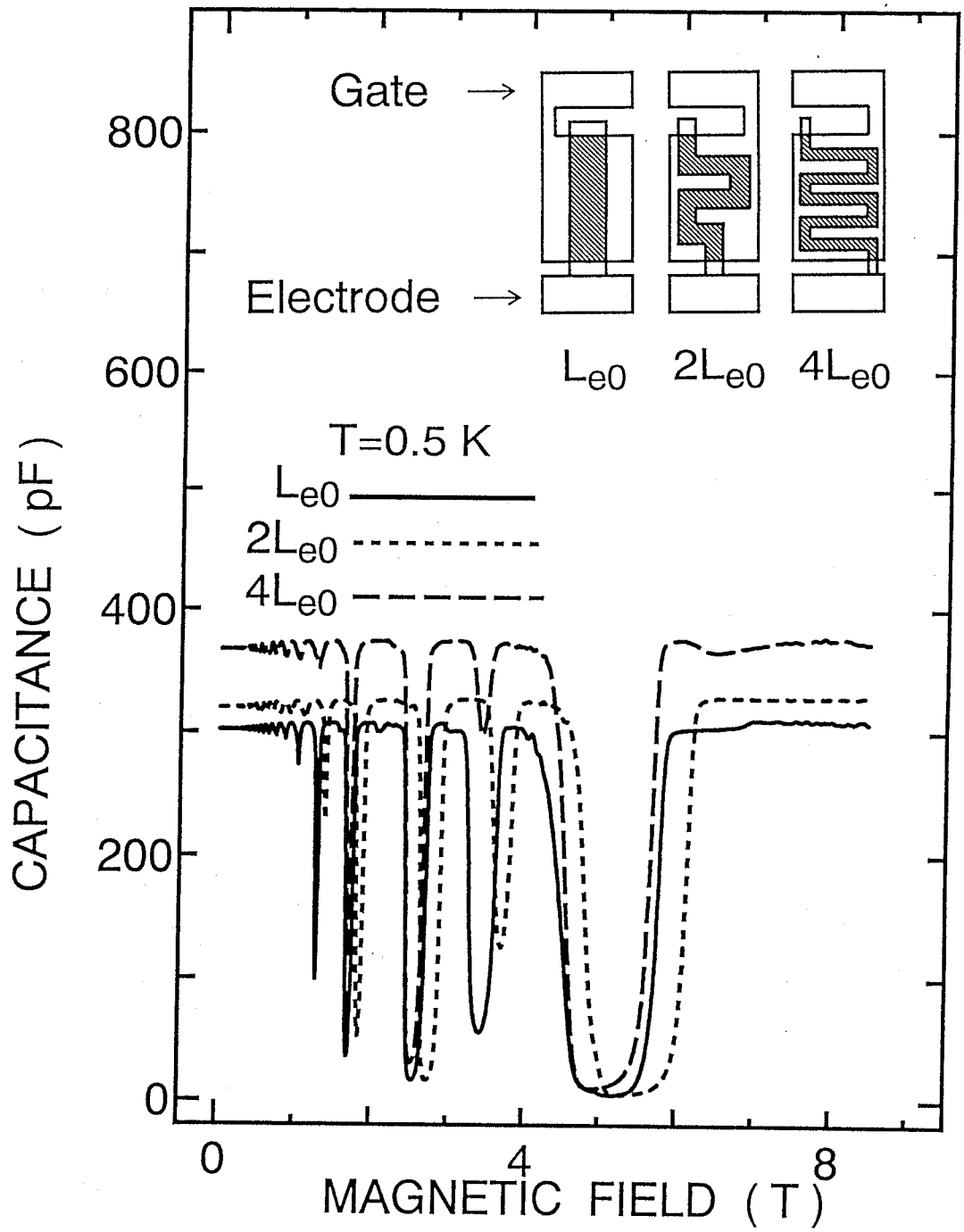

Fig. 60. Magnetocapacitance of the samples with various edge lengths and nearly same gate area as shown schematically in the inset.

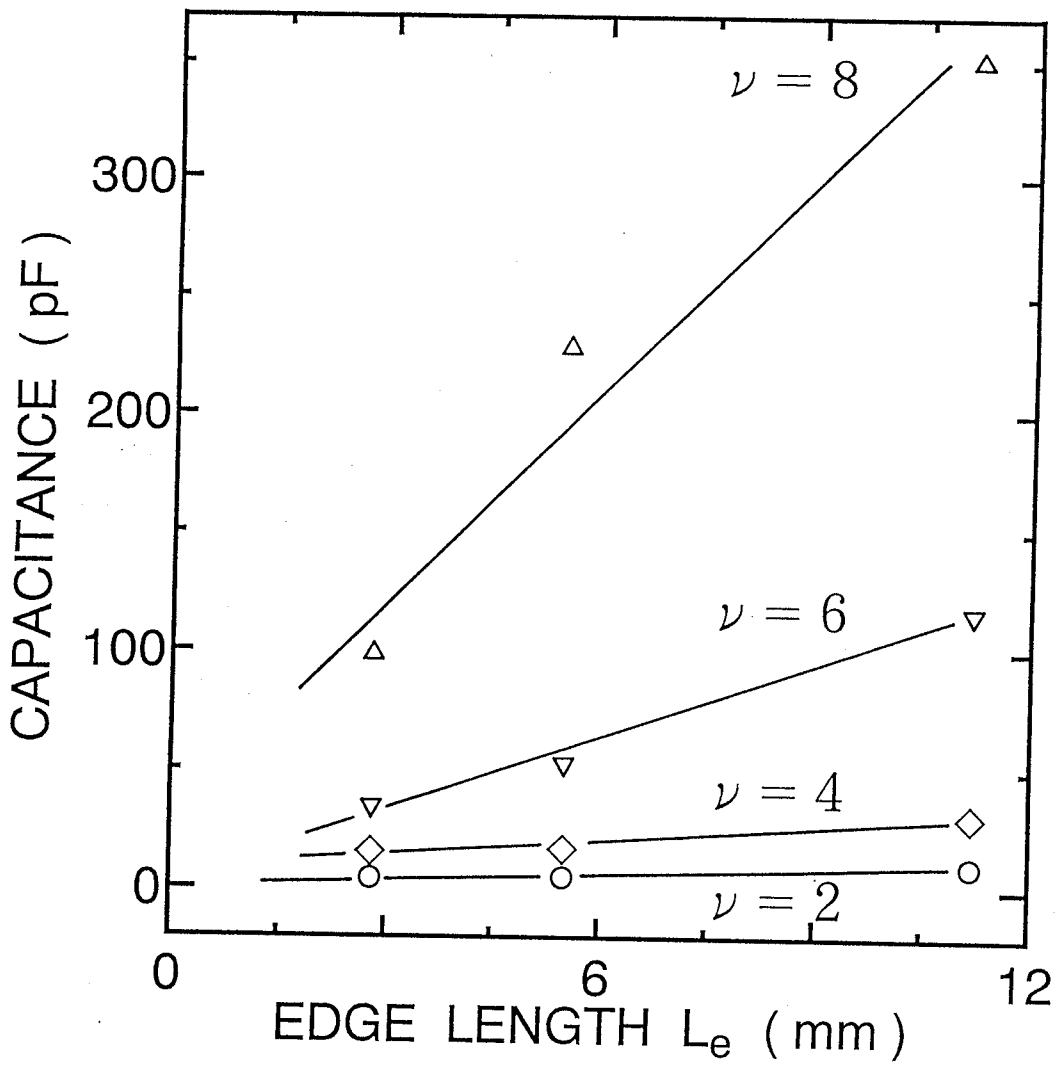

Fig. 61. Bottom values of magnetocapacitance at various ν are plotted with the edge lengths. Bottom values are proportional to the edge length. Solid lines are provided to a guide to the eye.

4.3 Edge state in Si-MOS FETs

4.3.1 Introduction

The SdH oscillation of the nonlocal resistance was originally observed in the high mobility GaAs/AlGaAs heterostructure[6,7] as discussed in the previous section. This phenomenon is understood by taking account of both edge and bulk (extended) states. Since the mobility of the Si-MOS FETs is much less (typically $\approx$ 1/100) than that of the GaAs/AlGaAs system, the edge state has not been investigated in the Si-MOS system. But the observed resistivity θ_{xx} and θ_{xy} depended strongly on the sample shape of the Hall bar type, and did not agree with the value obtained in the Corbino geometry[4] which is only affected by the longitudinal conductivity σ_{xx}. The phenomena strongly suggest that the current carrying edge states exist in the Si-MOS FETs at high magnetic fields. To investigate the edge current in this system, the nonlocal SdH effect has been studied in three samples with different mobility, and the results of the experiment will be discussed by taking account of the edge state[36].

4.3.2 Samples

The Hall devices of the Si-MOS structures used for this experiment were 250 μm long, 50 μm wide with two pairs of Hall probes, as shown in Fig. 62. Three samples A, B and C were used. The SiO_2 layer of the sample A and B was made by thermal annealing in diluted O_2 gas, and made by Ar/O_2 spattering[14] for the sample C. The maximum mobility, affected by the condition of the interface between Si and SiO_2, were different each other, as shown in Table 3. The probes consisted of n^+ high-doped region and a contact metal (Al). The contact resistance is below 50 Ω at 4.2 K. The measurements were performed at a

temperature of 0.5 K, otherwise specified. At the nonlocal resistance measurement, the separation length between the nominal current path and the voltage probes is 90 μm (Fig. 62(b),(c)). In the Landau levels in the Si–MOS FETs, there are two kinds of degeneracies, due to the spin and valley in the k–space. The spin–split from n–*th* Landau level is denoted by n↑ or n↓. The valley splitting is also observed at the n≤1 Landau levels, but it is not discussed.

4.3.3 Nonlocal conduction through edge channel in Si–MOS FETs

The magnetic field dependence of the transport properties of the sample A is shown in Fig. 63. The applied gate voltage is 3.5 V ($Ns=3.9\times10^{11}$ cm^{-2}, $\mu=1.25\times10^{4}$ cm^2/Vs) and current is 30 nA. The longitudinal resistance R_L shows SdH oscillations, and the plateaus at the quantum Hall resistance appear in R_H (Fig. 63(b)). The nonlocal resistance R_{NL} shows peaks at high magnetic fields which were observed in the GaAs/AlGaAs wires. One might think that the origin of the R_{NL} would merely be the ordinary four terminal resistance, which should be measured by the van der Pauw method. Indeed, a very small value of the R_{NL} ($\approx$ 6 Ω) is measured at zero or low magnetic fields (Fig. 63(a)) and it is due to the relatively large sample width (50 μm) as compared with the separation length. But the high magnetic field behavior of the R_{NL} can not be understood by considering only the macroscopic conductivity tensor. The magnetic field dependence of R_{NL} and R_L is quite different, especially at high magnetic fields as shown in Fig. 63. The oscillation of R_{NL} is caused by the edge and bulk states, as discussed in section 4.1.3. At low fields, as the energy levels of the edge and bulk states are close to each other, electron scattering frequently occurs and the nonlocal resistance R_{NL} is reduced. Note that the peak heights of the R_{NL} shows drastic growth with increasing magnetic fields, and R_{NL} is practically zero at the field, where the quantum Hall effect occurs (B=4 T and B=8 T), similar to the result

obtained in the high mobility GaAs/AlGaAs system[6,7].

The peak amplitude of the SdH oscillation of R_L and R_{NL} at Landau levels (1↑) and (1↓) for several magnetic fields is shown in Fig. 64 for sample B. At respective magnetic fields, the gate voltage is so tuned as to show the resistance peak of the SdH oscillations at the Landau level. The peak value of σ_{xx} and σ_{xy} at a certain Landau level is independent of the magnetic fields[2], and the observed R_L peaks are almost constant for various magnetic fields. Since the scattering rate among edge and bulk state is inversely proportional to the magnetic fields, the R_{NL} is suppressed with reduction of magnetic fields.

The gate voltage dependence of R_{NL} and R_L at B=8 T is shown in Fig. 65 (a),(b),(c) for samples A, B and C, where the currents are 30 nA, 0.3 μA, 0.3 μA respectively. The measured resistance R_{NL} and R_L are not changed by varying currents 30 nA or 0.3 μA both in the sample B and sample C. In all samples, R_L shows SdH oscillations whose amplitude profiles are almost equal to each other, but the amplitudes of the R_{NL} SdH oscillations are quite different amount in different samples. In the high mobility sample A, the amplitude is about two times as large as those of other low mobility samples. The SdH oscillations due to the second Landau levels, which are spin-split and indicated by (2↑) and (2↓), appear in the gate voltage $10.2 < V_g < 14.6$ V. As shown in Fig. 65(a), peak height ratio of R_L for (2↑) and (2↓) is 1.3:1 , but that of the R_{NL} is 6.5:1. The same behavior is observed at other Landau number n=1 and 3. Similar trend is observed in the sample B and C, but peak heights are lower than those of the sample A. The effect due to the spin-splitting Landau level in R_{NL} SdH oscillations is more sensitive to the sample quality than that of the R_L (Fig.65). For example, when the energy of the bulk state ($=E_F$) coincides with Landau level (2↑), the topmost edge state is (1↓). The energy difference of the Landau levels between the bulk state (2↑) and

topmost edge state (1↓) is nearly equal to cyclotron energy (Fig.66(a)). The spatial separation between edge and bulk states is large enough not to interact with each other. On the contrary, when the E_F coincides with (2↓), the topmost edge state is (2↑) and the corresponding energy difference of the Landau levels is the 'Zeeman energy', which is much smaller than the cyclotron energy. In this case, many of the edge state electrons are scattered to the bulk state which is spatially close to the edge state, and R_{NL} is reduced (Fig.66(b)).

The current dependence of the R_{NL} and R_L of the sample B at B=8 T is shown in the range 0.3–10 μA in Fig. 67. The profiles of the R_L change slightly as the current is increased. On the other hand, the amplitude of the R_{NL} decreases with increasing current. We have checked that both R_L and R_{NL} have not been changed with current changing from 30 nA to 0.3 μA. The current dependence shows a critical behavior with abrupt decrease of R_{NL} with increasing current level (Fig. 67).

In Fig. 68, we demonstrate the temperature dependence of the R_{NL} and R_L of the sample B at B=8 T and the current 0.3 μA. The peak profiles of both R_{NL} and R_L does not change between T=0.5 K (solid line) and T=1.8 K (dashed line). At 4.2K the peak heights of R_{NL} are reduced about 1/3 compared with those at 0.5K. The nonlocal SdH effect decreases with increasing temperature before the QHE, as shown the minimum plateaus of R_L=0, disappears.

As the electrons in edge states are scattered and equalized their chemical potential are equalized to the bulk state, the nonlocal SdH effect is reduced with increasing current and/or temperature. These results strongly suggest that the transport properties of the high quality Si–MOS FETs in the QHE regime are affected by the edge state. The nonlocal SdH effect is one of the evidences that

the edge state plays an important role in the Si–MOS FETs at high magnetic fields and low temperatures.

Table 3: Device parameters of the Si–MOS FETs

sample	peak mobility (0.5 K)	process of the gate oxide
sample A	1.38×10^4 (cm^2/Vs)	thermal annealing
sample B	1.37×10^4 (cm^2/Vs)	thermal annealing
sample C	7.3×10^3 (cm^2/Vs)	Ar/O_2 sputtering

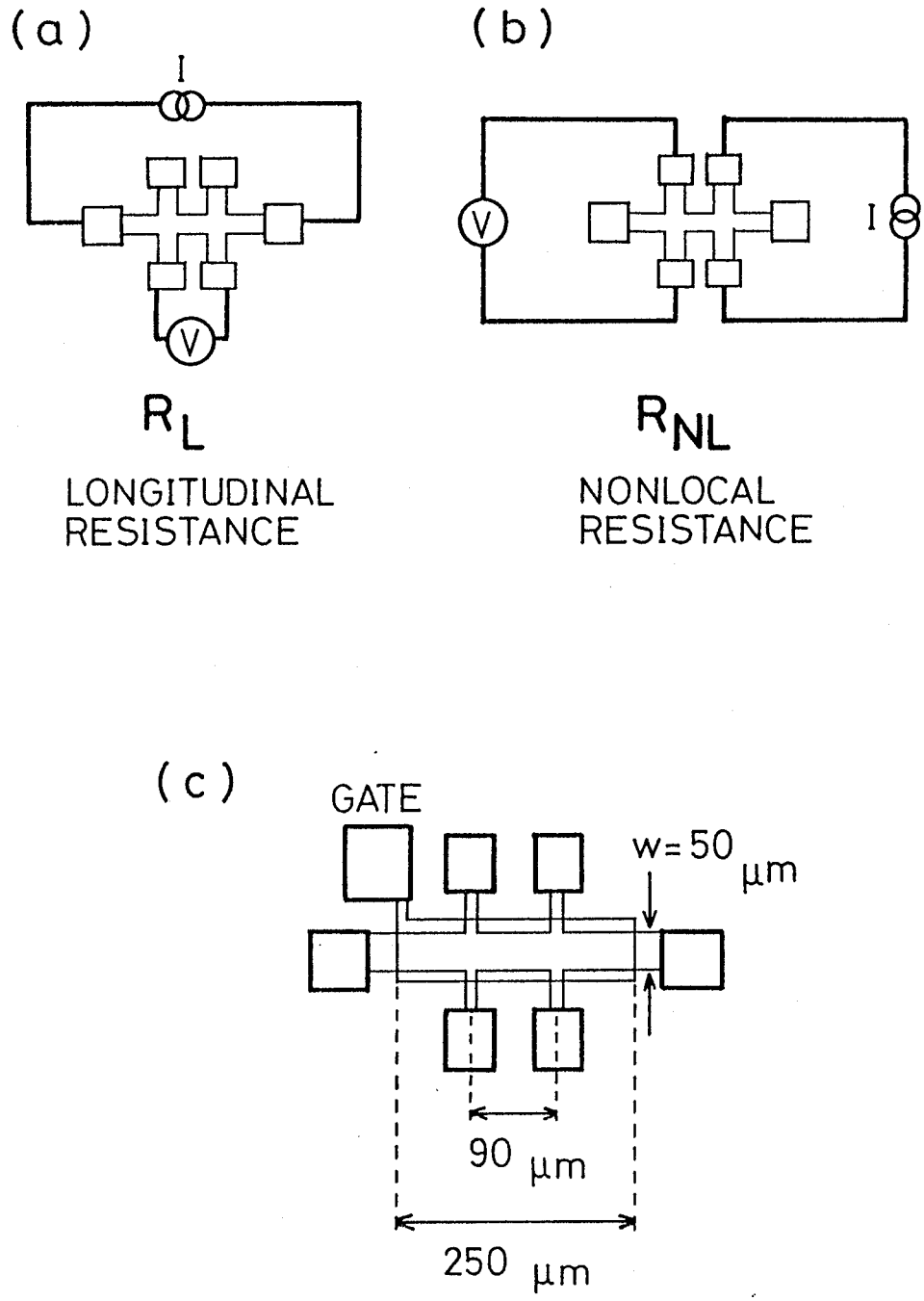

Fig. 62. Schematic layout of the four-terminal measurements and the samples. (a) Ordinary longitudinal resistance R_L. (b) The nonlocal resistance R_{NL} where the voltage probes are spatially separated from the nominal current path. (c) Schematic view of samples used in this experiments.

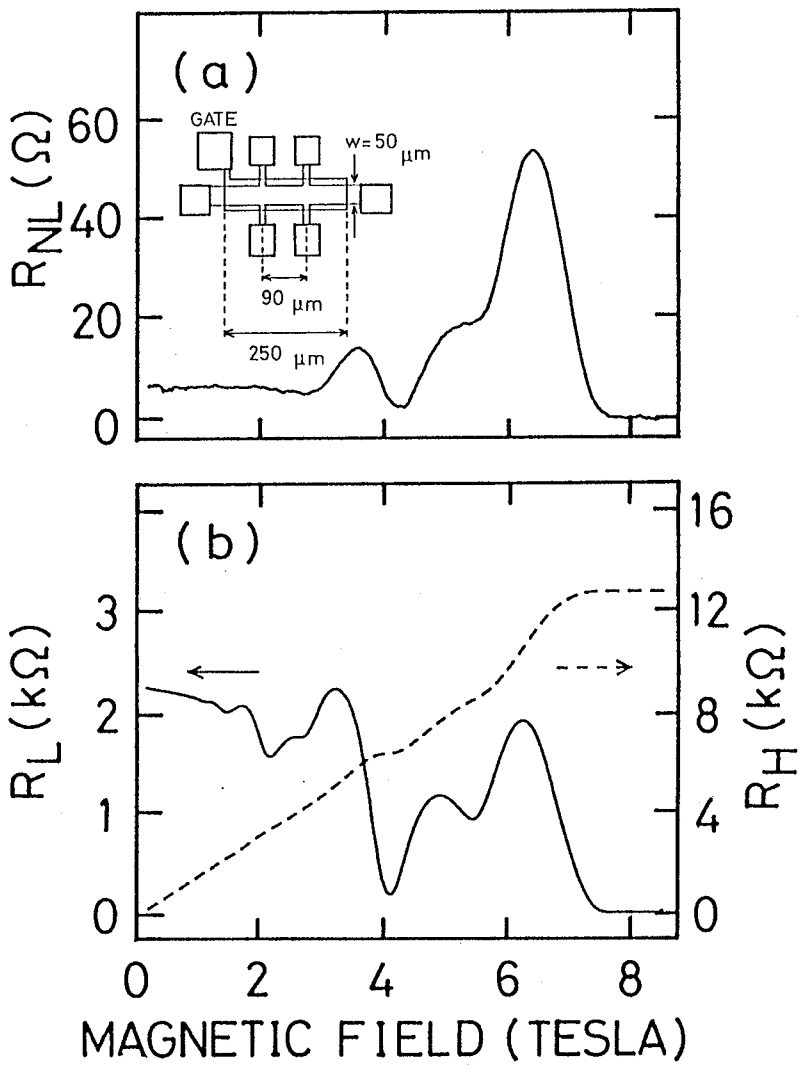

Fig. 63. (a) Nonlocal SdH oscillations and (b) longitudinal resistance R_L (solid line) and Hall resistance R_H (dashed line) in the sample A at T=0.5 K with V_g=3.5 V, I=30 nA.

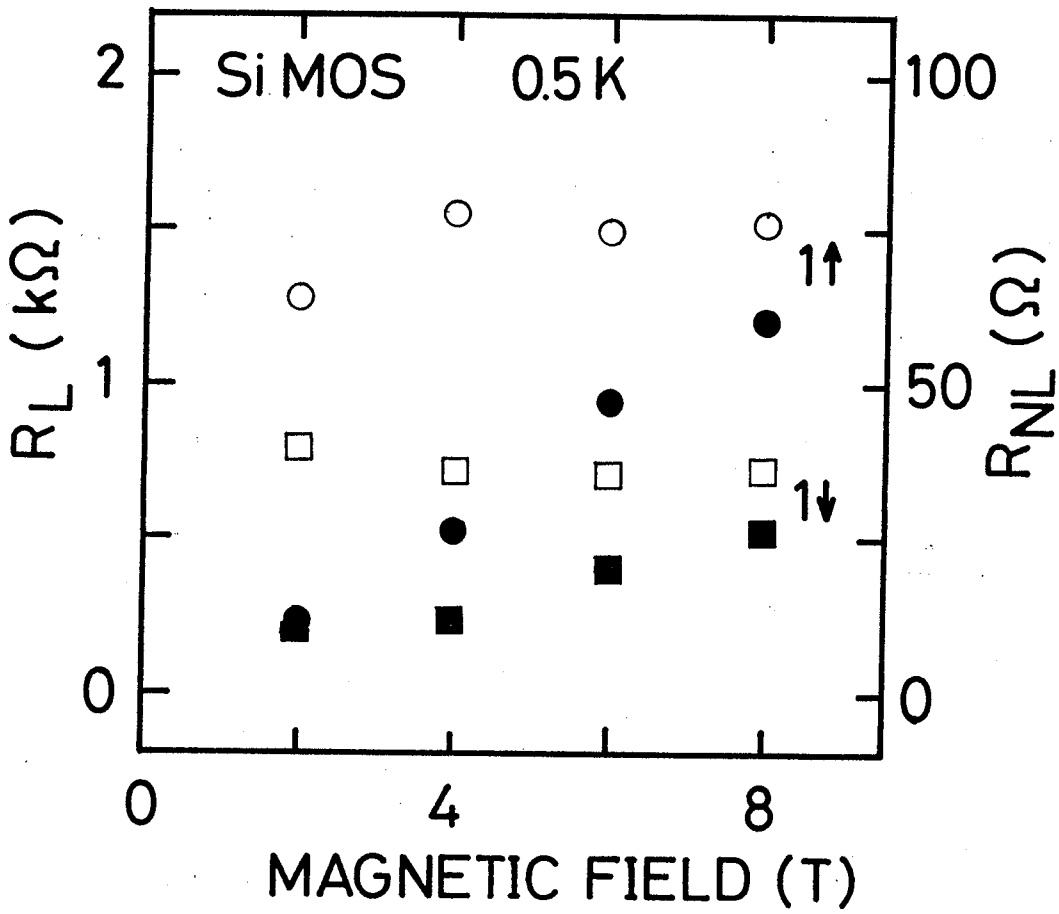

Fig. 64. Peak values of the SdH oscillation of R_L (open marks) and R_{NL} (closed marks) at Landau levels (1↑) (circle marks) and (1↓) (square marks) of the sample B. The gate voltage was tuned to show the peaks of the SdH oscillation from Landau levels (1↑) and (1↓) at respective magnetic fields. The temperature and current were T=0.5 K and I=0.3 μA.

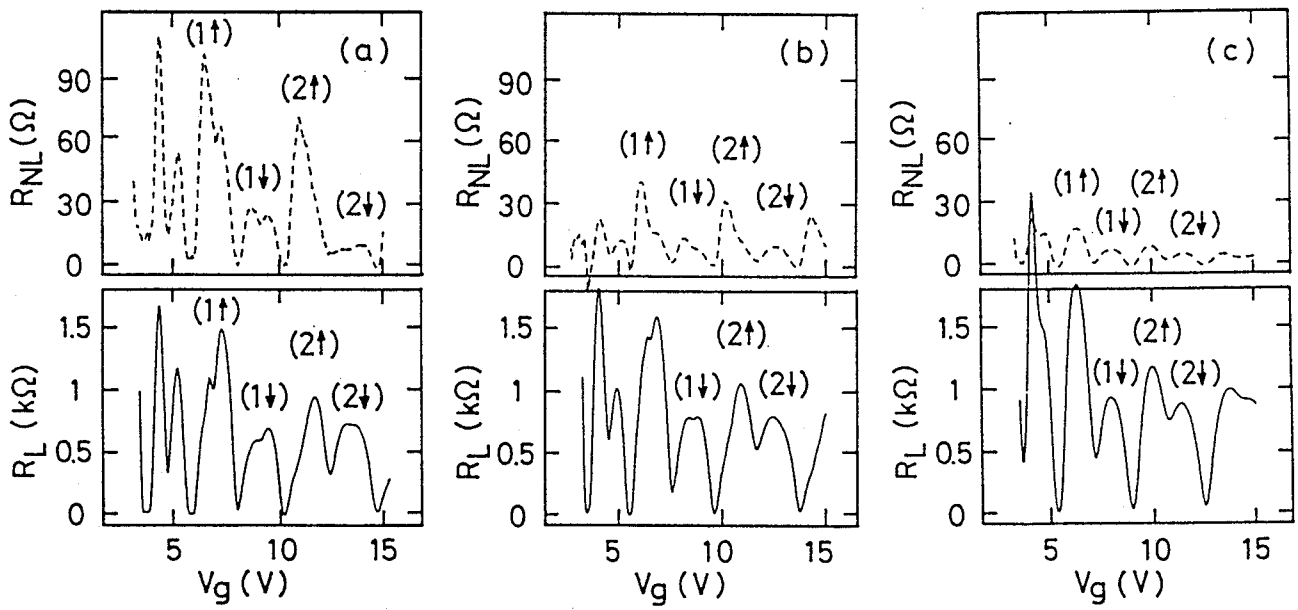

Fig. 65. Nonlocal resistance R_{NL} (dashed line) and longitudinal resistance R_L (solid line) as a function of the gate voltage at T=0.5 K and B=8 T. (a) for sample A with I=30 nA, (b) for sample B with I=0.3 μA, (c) for sample C with I=0.3 μA. The mobility of the sample μ is shown in table Fig.a, $\mu_A \geq \mu_B >> \mu_C$. The spin-split Landau levels n denoted by (1↑), (1↓), (2↑), (2↓) are shown.

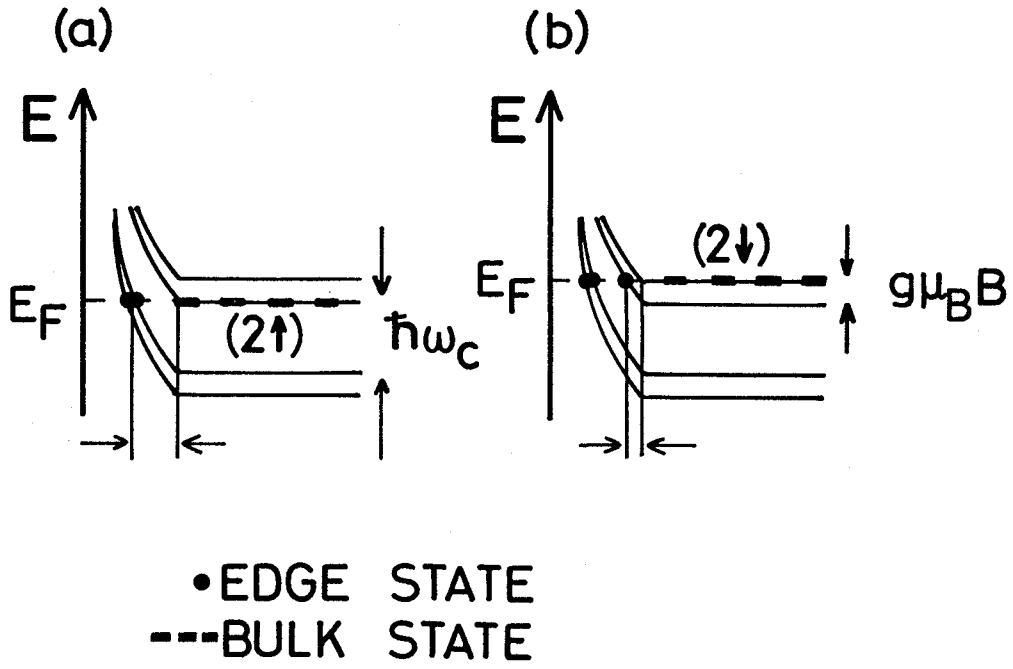

Fig. 66. Schematic illustrations which explain the reduction of R_{NL} at Landau levels (n↓). (a): When E_F coincides with (2↑), the spatial separation between the bulk and edge states is much larger than in case E_F coincides with (2↓). (b): The energy difference of the Landau levels between edge and bulk state is 'Zeeman energy $g\mu_B B$' which is much smaller than $\hbar\omega_c$. The spatial separation between edge and bulk states are small enough to interact each other.

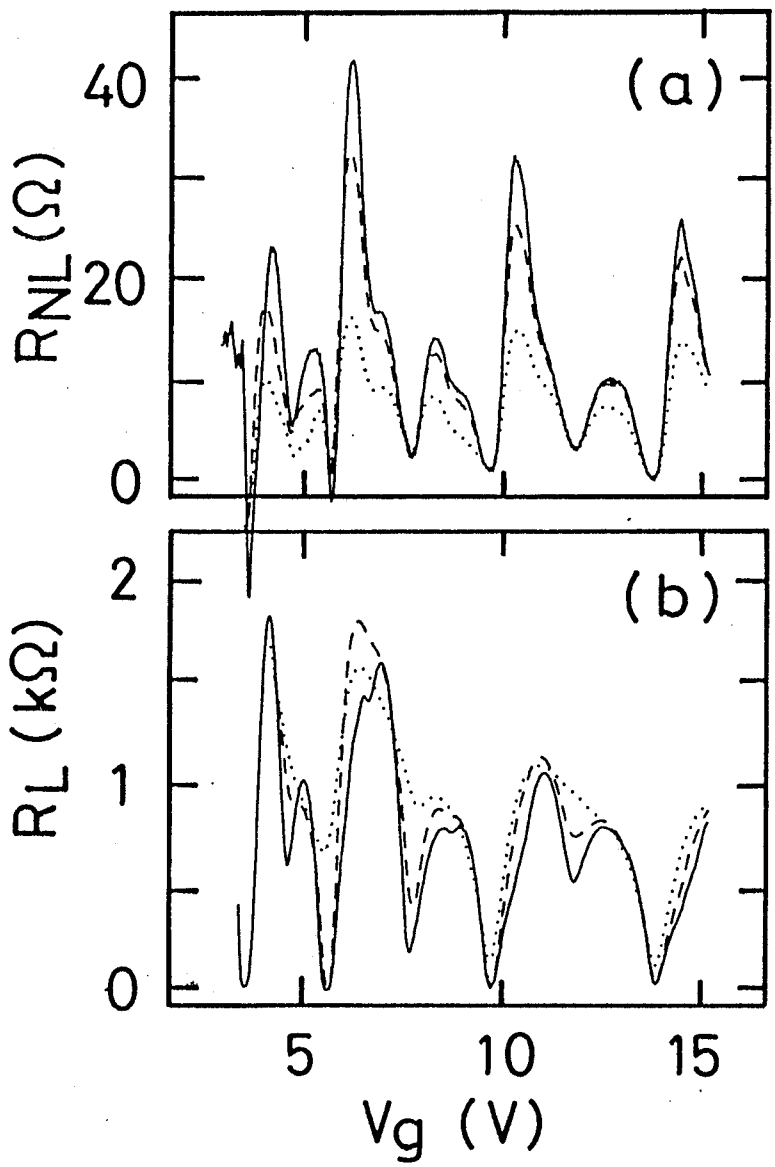

Fig. 67. The current dependence of the nonlocal resistance R_{NL} (a) and longitudinal resistance R_L (b) at T=0.5 K, B=8 T with current 0.3 μA (solid line), 3 μA (dashed line), 10μA (dotted line).

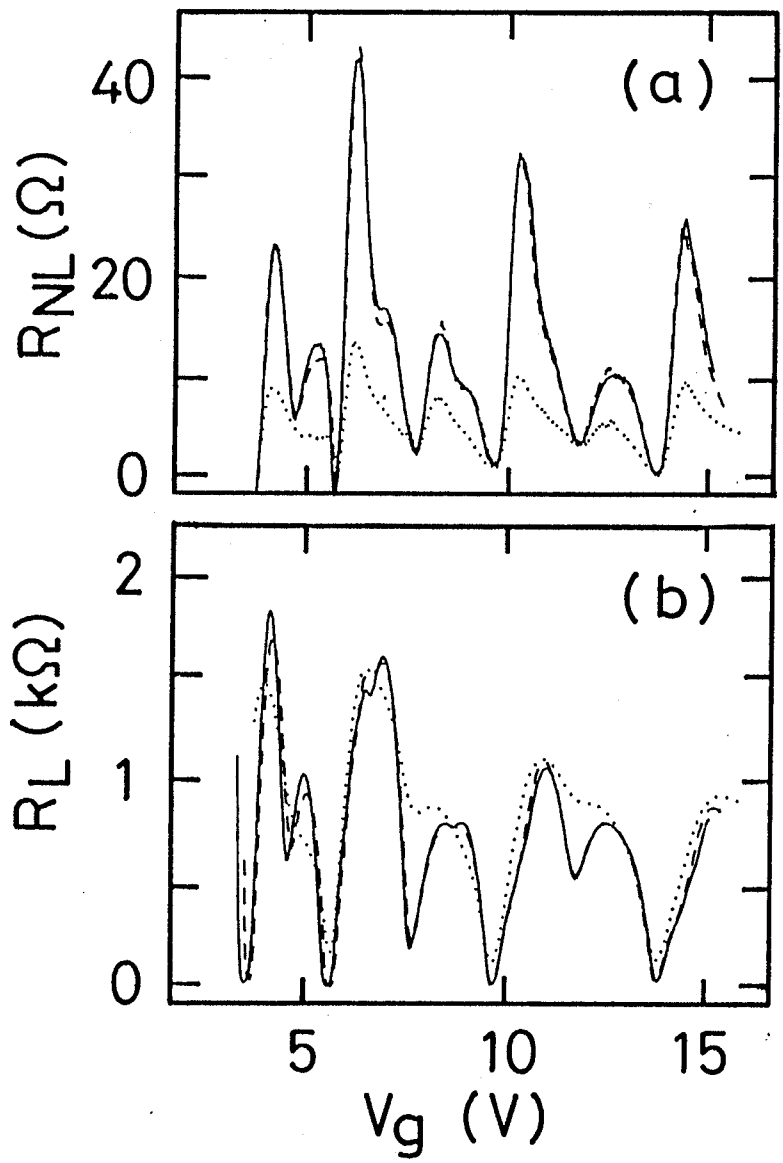

Fig. 68. The temperature dependence of the nonlocal resistance R_{NL} (a) and longitudinal resistance R_L (b) at B=8 T with I=0.3 μA. T=0.5 K (solid line), 1.8 K (dashed line), 4.2 K (dotted line).

5 Concluding Remarks

The quantum transport of two-dimensional electron systems (2DES) in GaAs / AlGaAs heterostructures and Si-MOS FETs is investigated at high magnetic fields up to 8 T and low temperatures between 0.5 and 4.2 K.

The mesoscopic size ($\approx\mu$m) and macroscopic size ($\approx$mm) multi-terminal wires are fabricated from a GaAs/AlGaAs heterostructure wafers. The magnetoresistance shows nonlocal features, such as a geometry dependent resistivity, an influence of the contact probe on the transport and a current dependent resistivity. These phenomena can not be explained only by considering local conductivity σ_{xx} and σ_{xy}. The nonlocal features in 2DES are understood as the edge state and bulk state coexist and act as current carrying channels.

A nonlocal resistance, where the voltage probes are well separated from the nominal current path, shows peaks similar to usual SdH oscillations. The appearance of the nonlocal resistance at the separation length $\Delta L = 0.5$ mm suggests that the equilibration length of the chemical potential between edge and bulk currents may be more than 0.5 mm. It is shown that the observed nonlocal resistance scales with $\Delta L/W$ and agrees with those of the calculated values based on the Landauer-Büttiker formula. The nonlocal features due to the edge current is reduced with increasing temperatures, current, and carrier concentrations, because the interaction (scattering) between bulk and edge channels becomes stronger.

In the cases that the extra probes are contained between the current and voltage probes, the nonlocal resistance is much reduced. The extent of the nonlocal resistance depends on the sample geometry and the number of edge channels.

A negative four-terminal resistance is observed when the property of a probe is

not ideal. The anomalous transmission probability of the edge and bulk channels from the probe can cause an inverse population of electrons in the channels when the probe is used as a current source. By using the probe as a voltage probe, the chemical potential of the channels are selectively detected. The negative resistance is understood by considering the property of the non-ideal probe and non-equilibrium conduction in the edge and bulk states. The high contact resistance probe is apt to have an anomalous transmission probability to the edge and bulk channel, which is smaller for the channels belonging to the lower index Landau levels. It is emphasized that the fabrication process of the probes is very much important to make a *'good probe'* for electron transport measurement, such as the precision measurements of QHE.

The influence of the property of the probe on the quantum transport is studied by using the probe whose transmission probability of the in and out going channels is artificially controlled by the gate. It is demonstrated that the anomalous selective transmission of channels can be realized with a gate controlled Corbino-like probe, and negative resistance appears in the *'non-ideal'* probe. The extent of chemical potential equilibration among edge channels by the probe is estimated based on the Landauer-Büttiker formalism. The reciprocity of the resistance is observed in the measurement with the non-ideal probe. The Landauer-Büttiker formula is valid to explain the transport property of 2DES using the non-ideal probes.

The influence of the bulk and edge states on the nonlocal resistance is investigated by cutting the bulk and edge current with the gate. The 'bulk current' corresponding to the down-spin Landau level peak of the SdH oscillations comes from the overlapping down-spin and up-spin states, while the up-spin Landau level peak comes from mostly the up-spin state. The influence of the extra probes on the transport has been examined by cutting the bulk and edge currents in the

extra-probes by the gate. The electronic transport is actually affected by the contact probe, since equilibrium of chemical potential among channels occurs in the probe.

The magneto-resistance of the GaAs/AlGaAs wires, whose brinks are covered with Schottky gates, is measured to investigate the influence of the confinement potential of the 2DES on the quantum transport. The nonlocal features of the electronic transport in 2DES is influenced by the confinement potential of 2DES at the sample edge. It is suggested that the mixing among channels is enhanced, when the gate voltage about its pinch off value is applied, because the spatial separation of the channel is closed.

The magnetocapacitance between a metal gate on the sample and 2DES in GaAs/AlGaAs heterostructure shows minima at the quantum Hall plateau regime. The bottom values of the magnetocapacitance at the quantum Hall plateaus is not proportional to the gate area but the edge length. It is found that the minimum capacitance is governed by the area of the current carrying edge state, and is not related to the density of states at Fermi level. The width of the edge state is estimated, and it is much larger than the magnetic length and the cyclotron radius.

In the Si-MOS FETs, the magneto-oscillation of the nonlocal resistance is observed, and its temperature and current dependence is similar to that observed in the GaAs/AlGaAs heterostructures. These results strongly suggest that the transport properties of the high quality Si-MOS FETs in the QHE regime are affected by the edge state. The nonlocal SdH effect is one of the evidences that the edge state plays an important role in the Si-MOS FETs at high magnetic fields and low temperatures.

The subjects to be investigated in future are listed as follows;

(1) In the capacitance measurements, the estimated edge width might be affected by the finite conductivity σ_{xx}. In order to estimate the edge channel width more precisely, the effect of the σ_{xx} should be considered.

(2) More quantitative analysis is needed to understand the nonlocal features of the quantum transport about the amplitude of the observed resistance, the effect of extra probes, and the extent of equilibrium of the chemical potential distribution among channels.

Acknowledgments

The author would like to acknowledge the many people who have helped him to create this thesis.

He would like to express his sincere gratitude to Professor Kazuo Murase for valuable discussions, direction, continuous support and encouragement. He also wishes to express his thanks to Professor Sadao Takaoka for guidance on the experiment, encouragement and stimulating discussions.

He thanks Mr. K.Tsukagoshi for assistance in the experiment on the mesoscopic system, Mr. T.Toshinou for his assistance in the Si–MOS experiment, and Mr. H.Kurimoto for experimental assistance on the contact resistance and capacitance measurements.

He is particularly indebted to Mr. Tatsuo Sawasaki for his collaboration on the experiment and valuable discussions.

The author would like to thank Dr. S.Nishi of Oki Electric Industry Co.,Ltd., and Mr. K.Kasahara of NEC Corp. for providing high mobility MBE grown wafers.

He also wishes to thank Dr. S.Suyama and Dr. T.Serikawa for providing high quality Si–MOS FETs devices.

The author gratefully acknowledges Prof. S.Namba and Prof. K.Gamo for providing facilities for microfabrication. He also would like to thank Dr. Y.Takagaki, Mr. F.Wakaya, Mr. J.Takahara and Mr. K.Mino for their support and helpful advice on microfabrication technology.

The author would like to thank Prof. J.Wakabayashi and Prof. S.Kawaji for helpful advice of the construction of the ^{3}He refrigerator system.

This work was supported by a Grant-in-Aid for Scientific research on priority Area, "Electron Wave Interference Effects in Mesoscopic Structure" from the Ministry of Education, Science and Culture.

The author acknowledges for financial supporting by JSPS Fellowships for Japanese Junior Scientists.

The author wishes to express his thanks to Prof. S.Ishida, Dr. S.Sugai, Dr.K.Inoue, Dr. O.Matsuda, and all the members of the Murase laboratory for their cooperation and encouragement.

Appendix 1

The properties of the probe T_0/T_1 and equilibration length of the chemical potential distribution L_e, as shown in Fig. 69, is estimated from the Landauer–Büttiker formalism at ν=2. Here, T_0 and T_1 is the transmission probability of the outer and inner edge channels. The chemical potential of edge currents coming from the probe (6) is denoted by μ_0. After passing the probe (1), the chemical potential of the edge current shows an inverse distribution;

μ_0 (outer edge) , (28)

and

$\mu_1 = \mu_0 + hI / e$ (inner edge) . (29)

They are equilibrated in the conducting path. The chemical potential just before the probe (2) is;

$\mu'_0 = \mu_0 + (1-m)hI / 2e$ (outer edge) , (30)

$\mu'_1 = \mu_0 - (1-m)hI / 2e$ (inner edge) . (31)

where $m = \exp (-X / L_e)$

X: distance along the sample edge,

L_e: equilibration length .

The chemical potential of the probe 2 (μ_{c2}) is

$\mu_{c2}(V_{G2}=+0.1\ V) = \mu_0 + (1 - \alpha m)hI / 2e$, (Fig.41(b)) (32)

$\alpha = (T_0 - T_1) / (T_0 + T_1)$

and

$\mu_{c2}(V_{G2}=-0.24\ V) = \mu_0 + (1 - m)hI / 2e$, (Fig.41(c)) (33)

Thus the Hall resistance is written as;

(b) $R_H(51,62) = (\mu_{c2} - \mu_{c6}) / eI = (1 - \alpha m)h / 2e^2$
at $V_{G1} = 0.1$ V and $V_{G2} = 0.1$ V, (34)

(c) $R_H(51,62) = (1 - m)h / 2e^2$ at $V_{G1} = 0.1$ V and $V_{G2} = -0.24$ V. (35)

That is, the observed deviation of R_H from the quantized value $h/2e^2$ is (b): $\alpha mh/2e^2$ and (c): $mh/2e^2$ respectively. The ratio of these deviation is α, the ratio T_0 / T_1 is obtained by

$\alpha = (T_0 - T_1) / (T_0 + T_1) = 170\ \Omega / 400\ \Omega = 0.42$
$T_0 / T_1 = 2.4$

and m is obtained by

$m = \exp (-X / L_e) = (mh / 2e^2) / (h / 2e^2) = 400\ \Omega / 12.9\ k\Omega$,
In this sample geometry, X = 2.54 mm.
Thus the chemical potential equilibrium length L_e is estimated as 700 μm.

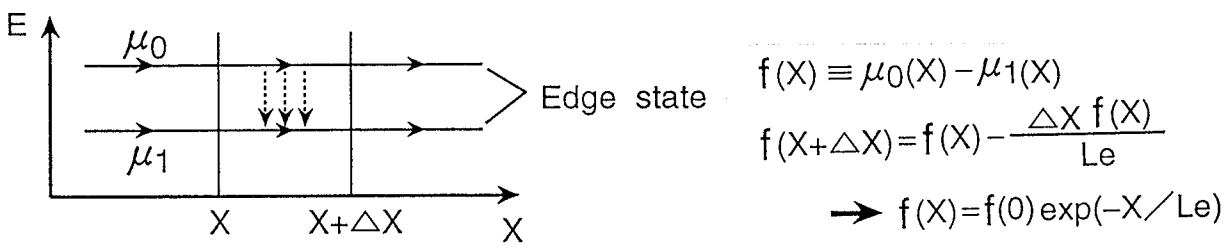

Fig. 69. Definition of the chemical potential equilibrium length L_e.

Appendix 2

Using the model proposed by McEuen *et al.*, the peak amplitude of longitudinal resistance R_L is calculated without adjustable parameter. The Landau index n=4, thus the number of edge channel m=4, and the spin degeneracy is considered. The formula explained in section 4.1.2 is modified as;

$$I_1 = (2e / h)[m (\mu_1 - \mu_4) + \mu_1^b (\text{out}) - \mu_1^b (\text{in})] = \text{I} , \quad (36)$$

$$I_2 = (2e / h)[m (\mu_2 - \mu_1) + \mu_2^b (\text{out}) - \mu_2^b (\text{in})] = -\text{I} , \quad (37)$$

$$I_3 = (2e / h)[m (\mu_3 - \mu_2) + \mu_3^b (\text{out}) - \mu_3^b (\text{in})] = 0 , \quad (38)$$

$$I_4 = (2e / h)[m (\mu_4 - \mu_3) + \mu_4^b (\text{out}) - \mu_4^b (\text{in})] = 0 , \quad (39)$$

where μ_j is the chemical potential of j$-th$ probes, and μ_j^b(in) and μ_j^b(out) are the chemical potentials of the bulk channels coming in and out of the j$-th$ barrier. They are expressed as

$$\mu_1^b (\text{in}) = \mu_4^b (\text{out}) , \quad (40)$$

$$\mu_2^b (\text{in}) = (1 - t_5) \mu_3^b (\text{out}) + t_5 \mu_1^b (\text{out}) , \quad (41)$$

$$\mu_3^b (\text{in}) = \mu_2^b (\text{out}) , \quad (42)$$

$$\mu_4^b (\text{in}) = (1 - t_5) \mu_1^b (\text{out}) + t_5 \mu_3^b (\text{out}) , \quad (43)$$

$$\mu_j^b (\text{out}) = \mu_j t_j + (1 - t_j) \mu_j^b (\text{in}), \qquad (j = 1 \textit{ to } 4) . \quad (44)$$

The longitudinal resistance R(12,43) is derived analytically as;

$$R(12,43) = (\mu_4 - \mu_3) / \text{Ie} , \quad (45)$$

where

$$\mu_4 = [\ \{\ t_1 r_2 r_5\ (m+t_3\ (1-m))\ /\ (t_3+m)\ -t_1\ -t_2 t_5 r_1\ \}\ h\ I\ /\ 2e$$
$$+\ \{\ t_1 m+t_2 t_5\ (m+t_1\ (1-m)-t_1 r_2 r_5 m\ +\ (m+t_3(1-m))\ /\ (t_3\ +m)\ \}\mu_1\ ]$$
$$/\ (\ m\ t_2 t_5 r_1\ )\ ,$$

$$\mu_3 = r_2 t_3\ (\ h\ I\ /\ 2e\ -\ m\ \mu_1\ )\ /\ [\ t_2(t_3\ +\ m\ )\ ]\ ,$$

$$\mu_1 = h\ I/2e\ (\ A\ -\ B\ )\ /\ (\ C\ -\ D\ )\ \ ,$$

$$A = (\ m+t_1 t_4-m\ r_1 r_4 r_5\ )\ [\ t_1+r_1 t_2 t_5-t_1 r_2 r_5\{m+(1-m)\}/(m+t_3)\ ]\ ,$$

$$B = m\ r_1 t_5\ [\ t_1 r_2 r_4 t_5\ \{m+(1-m)t_3\}\ /\ (m+t_3)\ -\ t_2\ (r_1 r_4 r_5-1)\ ]\ ,$$

$$C = (\ m+t_1 t_4-m\ r_1 r_4 r_5\ )\ [\ m\ t_1+t_2 t_5\{m+(1-m)t_1\}$$
$$-m\ t_1 r_2 r_5\{m+(1-m)t_3\}\ /\ (m+t_3)\ ]\ ,$$

$$D = m r_1 t_5\ [\ t_2(m+t_1)\ +\ m\ t_1 r_2 r_4 t_5\{\ m+(1-m)t_3\}/(m+t_3)\ -t_2 r_4 r_5\{m+t_1(1-m)\}\ ]\ ,$$

where $r_j = 1 - t_j$, $(j = 1\ to\ 5)$.

and $t_j = [\ 1 + (\ 2e^2/h\ )\ \rho^b\ (\ L_j/W_j\ )\ ]^{-1}$, $(j = 1\ to\ 5)$

The ratio of the length and width of each segment L_j/W_j in the sample is $L_j / W_j = 6.5$ (for $j = 1\ to\ 4$), $L_5 / W_5 = 13.25$, respectively. The value of t_j is written as;

$$t_j = \{\ 1 + (\ 1 - t_5\ )L_j W_5\ /\ (\ t_5 W_j L_5)\ \}^{-1} \qquad (j=1\ to\ 4\ ).$$ (46)

Thus, R(12,43) can be expressed with a parameter t_5. The peak value of R(12,43) is searched by sweeping t_5 from 0 to 1.

The maximum value of R(12,43) at n=4 Landau level is calculated as 134 Ω.

References

1 T.Ando, A.B.Fowler and F.Stern, Rev. Mod. Phys. **54**, 437 (1982).

2 T.Ando, Y.Matsumoto, Y.Uemura, M.Kobayashi and K.F.Komatsubara, J. Phys. Soc. Jpn. **32**, 859 (1972).

3 K.von Klitzing, G.Dorda and M.Pepper, Phys. Rev. Lett. **45**, 494 (1980).

4 S.Kawaji, J.Wakabayashi, M.Namiki and K.Kusuda, Surf. Sci. **73**, 121 (1987).

5 B.E.Kane, D.C.Tsui, and G.Weimann, Phys. Rev. Lett. **59**, 1353 (1987).

6 P.L.McEuen, A.Szafer, C.A.Richter, B.W.Alphenaar, J.K.Jain, A.D.Stone, R.G.Wheeler, and R.N.Sacks, Phys. Rev. Lett. **64**, 2062 (1990).

7 S.Takaoka, H.Kubota, K.Murase, Y.Takagaki, K.Gamo, and S.Namba, Solid State Commun. **76**, 293 (1990).

8 M.Büttiker, Phys. Rev. **B38**, 9375 (1988).

9 B.I.Halperin, Phys. Rev. **B25**, 2185 (1982).

10 P.Streda, J. Phys. **C15**, L717 (1982).

11 S.Komiyama, H.Hirai, M.Ohsawa, and Y.Matsuda, Phys. Rev. **B45**, 11085 (1992).

12 R.Landauer, IBM J. Res. Dev. **1**, 233 (1957).

13 S.Komiyama and H.Hirai, Phys. Rev. **B40**, 7767 (1989).

14 S.Suyama, A.Okamoto, S.Shirai, T.Serikawa, S.Takaoka, and K.Murase, J. Appl. Phys. **71**, 494 (1992).

15 Y.Takagaki, K.Gamo, S.Namba, S.Ishida, S.Takaoka, K.Murase, K.Ishibashi and Y.Aoyagi, Solid State Commun. **68**, 1051 (1988).

16 S.Komiyama, H.Nii, M.Ohsawa, S.Fukatsu, Y.Shiraki, R.Itoh, H.Toyoshima, Solid State Commun. **80**, 157 (1991).

17 M.Bütikker, IBM J. Res. Develop. **32**, 317 (1988).

18 K.Oto, T.Sawasaki, K.Tsukagoshi, S.Takaoka, K.Murase, K.Gamo, and S.Namba, Proc. 21st Int. Conf. Physics of Semiconductors, Beijing, China, Aug. 10–14, 1992.

19 T.Sawasaki, K.Oto, S.Takaoka, K.Murase, K.Gamo, and S.Namba, Proc. Int. Sympo. Intelligent Design and Synthesis of Electronic Material Systems, Osaka, Japan. 1992, (Ed. by S.Gonda) p.169.

20 G.Müller, D.Weiss, S.Koch, K.von Klitzing, H.Nickel, W.Schlapp, and R.Lösch, Phys. Rev. B**42**, 7633 (1990).

21 G.Müller, D.Weiss, A.V.Khaetskii, K.von Klitzing, S.Koch, H.Nickel, W.Schlapp, and R.Lösch, Phys. Rev. B**45**, 3932 (1990).

22 S.Komiyama and H.Nii, Physica B **184**, 7 (1993).

23 K.Oto, T.Sawasaki, S.Takaoka, K.Murase, K.Gamo and S.Namba, *Work Book of 2nd Int. Symp. on New Phenomena in Mesoscopic Structures*, Maui, Hawaii, p.116 (1992).

24 S.Takaoka, T.Sawasaki, K.Tsukagoshi, K.Oto, K.Murase, K.Gamo, and S.Namba, Solid State Commun. **80**, 571 (1991).

25 K.Tsukagoshi, S.Takaoka, K.Oto, K.Murase, Y.Takagaki, K.Gamo, and S.Namba, Phys. Rev. B**46**, 5016 (1992).

26 Th.Englert, D.C.Tsui, A.C.Gossard, and Ch.Uihlein, Surf. Sci. **113**, 295 (1982).

27 S.Takaoka, K.Tsukagoshi, K.Oto, K.Murase, Y.Takagaki, K.Gamo, and S.Namba, Physica B **184**, 21 (1993).

28 K.Tsukagoshi, K.Oto, S.Takaoka, K.Murase, Y.Takagaki, K.Gamo, and S.Namba, Solid State Commun. **80**, 797 (1991).

29 D.B.Chklovskii, B.I.Shklovskii, and L.I.Glazman, Phys. Rev. **B46**, 4026 (1992).

30 M.Kaplit and J.N.Zemel, Phys. Rev. Lett. **21**, 212 (1968).

31 R.K.Goodall, R.J.Higgins and J.P.Harrang, Phys. Rev. B**31**, 6597 (1985).

32 T.P.Smith, B.B.Goldberg, P.J.Stiles and M.Heiblum, Phys. Rev. B**32**, 6597 (1985).

33 V.Mosser, D.Weiss, K. von Klitzing, K.Ploog and G.Weimann, Solid State Commun. **58**, 5 (1986).

34 J.I.Lee, P.J.Stiles and M.Heiblum, Surf. Sci. **263**, 120 (1992).

35 C.W.J.Beenakker, Phys. Rev. Lett. **64**, 216 (1990).

36 K.Oto, S.Takaoka, K.Murase, S.Suyama and T.Serikawa, Surf. Sci. **263**, 303 (1992).